CAPILLARITY IN LITHOGRAPHICALLY PATTERNED MICRO CHANNELS

Haadi Javed

NOVEMBER, 2013

A thesis submitted in partial fulfilment of the requirements of Nottingham Trent University for the degree of Doctor of Philosophy

Acknowledgments

If we knew what it was we were doing, it would not be research, would it???

— Albert Einstein

Contents

4   Capillarity in Glass Tubes and Smooth Rectangular Channels

Abstract

The spontaneous capillary-driven filling of micro channels is important for a wide range of applications. Reporting for the first time for vertically mounted open top channels, in this work the theory for capillary rise in channels of rectangular cross-section has been tested and verified, taking into account the effects of surface topography assuming a Wenzel state. The theory has been tested via capillary rise experiments using polydimethylsiloxane oils of viscosity 96.0, 48.0, 19.2 and 4.8 mPa s within the 400μm and 600μm closed square glass tubes and SU8 open top smooth walled rectangular cross-section channels having width 400μm and 600μm and depth 135μm. It has been shown that capillary rise heights in plane open top walled channels (with roughness factor of 1) can be fitted using the exact numerical solution and that these are similar to fits using the analytical visco-gravitational solution. The viscous friction contribution was found to be higher than predicted by theory assuming a non-rigidified liquid–air boundary, but far below that for a rigidified boundary, which is recently reported for imbibition into horizontally mounted open micro channels. It has also been observed that fingers of liquid spreading along the internal edges of the smooth walled channels in advance of the main body of liquid consistent with wetting expectations. These fingers were observed to be thicker and larger in size for wider and shallower channels. The data from the experiments in which prominent liquid fingers were observed was fitted using the visco-gravitational approximation and it was found that the rise heights were far less than the expected heights especially in wider and shallower channels. In SU8 open top channels, Wenzel roughness was introduced on the walls in the form of triangular steps to provide additional surface area to rising liquid. The experiments were performed with 300- 350μm deep open top rough walled SU8 channels of width 400μm and 600μm using PDMS oils of viscosity 19.2, 48 and 96 mPas. The equilibrium height was observed to be increased in channels with greater roughness. The data was fitted using the visco-gravitational solution and the fitted height was found to be increased with roughness but not as much as expected from a Wenzel consideration. This deviation of fitted height from its predicted value was found to be more in the channels with greater roughness factors. The stick-slip behaviour of the liquid fingers was observed along the roughness steps.

1   Introduction

The main aim of the project was to study the liquid flow behaviour i.e. penetration and the rate of flow of liquid through lithographically patterned open top and closed rectangular micro channels. The effect of the increased surface area of channel walls on the capillary induced imbibition (hemi-wicking) by introducing symmetric triangular steps on the channel walls is studied. The geometry of the channels was altered by changing the roughness factor of the side walls. This could be achieved by increasing the surface area of the side walls that liquid faces while flowing within the channel.

The *Second chapter* of this thesis contains the literature review and background theory related to capillarity and its defining equation from which various solutions are derived governing capillarity at different time regimes one of which is Bousanquet solution. This solution leads to visco-gravitational model that is the best approximation for the series of experiments performed to validate this model.

The Third Chapter describes the experimental techniques adopted to perform the series of experiments to investigate the phenomenon of capillarity in open and closed top rectangular channels The experimental setup is described which is comprised of *five* major tasks, the *first* of which was to set up a video-microscope system capable of monitoring capillary flow at high speed and acquiring data from micro channel samples. The *second* task was to design photolithographic masks with an array of parallel micro channels. The parallel nature of the channels allows comparison and to achieve calibration data within a single experiment. A number of masks were designed with differing widths ranging from 150 to 600 microns and lengths from 1 to 5 cm. The channels were having same shape but different width, and, same width but different roughness factors. The *third* task was to use these masks to fabricate open top channels in SU-8 photoresist using the lithographic techniques. The *fourth* task was to use these samples and transitions regulating how capillary penetration and fluid flow occurs were studied. The surface chemistry of the micro-channels was varied to make it more hydrophilic. At final stage, the *fifth* task was to study the shape and speed of liquid fingers spreading in advance to the main meniscus body along the edges of the channels.

The *fourth chapter* comprises of investigations regarding capillary rise in plane capillaries including circular glass tubes, closed square glass tubes and SU8 open rectangular micro channels. It has been shown that visco-gravitational solution is the best model to describe capillary phenomenon for these particular dimensions of capillaries used in this experimental setup.

The study on capillary fingers are included in *fifth chapter*. These fingers rise along the corners of the capillaries where side walls meet the bottom surface in case of open top channels along all four corners of closed tubes The effect of various physical parameters on the speed and shape of liquid fingers is investigated. The visco-gravitational solution is applied to the capillary flow with prominent fingers and the corresponding capillary co-efficient '*b*' is measured in each case.

In *sixth chapter*, the flow of PDMS oils of various viscosities and propylene glycol is investigated in SU8 rough open top micro channels. The effect of roughness on the liquid flow is discussed and it has also been shown how the width and depth of capillaries and various viscosities of liquid effect the rise height. The data in each case is fitted using visco-gravitational solution and the fitted values of viscous and capillary terms '*a*' and '*b*' are compared to their corresponding predicted values in each case. As in case of rough channels, the rise height obtained is not as much as predicted by theory using the actual roughness factors, therefore, the effective roughness factors are calculated for various rough channels, that gives the same rise height as predicted.

## 2	*Literature Review and Background Theory*

2.1   Surface Tension

Surface tension is the increase in free surface energy per unit area and it is also measured by force per unit length (Gast., 1997). It is typically measured in N/m.

The surface tension as explained by Arthur W Adamson (1997) considering a soap film stretched on a wire frame where one of the ends of the frame is movable as shown in Fig. 2.1. The work is done to stretch the soap film by the amount of dx and surface tension is, the restorative force, on the sliding bar of the frame in the opposite direction to the stretching. This is given by the equation

$$Work\ done = \gamma_{LV}\ l\ dx\ =\ \gamma_{LV}\ dA \tag{2.1}$$

where γ_{LV} is referred as surface tension, A is the area of the frame.
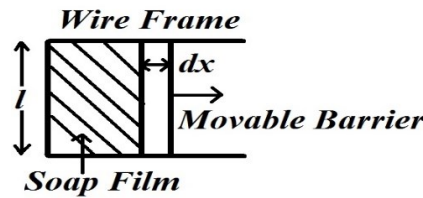
Fig. 2.1   *A soap film stretched across the wire frame with one movable side*

The cohesive force between the molecules in the liquid is equally distributed in all directions with neighbouring molecules. However the molecules at the surface of the liquid are exhibiting the strong attractive force on the inner molecules, and results of a thin elastic membrane at the surface as shown in Fig. 2.2. The surface tension is a restorative force which acts to reduce the surface area of the liquid (Gentle, 2005) or in other words, the amount of energy required to increase a unit surface area is known as surface tension. At the surface, liquid molecules do not find other like molecules in all directions above them, due to this reason they stick to the other like molecules directly associated with them on the surface more strongly resulting in the formation of a surface film.

5
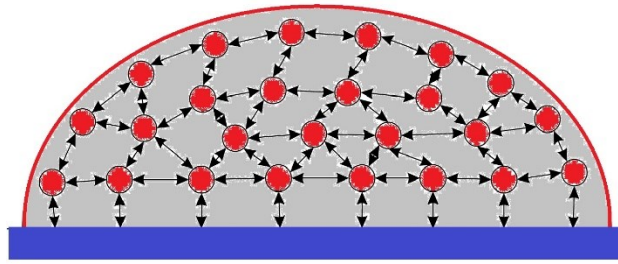
Fig. 2.2   *Molecular interaction in the liquid and at the boundaries of the liquid.*

The molecules experience a strong attractive force between the two like molecules which is referred to as a cohesive force. An attraction force between the unlike molecules such as liquid molecule and solid surface is referred to as adhesive force.

Wetting of the solid surface is governed by balancing between the cohesive and adhesive force. If the cohesive force of the molecules in the liquid is stronger than the adhesive force between the liquid and the surface then liquid does not wet the solid surface, for example mercury on the glass substrate. The complete wetting occurs when the adhesive force is stronger than the cohesive force, for example water molecules in a glass tube. The shape of liquid droplets is a result of surface tension. The spherical shape of droplets is caused by cohesive forces of the surface film. "Small droplets on solid surfaces" have spherical cap shapes, but large ones have a flattened shape due to gravity. Surface tension exists in all liquids to some degree.

2.2   Capillarity

Capillarity is the phenomenon of flow of liquid into narrow tubes or pores as a result of surface tension; it is the study of liquid-air and liquid-solid interfaces. The liquid-air interfaces are deformable, i.e. they are free to change their shape in order to minimize the surface energy (de Gennes et al., 2004). Adhesion of liquid molecules to the surface of solid and cohesive forces between other liquid molecules play the major role in capillary phenomenon. If adhesive forces between the molecules of liquid and solid are stronger than the cohesive forces between liquid molecules, the capillary action is observed and the liquid is more likely to imbibe along the solid surface. In this case, the angle between the tangent to liquid surface and solid surface at the point of contact is less than 90º and the liquid is said to be wetting liquid. The examples are rise of water or silicon oil in glass tubes. In contrast, if adhesive forces are weaker than the

cohesive forces, the liquid tends to be supressed near the solid surface. In this case the contact angle that liquid makes with solid surface is more than 90° and the liquid is called non-wetting liquid. For example, when mercury is subjected to rise in a glass tube, its surface is supressed near the solid surface.

The liquid meniscus rises as a result of adhesion of liquid to the walls of a container which exerts an upward force on the liquid at the edges. The surface tension causes the molecules to form a film at the surface, which in turn makes this entire film to move upwards instead of molecules at the edges only.

(a)   (b)   (c)
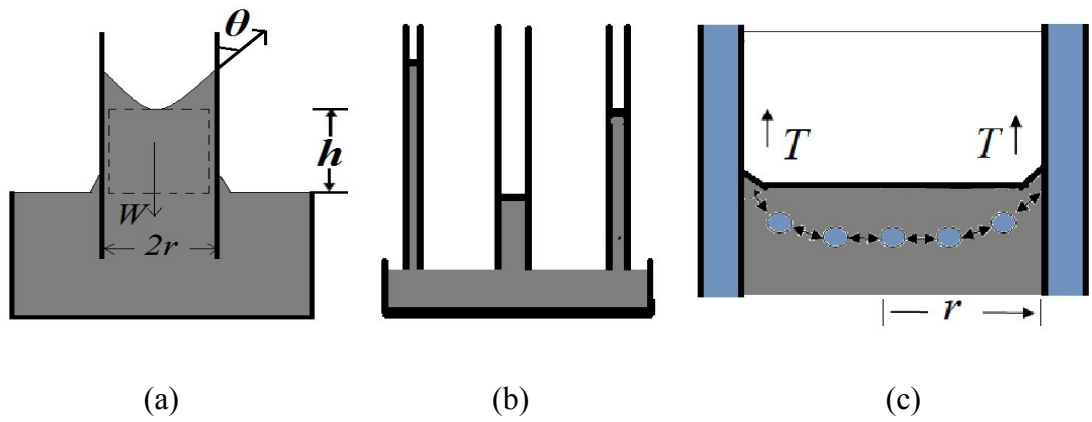
Fig. 2.3   *(a) Dependence of height on weight of liquid, (b) Capillary action in tubes having various radii and (c) Surface Tension*

The surface tension of a liquid determines how high it can climb within a capillary. The upward force which is vertical component of surface tension that acts around the circumference in the case of a circular capillary is given as;

$$F_{upward} = 2\pi r \, \gamma_{LV} \cos\theta \qquad (2.2)$$

where γ_{LV} is surface tension of liquid, r is radius of the tube and θ is the contact angle that the liquid makes with solid surface. The height h reached by the liquid as a result of capillary action is given by the balance of weight of liquid acting downwards, and an upward force F_{upward} and is given by the following relation:

$$h = \frac{2\gamma_{LV} \cos\theta}{\rho rg} \qquad (2.3)$$

here ρ is liquid density and g is acceleration due to gravity. In case of non-wetting liquids, $\theta \geq 90^{\circ}$ the height h becomes negative which shows the capillary drop.

2.3 Viscosity

2.3.1 Dynamic Viscosity

Dynamic viscosity is also referred to as absolute viscosity or simply viscosity. The measure of the resistance between the different layers of a fluid that slide past each other with different velocities is regarded as viscosity. In other words, fluid thickness or friction between the layers determine its viscosity. Honey is said to be more viscous as it is very thick and hard to flow as compared to water which is considered to have relatively less viscosity. If a fluid is deformed by shear stress or tensile stress, then viscosity can be measured by the formula;

$$(Shear\ Stress) = \eta\ (Shear\ Rate) \tag{2.4a}$$

It be defined considering a situation where a layer of Newtonian fluid is trapped between two very large horizontal plates, one fixed and one moving horizontally at constant speed. If the speed of the top plate is small enough, the fluid particles will move parallel to it, and their speed will vary linearly from zero at the bottom to u at the top. Each layer of fluid will move faster than the one just below it, and friction between them will give rise to a force resisting their relative motion. In particular, the fluid will apply on the top plate a force in the direction opposite to its motion, and an equal but opposite one to the bottom plate. An external force is therefore required in order to keep the top plate moving at constant speed. The magnitude F of this force is found to be proportional to the speed u and the area A of each plate, and inversely proportional to their separation y. That is,

$$\frac{F}{A} = \eta\ \frac{u}{y} \tag{2.4b}$$

The proportionality factor η in this formula is the dynamic viscosity of the fluid. The ratio $\frac{u}{y}$ is called the rate of shear deformation or shear velocity, and is the derivative of the fluid speed in the direction perpendicular to the plates. It is measured in units of Pa.s

which is fairly a larger unit, therefore, mPa.s is commonly used unit for this. The plot of shear rate vs. shear stress which is linear for Newtonian liquids is shown in Fig. 2.4, the slope of which gives the measure of viscosity.
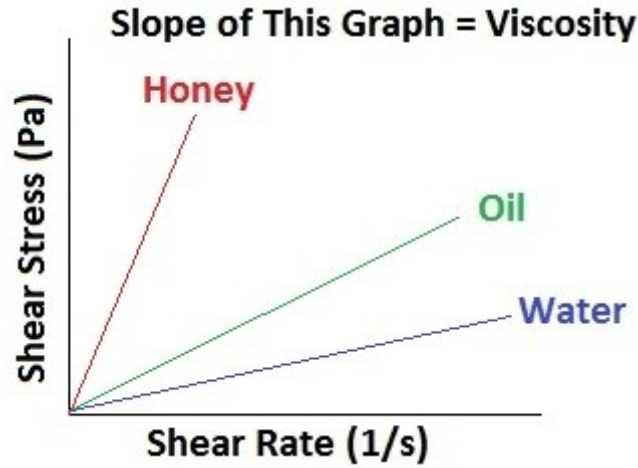
Fig. 2.4   *Viscosity for different types of Newtonian liquids is given by the slope of the graph between shear rate and shear stress*

2.3.2   Kinematic Viscosity:

The ratio of the viscous force to the fluid density ρ is known as kinematic viscosity. In other words, it is the ability of the fluid to transport momentum. Mathematically,

$$\upsilon = \frac{\eta}{\rho} \qquad (2.5)$$

For SI units, it is expressed as m²/s. Kinematic viscosity is also expressed in stokes (St) or centistokes (cSt), for cgs units.

2.4   Wetting

When a droplet of a liquid comes into contact with the solid surface it can either wet, partially wet or does not wet the surface at all depending on the contact angle it makes with the solid surface. The wetting behaviour can be quantified by measuring the contact angle of the drop with the solid surface.

2.4.1 Contact Angle

Wetting is measured quantitatively by the contact angle a liquid makes with the solid surface. It is the internal angle between the liquid/vapour and solid/liquid interface. It is measured when a liquid droplet is dispensed on a solid surface. The two-dimensional angle between the solid and the droplet with the vertex at the three-phase line as shown in Fig.2.5 where the arrows represent a direction for the interfacial forces.
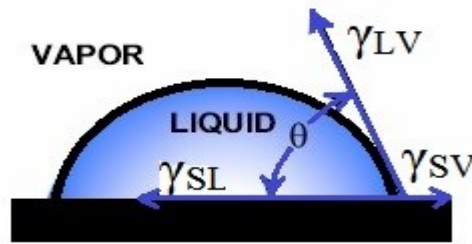
Fig. 2.5 *Contact angle*

2.4.2 Young's Law

Thomas Young, a British physicist, explained the behaviour of wetting in terms of three interfacial tensions and derived the equilibrium contact angle with relation to the three interfacial tensions, i.e. liquid-solid interfacial tension γ_{SL}, solid-vapour interfacial tension γ_{SV} and liquid-vapour interfacial tension γ_{LV} (Young, 1805). The three interfacial tensions influence the shape of the droplet on the solid surface.

If a liquid droplet of constant volume is placed on a plane surface and starts spreading, as shown in Fig. 2.6, The three phase contact line moves increasing by the drop contact area ΔA, hence the solid-vapour interface is replaced by the solid-liquid interface and in addition the liquid-vapour surface area increased by $\Delta A \cos\theta$
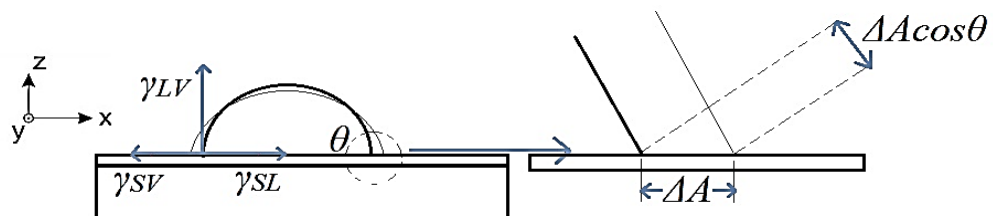
Fig. 2.6 *Schematic representation interfacial spreading by balancing the three interfacial tensions.*

$$\Delta F = (\gamma_{SL} - \gamma_{SV})\Delta A + \gamma_{LV}\Delta A \cos \theta \qquad (2.6)$$

When a thermodynamic equilibrium is reached between the three phases: solid, liquid, and gas, $\Delta F = 0$, the eq. (2.6) becomes;

$$\gamma_{SV} = \gamma_{SL} + \gamma_{LV} \cos \theta_e \qquad (2.7)$$

where θ_e is contact angle called Young's angle, γ_{SL} is solid/liquid interfacial free energy, γ_{SV} is solid surface free energy and γ_{LV} is the liquid surface free energy. This is known as *Young's equation* and is used to describe the interactions between the forces of cohesion and adhesion and measure what is referred to as surface energy (Quéré., 2008; Bonn, 2009). Young's equation is one of the oldest and most used equations in liquid physics. Eq. 2.2 can be re-written as;

$$\cos \theta_e = \frac{(\gamma_{SV} - \gamma_{SL})}{\gamma_{LV}} \qquad (2.8)$$

1.4.3   Types of Wetting

There are three types of wetting which are shown in Fig. 2.7

γSV = γSL   *Super-hydrophobic*

Complete Wetting   *Partial Wetting (θ > 0º)*   *Non-wetting*
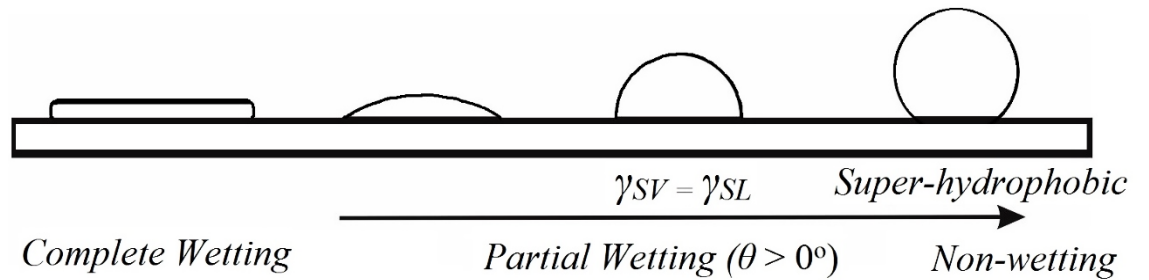
Fig. 2.7   *The representation of three wetting states i.e. two extreme wetting states with partial wetting between these two states.*

Complete wetting:

If the interfacial tension of the solid-vapour is equal to the sum of the solid-liquid and liquid-vapour interfacial tensions $\gamma_{SV} = \gamma_{LV} + \gamma_{SL}$, then at the equilibrium state the liquid completely wets the solid surface and this is called a complete wetting

(shown in Fig. 2.7). For example a water drop on the bare metallic or ceramic surfaces, although the presence of an oxide layer, or contaminants, on the solid surface can significantly increase the contact angle. These kind of materials are called as hydrophilic surfaces. In other words, a drop with a small contact angle, i.e. approaching zero, is completely *hydrophilic* as shown in Fig. 2.7. This condition reflects better wetting, better adhesiveness, and higher surface energy. Solids such as metals, glasses, and ceramics are known as 'hard solids' because the chemical bonds that hold them together (e.g., covalent, ionic, or metallic) are very strong. Thus, it takes a large input of energy to break these solids so they are termed "high energy." Most molecular liquids achieve complete wetting with high-energy surfaces.

Partial wetting:

If the interfacial tension of the solid-vapour is smaller than the sum of the solid-liquid and liquid-vapour interfacial tensions $\gamma_{SV} < \gamma_{LV} + \gamma_{SL}$, then it will perform a partial wetting which means the equilibrium contact angle of the drop should be greater than 0° and less than 180° as shown in Fig. 2.8.
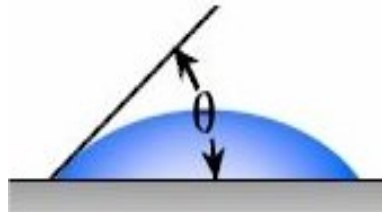
Fig.2.8   *Hydrophilic Surface*

Non-Wetting:

If the adhesive force between the liquid molecules and solid surface is much smaller than the cohesive force in the liquid, then the liquid wets a very small limited area of the solid surface and the contact angle would be more than 150°. For example, water drop on the super hydrophobic surface, e.g. micro pillars (Onda, 1996; Bico, 2001). This condition is exemplified by poor wetting, poor adhesiveness and the solid surface free energy is low.
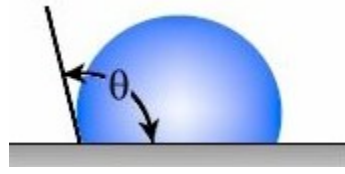
Fig. 2.9   *Hydrophobic Surface*

2.4.4   Contact Angle Hysteresis

The contact angle, while the volume of the drop is increasing, just before the wetting line starts to advance is called *advancing contact angle* θ_a. If the volume of the drop is decreased, the contact angle determined just before the wetting line is receding is called *receding contact angle* θ_r. Usually the angle θ_a is significantly higher than the angle θ_r. The difference $\theta_a - \theta_r$ is called *contact angle hysteresis*. Contact angle hysteresis is generally attributed to surface roughness, surface heterogeneity or solution impurities adsorbing on the surface.

Advancing and receding contact angles can be determined using the tilt plate method or by adding or removing liquid volume method as shown in Fig. 2.10

(a)   (b)
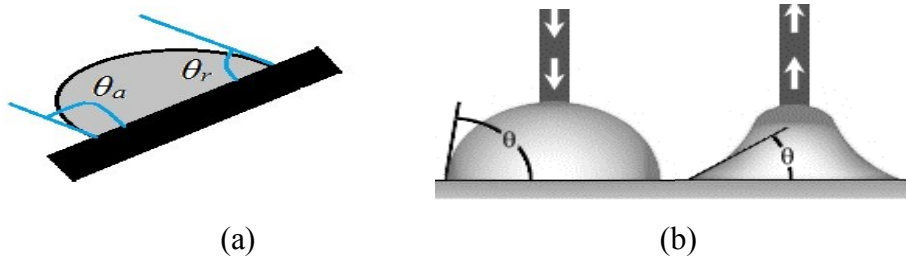
Fig. 2.10   A*dvancing and receding angle measurement by (a) tilt plate method and (b) add or remove liquid volume method*

2.5   Capillary Length

Capillary length is a characteristic length scale for fluid subject to a body force from gravity and a surface force due to surface tension (Batchelor, 1967). The capillary length is defined as:

$$L_C = \sqrt{\frac{\gamma_{LV}}{\rho g}}$$
(2.9)

where g is the acceleration due to gravity and ρ is the density of the fluid, and γ_{LV} is the surface tension of the fluid-fluid interface. For polydimethylsiloxane (PDMS) oil it comes out to be 1.45mm. If the interface's radius of curvature is much less than the capillary length, the effect of gravity can be neglected compared to that of surface tension on the shape of a liquid/air interface (Fig. 2.3).

2.6   Liquid-Solid Interaction on Rough Surface

To control the liquid and solid interaction, surface chemistry can be used to alter the molecularly determined hydrophobic/hydrophilic properties of the surface (Vogler, 2001). Whilst surface chemistry can cause a droplet of liquid to spread into a film on a particular smooth and flat solid surface, there are many liquids for which a droplet will only partially spread on the same surface. However, if the solid surface is rough or topographically structured on a suitably small length scale the extra surface area can amplify the spreading tendency of a liquid so that it is drawn completely into a film rather than remaining as a partially wetting droplet (McHale, 2004; Aqil, 2006). This type of induced wetting is also known as hemi-wicking and is characteristic of a transition from a non-porous state to a pseudo two-dimensional porous state of the material (Shirtcliffe, 2005).

However, these obstacles to the flow can cause the advancing front to pin for contact angles greater than a certain threshold value, thus halting the filling. It is also possible that far from acting as obstacles, if the additional surface area is wetting/hydrophilic, the effect can be to reduce the threshold value of the contact angle. Moreover, the rate of rise of liquid within a capillary tube, which is usually described by the Lucas-Washburn law (de Gennes, Brochard-Wyart, & Quéré, 2004; Gast., 1997; Dreyer, 2008), can also be expected to be modified (Quéré, 2003; Quéré, 2008).

2.6.1   Wenzel's Model

Wenzel model describes the homogeneous wetting of textured surfaces. However, it only applies when the drop size is sufficiently large compared with the surface roughness scale. In a Wenzel state, the liquid fills the voids below the liquid and thus occupies more surface area. The additional parameter in this case is roughness (*r*). Wenzel's formula states that solid surface energy (when the contact angle is greater than

90°) is a function of cosine of the contact angle multiplied by factor (*r*), and is defined by the following equation for the contact angle on a rough surface (Wenzel, 1936)

$$\cos \theta_W = r \cos \theta_e \qquad (2.10)$$

where θ_W is the apparent (rough surface) contact angle, θ_e refers to the Young contact angle (on ideal smooth surface) and *r* refers to the roughness factor (which is 1 for an ideal smooth surface). The *roughness factor*, *r*, is a measure of how surface roughness affects a homogeneous surface. The roughness factor is defined as the ratio of true area of the solid surface to the apparent area (explained in detail in sec. 3.2.2). Wenzel state is shown in Fig. 2.11
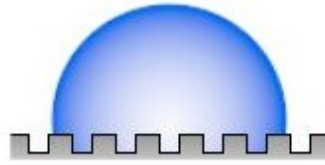
Fig. 2.11   *Wenzel State*

2.6.2   Effect of Roughness of the Surfaces on Contact Angle

According to Wenzel's equation, roughness will decrease the contact angle when the apparent contact angle is under 90° but will increase the contact angle when the apparent contact angle is over 90°. Thus, we can say that increased roughness will decrease the measured contact angle on hydrophilic surfaces but increase the measured contact angle on hydrophobic surfaces (in case of water). In other words, increased roughness amplifies both hydrophilicity and hydrophobicity (but not necessarily linearly) (Clegg, 2008)

2.6.3   Cassie-Baxter Law

While dealing with heterogeneous surfaces as shown in Fig. 2.12, a more complex model is needed to measure how the apparent contact angle changes when various materials are involved and is explained by Cassie-Baxter equation

$$\cos \theta_{CB} = r_f f \cos \theta_e + f - 1 \qquad (2.11)$$

where r_f is the roughness ratio of the wet surface area and f is the fraction of solid surface area wet by the liquid. It is important to realize that when $f = 1$ and $r_f = r$, the Cassie–Baxter equations becomes the Wenzel equation.
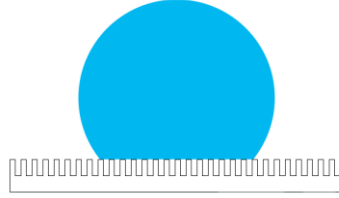
Fig. 2.12   *Cassie-Baxter State*

2.6.4   Hemi-wicking

The roughness features on a surface affect the contact angle of liquid with the solid surface. Due to the change in contact angle, wetting properties such as hydrophilicity/oleophilicity and hydrophobicity/oleophobicity are altered. The advancement in techniques for micro and nano texturing is used to induce the variation in wetting behaviour. Fig. 2.13 describes how contact angle of various liquids change on rough fluorinated surface compared to the angle on the smooth surface of the same material (Shibuichi et al., 1996).

The curve in the Fig.2.13 shows that how roughness can amplify the wetting behaviour for different liquids. On right hand side $\cos \theta_e > 1$, the first slope describes Wenzel's law whereas the next slope indicates the superhydophilicity and shows hemi-wicking of surrounding grooves of the surface.

In the case of Cassie–Baxter state, the air is trapped underneath the liquid droplet which rests on the top of the ridges or imperfections of the solid surface. The air gaps are started to be filled by liquid from the middle of the droplet during the wetting transition from the Cassie state to the Wenzel state, which forms a "mushroom-like state," as seen in Fig. 2.14 (Okumura, 2008). The condition of liquid penetration is given by the following equation:

$$\cos \theta_C = \frac{1 - f}{r - f} \tag{2.12}$$

where θ_C is the critical contact angle, f is the fraction of solid/liquid interface where drop is in contact with surface and r is solid roughness (for smooth surface, $r = 1$).

16
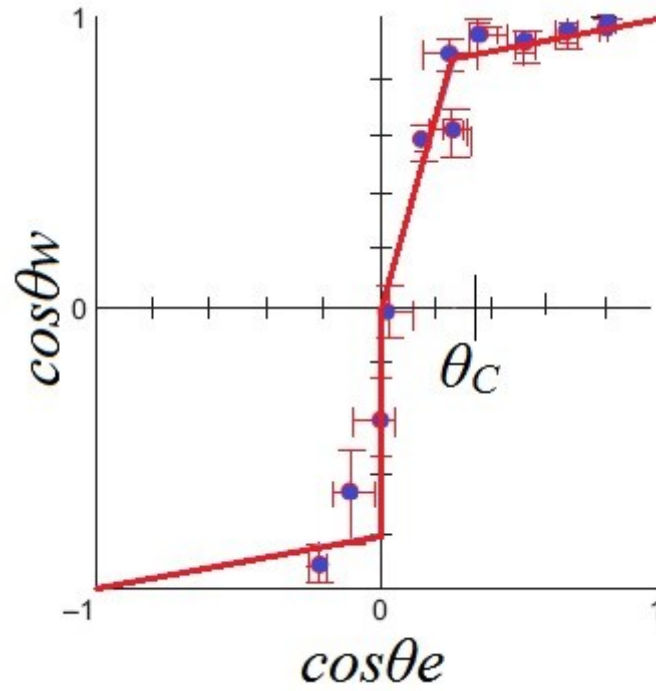
Fig. 2.13 *Cosine of the effective angle (on rough surface) versus cosine of the Young's angle (on a smooth surface) of the fluorinated surface using different liquids (Shibuichi et al., 1996)*

Fig. 2.14 *Hemi-wicking*

The surface free energy is reduced as the penetration front advances. Wenzel state occurs when it reaches the edges of the drop. Due to the roughness of the solid surface, the solid can be considered as an absorptive material, this phenomenon of spreading and imbibition is called *hemi-wicking*. The spreading/imbibition occurs at the contact angles having values $0 \leq \theta < \dfrac{\pi}{2}$ (Quéré., 2008). The range of contact angle for which the Wenzel state occurs is $\theta_c < \theta < \dfrac{\pi}{2}$. The penetration front continues to spread and goes beyond the liquid surface when the contact angle is less than θ_c, as shown in

Fig. 2.13 and 2.14. After the formation of the film, the Wenzel model is no longer applicable as it smooth the surface roughness. In this state, the equilibrium condition is achieved and Young's relation is valid (Okumura, 2008):

$$\cos \theta_{CB} = f \cos \theta_C + (1 - f) \qquad (2.13)$$

By altering the surface roughness, it is possible to achieve a transition between both super hydrophobic and hydrophilic regions. Hence we can say that if the solid surface is rough or topographically structured on a suitably small length scale the extra surface area can amplify the spreading tendency of a liquid so that it is drawn completely into a film rather than remaining as a partially wetting droplet (McHale, 2004). This type of induced wetting is also known as *hemi-wicking* and is characteristic of a transition from a non-porous state to a pseudo two-dimensional porous state of the material.

2.7 Capillary Rise in Glass Tubes and Micro Channels

The imbibition of liquids into capillaries plays vital role to so many applications such as printing (Schoelkopf et al., 2002), lab-on-chip (Brody et al., 1996; Squires and Quake, 2005), porous media (e.g. Marmur and Cohen, 1997; Siebold, 2000) and soil water repellency (Shirtcliffe et al, 2006). These problems are governed by the principles that are based upon the balance of capillary forces, viscous forces, inertial forces and hydrostatic pressure. Hydrostatic pressure is the pressure exerted by the liquid at rest and is given by

$$P = \rho g h \qquad (2.14)$$

where ρ is the liquid density, g is acceleration due to gravity and h is the liquid depth. The capillary imbibition can be controlled effectively by understanding precisely the nature of this phenomena. There are different time regimes for capillary driven flow. At the very early stage, imbibition is dominated by inertial force, described by Quéré (1997). For longer time regime, mainly the viscous force controls the capillary flow as discussed by Lucas (1918) and Washburn (1921) while Fries and Dreyer (2008a) discussed the transition between these regimes for capillary driven imbibition.

The gravitational effects can be neglected in the system of horizontally mounted capillaries and exact analytical Bousanquet solution (Bousanquet, 1923) describes these time stages. This solution is valid for both open and closed capillaries (e.g. Bouaidet et al., 2005; Jokinen and Franssila, 2008). Bousanquet solution gives the Lucas-Washburn solution at the longer time regime. Fig. 2.15 shows the Quere, Washburn and Bousanquet solutions for the experimental data of pentane in a circular glass tube of radius 191 μm. The contact angle with vertically held glass tube was observed to be 73° (Siebold et al., 2000)
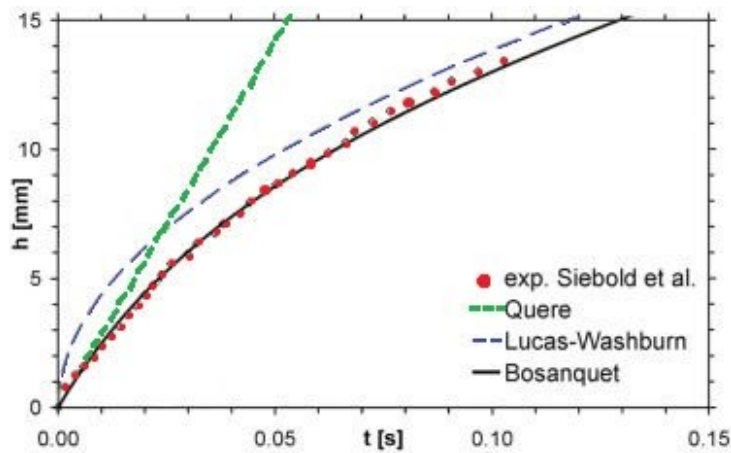
Fig. 2.15   *Three Models for the experimental data from Siebold et al. (solid symbols)*

Closed and Open Channels:

A capillary with all solid walls is taken as closed channel while open channels is the one with one wall open to air and in this case, liquid-air interface is taken as the effective wall.

As capillary driven imbibition is fundamental to microfluidics, it has been studied for various types of cross-sectional shape channels, such as circular (Strange et al., 2003), rectangular (Ichikawa et al., 2004; Jong et al., 2007; Zhu and Petkovic-Duran, 2010) and grooved/triangular (Yost and Holm, 1995; Romero and Yost, 2006; Baret et al., 2007). Moreover, the same approach has been taken for channels defined by hydrophilic paths on a hydrophobic substrate (Darhuber et al., 2001) and by the space between two parallel plates (Rosendahl et al., 2004) under the assumption of flow with low Reynolds number and liquid imbibing in a cylindrical/slab-like manner.

19

2.8   Capillarity in Vertically Held Capillaries

Gravitational effect becomes very important when the capillaries are held vertically and exact analytical solutions for capillary imbibition are no longer possible in general. However, a visco-gravitational solution for time as a function of meniscus position does exist for the equivalent of the Lucas-Washburn regime (e.g. Krotov and Rusanov, 1999; Hamraoui et al. 2000, Ahmed and Nylander, 2002), including for liquid-liquid systems (Mumley et al, 1986). In these problems, the role of the shape and wetting state of the walls are critical.

Advances in lithographic fabrication techniques are increasing the range of studies in which capillary aspects of imbibition and rise are critical. These advances are leading to studies with microfluidic (e.g. Yang et al, 2011) and nanofluidic capillaries widths of a few tens of nm (Han et al., 2006) or with depths as small as 6 nm (Oh et al, 2009). Whilst non-constant channel cross sections have been a focus of study experimentally and theoretically (Legait, 1983; Staples and Shaffer, 2002, Reysatt et al, 2008; Liou et al, 2009), increased solid-liquid contact area, and hence increased capillary pull can be achieved using a range of in-channel structures. In a series of studies, Bico and co-workers studied imbibition using hemi-wicking, which amplifies the capillary pull using wall roughness (Bico 2000, Bico et al., 2002; Bico and Quéré, 2003; Ishino et al, 2007); ideas recently applied to rough Cu_6Sn_5/Cu intermetallic surfaces (Liu et al, 2011). Their work used average parameters to characterize the capillary effect of roughness and topographic structures. This has been complemented by modelling studies by Kusumaatmaja et al. (2008) and Mognetti and Yeomans (2009) focused on feature shape and channel filling patterns, finite element modelling and experiments incorporating both capillary and viscous effects of flow through micropost (Srivastavea et al., 2010), and experimental studies using, e.g. stars, octagons and squares (Chen et al., 1999).

In the section 2.9, an overview of the theoretical basis of capillary driven rise and imbibition is given. It has been done in a form that brings out the coherence of the equations and their solutions for different channel shapes in different orientations. Simple interpolation formulae for the viscous friction associated with open and closed rectangular channels of different aspect ratio has been given. It has been shown how within this formulation different contact angles on the various channel walls can be

20

incorporated using surface free energy changes, including considerations of surface roughness or topography as required for hemi-wicking. The exact numerical solution for capillary-driven imbibition is compared to the various analytical solutions of the approximate equations with and without gravity. A condition is obtained for the cross-over time and rise height below which the Bousanquet solution is the best approximation and above which the visco-gravitational solution is a more accurate description.

It has been found that fits to the numerical solution of the exact differential equation describing capillary rise, neglecting the fingers (will be discussed later in section 2.10), up to the point where the fingers reach the ends of the channels can describe the rise of the central meniscus of the liquid in both of these cases.

2.9   Theoretical Approach

In this section the standard approach to describe capillary driven imbibition is reviewed to provide a common notation and clarity on the assumptions used, particularly with regards the wetting of the surfaces. The aim is to consider the structure of the equations for uniform cross-section open and closed channels, but independent of precise geometry.

2.9.1   Capillary Equation for Circular Tube

Consider a smooth circular tube of radius R and there are no-slip boundary conditions at solid-liquid interfaces. Contact angle of liquid on tube wall is given by Young's law θ_e (experimental fits may need to replace θ_e by the advancing contact angle). Detailed shape of meniscus is ignored and the liquid flow is considered as Laminar. ρ is the liquid density, η is viscosity and γ_{LV} is the surface tension of liquid used as shown in Fig. 2.16. The equation for capillary flow can be derived by equating rate of change of momentum of liquid with the sum of various forces acting on the liquid (Chebbi, 2007; Fries, 2008a; Bousanquet, 1923; Washburn, 1921).
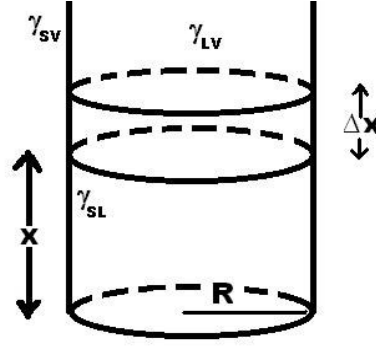
Fig. 2.16   *Round glass capillary tube*

Defining Equation

The defining equation for capillary rise is given by equating the rate of change of momentum to the various forces, i.e.

Rate of Change of Momentum = Capillary Force + Gravity Force + Viscous Force

$$\rho x \frac{d^2 x}{dt^2} + \rho \left(\frac{dx}{dt} \right)^2 = \frac{2\gamma_{LV} \cos\theta_e}{R} - \rho gx - \frac{8\eta x}{R^2} \frac{dx}{dt} \tag{2.15}$$

The forces described on the right and left hand side of the eq. (2.15) are calculated as follows:

Inertial Force

Liquid momentum is given by the relation mass×speed $= \rho\pi R^2 x \left(\frac{dx}{dt} \right)$ where x is length of tube of liquid. The force is rate of change of momentum, which is given as;

$$\rho\pi R^2 \frac{d}{dt} \left(x \frac{dx}{dt} \right) = \rho\pi R^2 x \frac{d^2 x}{dt^2} + \rho\pi R^2 \left(\frac{dx}{dt} \right)^2 \tag{2.16}$$

Capillary Force

The capillary force acting on the liquid, f_{cap}, is given by the following formula;

$$f_{cap} = 2\pi R \gamma_{LV} \cos\theta_e \tag{2.17}$$

22

Gravity Force

The gravitational force is given by the following relation:

$$f_{grav} = -\rho g \pi R^2 x \tag{2.18}$$

where $g = 9.81$ m s^{-2} is the acceleration due to gravity. (Note: If the orientation of capillary is other than vertical, then gravitational force is calculated as $f_{grav} = -\rho g \pi R^2 x (\sin \varphi)$, where '$\varphi$' is the angle of orientation of the tube to the horizontal)

Viscous Force

Assuming an incompressible, Newtonian liquid with a laminar flow, the profile is parabolic; the viscous force for flow down a tube can be deduced from the flow velocity profile which is;

$$f_{visc} = -8\eta \pi x \frac{dx}{dt} \tag{2.19}$$

2.9.2 Bousanquet Solution for Circular Tube

During the capillary rise, various forces can be neglected at certain time intervals, resulting in different defining equations. Due to this, the validity of these equations is limited to different time stages. One of these solutions is given by (Bousanquet, 1923), which is extracted from main defining equation by neglecting gravitational factor. This is the time stage when both inertial and viscous forces are effective. Actually it is the transition stage between purely inertial and purely viscous stage. Bosanquet, for this stage ignored gravitational term in eq. (2.15) which can be rearranged to give,

$$\frac{1}{2} \frac{d}{dt}\left(\frac{dx}{dt}^2\right) = b - gx - ax\left(\frac{dx}{dt}\right) \tag{2.20}$$

where the viscous coefficient a has dimensions of inverse time (s^{-1}) and is defined as:

$$a = \frac{8\eta}{\rho R^2} \tag{2.21}$$

and the capillary coefficient b has dimensions of speed^2 (m^{2}s^{-2}) and is defined as:

$$b = \frac{2\gamma_{LV}\cos\theta_e}{\rho R} \tag{2.22}$$

a and b are summarized for three types of capillaries later in section 2.9.7 and 2.9.8. Neglecting gravitational term in eq. (2.15) we get,

$$\rho x \frac{d^2 x}{dt^2} + \rho \left(\frac{dx}{dt}\right)^2 = \frac{2\gamma_{LV}\cos\theta_e}{R} - \frac{8\eta x}{R^2}\frac{dx}{dt} \tag{2.23}$$

or in terms of a and b,

$$\frac{1}{2}\frac{d}{dt}\left(\frac{dx}{dt}^2\right) = b - \frac{a}{2}\frac{dx}{dt}^2 \tag{2.24}$$

By solving the eq. (2.24), we get final Bousanquet solution as

$$x^2(t) = \left(\frac{2b}{a}\right)\left[t - \frac{1}{a}\left(1 - e^{-at}\right)\right] \tag{2.25}$$

Limiting Cases of Bousanquet:

Small t

$$x^2(t) \approx bt^2 \qquad \text{i.e.} \qquad x(t) \approx \sqrt{b}\, t \tag{2.26}$$

which is *inertial case* given by Quéré. The eq. (2.26) provides the solution at very initial stage when the capillary tube comes in contact with the surface of liquid when the inertial forces are dominant, Quéré neglected viscous and gravitational terms for this stage.

Large t

$$x^2(t) = \left(\frac{2b}{a}\right)\left[t - \frac{1}{a}(1)\right] \approx \left(\frac{2b}{a}\right)t \tag{2.27}$$

The above eq. is *Washburn-Lucas case* which is valid a for the flow period at longer time regime presented by Lucas (1918) and Washburn (1921). They neglected the influence of inertia and the influence of gravity in the defining eq. (2.15). Thus, Bousanquet simply provides the solution for all time regimes from very initial purely inertial stage to later purely viscous stage when gravitational effect is ignored.

2.9.3   Capillary Equation for Rectangular Channels

In the previous section 2.9.2, the capillary equation used for circular capillary tube experiments is presented. A similar equation can be derived for rectangular closed or open top channel, with smooth or rough walls and different contact angles on all the sides. Assume a closed top rectangular channel of width w and depth h. The top, bottom, left and right hand sides of the channel have the Young's angles θ_e^T, θ_e^B, θ_e^L and θ_e^R, and the *roughness factors* r_T, r_B, r_L and r_R respectively, where the *roughness factor* is defined as the ratio of actual surface area to the projected/geometrical surface area. It is assumed that there is no slip at walls (even in extreme hydrophobic case). Roughness is assumed to not effect drag (strongly questionable, but nonetheless assumed).
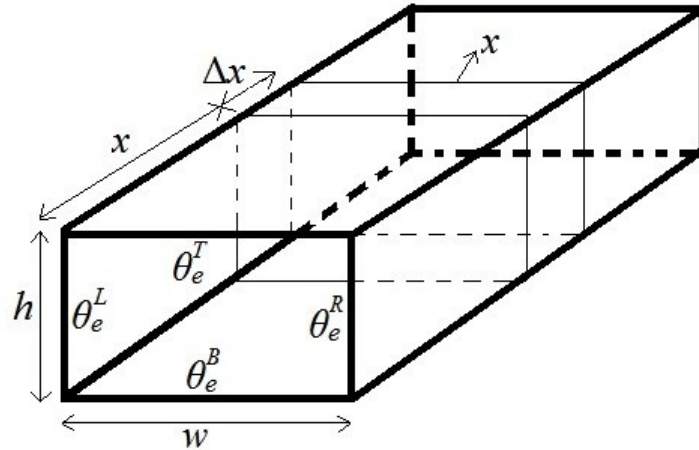
Fig. 2.17   *Closed Rectangular Channel*

The flow of liquid is considered to be laminar and ignoring the detailed shape of meniscus the equation for the flow of liquid in the micro channel can be derived by equating rate of change of momentum of liquid with the sum of various forces acting on the liquid.

Defining Equation:

Similar to circular tube case, the equation describing capillary-driven imbibition in rectangular channels is obtained by equating the rate of change of momentum to the sum of capillary force, gravitational force and viscous force.

For Closed Top Channels:

The defining equation for a closed top rectangular channel can be derived as (Ouali et al., 2013)

$$\rho \frac{d}{dt}\left(x \frac{dx}{dt}\right) = \frac{\gamma_{LV}}{h}\left[r_T \cos \theta_e^T + r_B \cos \theta_e^B + \varepsilon\left(r_L \cos \theta_e^L + r_R \cos \theta_e^R\right)\right] - \rho g x - \frac{12\,\eta x}{\varepsilon\zeta_c(\varepsilon)}\left(\frac{dx}{dt}\right)$$

(2.28)

In terms of Wenzel's angles, the above expression gives,

$$\rho \frac{d}{dt}\left(x \frac{dx}{dt}\right) = \frac{\gamma_{LV}}{h}\left[\cos \theta_W^T + \cos \theta_W^B + \varepsilon\left(\cos \theta_W^L + \cos \theta_W^R\right)\right] - \rho g x - \frac{12\,\eta x}{\varepsilon\zeta_c(\varepsilon)}\left(\frac{dx}{dt}\right) \qquad (2.29)$$

For Open Top Channels:

The defining equation for open top rectangular channels is given by

$$\rho \frac{d}{dt}\left(x \frac{dx}{dt}\right) = \frac{\gamma_{LV}}{h}\left[-1 + r_B \cos \theta_e^B + \varepsilon\left(r_L \cos \theta_e^L + r_R \cos \theta_e^R\right)\right] - \rho g x - \frac{12\,\eta x}{\varepsilon\zeta_o(\varepsilon)}\left(\frac{dx}{dt}\right) \quad (2.30a)$$

In terms of Wenzel's angles, the above expression gives,

$$\rho \frac{d}{dt}\left(x \frac{dx}{dt}\right) = \frac{\gamma_{LV}}{h}\left[-1 + \cos \theta_W^B + \varepsilon\left(\cos \theta_W^L + \cos \theta_W^R\right)\right] - \rho g x - \frac{12\,\eta x}{\varepsilon\zeta_o(\varepsilon)}\left(\frac{dx}{dt}\right) \qquad (2.30b)$$

where the terms on right hand side of eq. (2.28) and (2.30b) are indicating capillary force, gravitational force and viscous force. These forces can be calculated as follows:

Capillary Force:

The surface free energy change ΔF as the liquid advances in closed channel is caused by the changes in interfacial areas, i.e.

$$\Delta F = w \Delta x \left[r_T \left(\gamma_{SL}^T - \gamma_{SV}^T \right) + r_B \left(\gamma_{SL}^B - \gamma_{SV}^B \right) + r_L \left(\frac{h}{w} \right) \left(\gamma_{SL}^L - \gamma_{SV}^L \right) + r_R \left(\frac{h}{w} \right) \left(\gamma_{SL}^R - \gamma_{SV}^R \right) \right]$$

$$= -w \gamma_{LV} \Delta x \left[r_T \cos \theta_e^T + r_B \cos \theta_e^B + \left(\frac{h}{w} \right) \left(r_L \cos \theta_e^L + r_R \cos \theta_e^R \right) \right]$$

where Young's law has been used to replace the difference in interfacial tensions, i.e.

$$\cos \theta_e^i = \frac{\left(\gamma_{SV}^i - \gamma_{SL}^i \right)}{\gamma_{LV}}$$

The capillary force f_{cap} is then, $- \dfrac{\Delta F}{\Delta x}$, i.e.

$$f_{cap} = w \gamma_{LV} \left[r_T \cos \theta_e^T + r_B \cos \theta_e^B + \left(\frac{h}{w} \right) \left(r_L \cos \theta_e^L + r_R \cos \theta_e^R \right) \right]$$

Essentially, the relevant contact angle on the all sides of the channel are the Wenzel angles. By using $\cos \theta_W^i = r_i \cos \theta_W^i$ in the above equation we get,

$$f_{cap} = w \gamma_{LV} \left[\cos \theta_W^T + \cos \theta_W^B + \left(\frac{h}{w} \right) \left(\cos \theta_W^L + \cos \theta_W^R \right) \right] \tag{2.31}$$

For Closed Top Plane Channel:

If all the sides to the channels are smooth with roughness factor 1 and the same contact angles, i.e. $\theta_e^T = \theta_e^B = \theta_e^L = \theta_e^R = \theta_e$, the above eq. (2.31) comes out to be,

$$f_{cap} = 2 w \gamma_{LV} \cos \theta_e \left[1 + \left(\frac{h}{w} \right) \right] \tag{2.32a}$$

Taking the aspect ratio $\varepsilon = \dfrac{h}{w}$ in the above eq. we get

$$f_{cap} = 2 w \gamma_{LV} \cos \theta_e \left(1 + \varepsilon \right) \tag{2.32b}$$

For Open Top Channel with Rough Walls and Smooth Bottom Surface:

The above eq. (2.32b) gives capillary force in closed top channel with all sides smooth. Similarly, for open top channel with smooth bottom surface but two sides with same roughness factor, i.e. $r_L = r_R = r_s$ and same Wenzel angles i.e. $\cos \theta_W^L = \cos \theta_W^R = \cos \theta_W^S$, the capillary force is calculated as:

$$f_{cap} = w\gamma_{LV}\left[-1 + \cos \theta_e^B + 2\varepsilon \cos \theta_W^S\right] \tag{2.33}$$

If all the sides to the open top channel are smooth, the capillary force is given by,

$$f_{cap} = w\gamma_{LV}\left[-1 + \cos \theta_e(1 + 2\varepsilon)\right] \tag{2.34}$$

Gravity Force

The gravitational force is,

$$f_{grav} = -\rho gwhx \tag{2.35}$$

Viscous Force (Simplified version)

Assuming incompressible, Newtonian liquid with a laminar flow in a wide and flat channel (i.e. ε (=h/w) << 1), the profile is a 1-D parabolic shape. The viscous force (Fig. 2.18) for flow down a rectangular closed on top and bottom walls and on the bottom wall in case of open-topped channel (i.e. ignoring side walls) is;
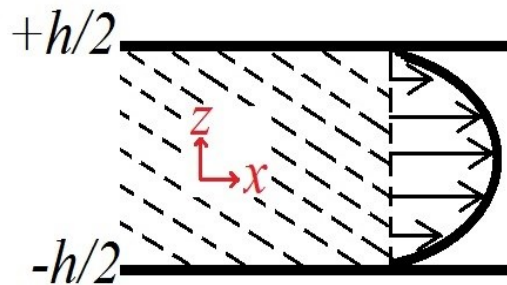
Fig. 2.18   *Viscous Force*

For closed top micro channel:

$$f_{visc}^{c} = -\frac{12\,\eta\,x}{\varepsilon\,\zeta_{c}(\varepsilon)}\left(\frac{dx}{dt}\right) \tag{2.36}$$

and for open top micro channel (Brody et al.,1996; Ichikawa et al., 2004), it comes out to be:

$$f_{visc}^{o} = -\frac{3\,\eta\,x}{\varepsilon\,\zeta_{o}(\varepsilon)}\left(\frac{dx}{dt}\right) \tag{2.37}$$

where ε is aspect ratio i.e. h/w and $\zeta_{c}(\varepsilon)$ and $\zeta_{o}(\varepsilon)$ are the aspect ratio functions for closed and open channels respectively. With aspect ratio in the range ε=0.0 to 2.0 (Ouali et al. , 2013) these functions are given as;

$$\zeta_{c}^{-1}(\varepsilon) \approx 1 + 0.362374\;\;\varepsilon + 1.020980\;\;\varepsilon^{2} \tag{2.38}$$

and,

$$\zeta_{o}^{-1}(\varepsilon) \approx 1 + 0.671004\;\;\varepsilon + 4.169711\;\;\varepsilon^{2} \tag{2.39}$$

2.9.4   Bousanquet Solution for Rectangular Channel

For Closed Top Channel:

Bosanquet solution can be derived by neglecting gravitational force in eq. (2.28) and writing as time derivatives of x^2, we get

$$\rho\frac{d}{dt}\left(x\frac{dx}{dt}\right) = \frac{2\gamma_{LV}}{h}\left[\cos\,\theta_{W}^{T} + \cos\,\theta_{W}^{B} + \varepsilon\left(\cos\,\theta_{W}^{L} + \cos\,\theta_{W}^{R}\right)\right] - \frac{12\,\eta\,x}{\varepsilon\,\zeta_{c}(\varepsilon)}\left(\frac{dx}{dt}\right) \tag{2.40}$$

By comparing the above eq. (2.40) to Bousanquet defining equation (2.24) gives,

$$a = \frac{12\,\eta}{\rho\,h^{2}\zeta_{c}(\varepsilon)} \tag{2.41}$$

and
$$b = \frac{\gamma_{LV}}{\rho h}\left[\cos\,\theta_{W}^{T} + \cos\,\theta_{W}^{B} + \varepsilon\left(\cos\,\theta_{W}^{L} + \cos\,\theta_{W}^{R}\right)\right] \tag{2.42}$$

<u>For Open Top Channel</u>**:**

Similarly, in the absence of gravity and writing as time derivatives of x^2, the eq. (2.30b) gives,

$$\frac{1}{2}\frac{d}{dt}\left(\frac{dx}{dt}^2\right) = \frac{\gamma_{LV}}{\rho h}\left[-1 + \cos\theta_w^B + \varepsilon\left(\cos\theta_w^L + \cos\theta_w^R\right)\right] - \frac{12\,\eta x}{\varepsilon\zeta_o(\varepsilon)}\left(\frac{dx}{dt}\right) \quad (2.43)$$

Comparing the above eq. (2.43) to Bousanquet defining equation (2.24)

$$\frac{1}{2}\frac{d}{dt}\left(\frac{dx}{dt}^2\right) = b - \frac{a}{2}\frac{dx}{dt}^2$$

gives

$$a = \frac{3\eta}{\rho h^2 \zeta_o(\varepsilon)} \quad (2.44)$$

and $\qquad b = \frac{\gamma_{LV}}{\rho h}\left[-1 + \cos\theta_w^B + \varepsilon\left(\cos\theta_w^L + \cos\theta_w^R\right)\right] \quad (2.45)$

2.9.5   Dimensionless Equations

The general equation describing capillary-driven imbibition for capillaries of any shape and dimensions held at any angle φ to the horizontal is given as,

$$\frac{1}{2}\frac{d}{dt}\left(\frac{dx}{dt}^2\right) = b - g\sin\varphi\,x - ax\left(\frac{dx}{dt}\right) \quad (2.46)$$

To obtain a dimensionless form of eq. (2.46) in order to minimize the complexity by reducing the various parameters, rescaling the position $x(t)$ and time coordinates t using $\quad T = at \quad$ and $\quad X = \frac{a}{\sqrt{2b}}x \quad$ gives;

$$\left(\frac{d^2X}{dT^2}\right) = 1 - G\sin\varphi X - \left(\frac{dX}{dT}^2\right) \quad (2.47)$$

where a dimensionless constant is defined as $G = \frac{g}{a}\sqrt{\frac{2}{b}}$. Bousanquet eq. (2.25) in terms of dimensionless equation is given by;

$$X^2(T) = T - [1 - \exp(-T)] \tag{2.48}$$

2.9.6 Visco-Gravitational Solution

When $T \gg 1$, the inertial term can be ignored, but gravity cannot be neglected, eq. (2.28) becomes,

$$0 = 1 - G \sin \varphi X - \left(\frac{dX}{dT}\right)^2 \tag{2.49}$$

As shown by Washburn (1921), and discussed by Fries and Deyer (2008b) (see also Mumley et al., 1986 and Krotov and Rusanov, 1999), this has an analytical solution, but for time as function of position rather than for position as a function of time. By rearranging eq. (2.49) to,

$$\frac{2X}{1 - G \sin \varphi X}\left(\frac{dX}{dT}\right) = 1 \tag{2.50}$$

an exact integration can be performed to get the visco-gravitational solution,

$$T = \frac{-2}{(G \sin \varphi)^2}[G \sin \varphi X + \log(1 - G \sin \varphi X)] \tag{2.51}$$

where $X=0$ at $T=0$ has been assumed. When $G \sin \varphi \to 0$, the $\log(1 - G \sin \varphi X)$ can be expanded and this gives $T \approx X^2$, which is the *Lucas-Washburn solution*. As $G \sin \varphi \to 1$, the logarithm diverges so that $T \to \infty$ and so at equilibrium the capillary rise height is $X_e = \frac{1}{G \sin \varphi}$, i.e. $x_e = \frac{b}{g \sin \varphi}$. Eq. (2.51) can be rewritten in terms of x and t as

$$t = -\frac{ab}{(g \sin \varphi)^2}\left(\frac{x}{x_e} + \ln\left(1 - \frac{x}{x_e}\right)\right) \tag{2.52}$$

In fitting experimental data for imbibition into vertical channels ($\varphi = 90^\circ$) the viscous-gravitational solution (eq. (2.51) or eq. (2.52)) can be used provided data is captured including both the early Lucas-Washburn stage $T \approx X^2$ and the approach to equilibrium as determined by $x_e \to \dfrac{b}{g}$. Eq. (2.52) is the analytical solution with time as a function of position.

2.9.7 The Viscous Coefficient '*a*' and The Capillary Coefficient '*b*'

For plane micro channels with smooth surfaces and the same contact angle on all surfaces $\theta_e^T = \theta_e^B = \theta_e^L = \theta_e^R = \theta_e$, roughness factor for all surfaces is taken as 1 (i.e. $r_T = r_B = r_L = r_R = 1$), the free surface vapor boundary in case of open top channels acts as a perfect hydrophobic surface (i.e. $\theta_e^T = 180^\circ$).

The viscous coefficient for circular tube, closed and open top plane channel is given as;

$$a = \begin{cases} 8\eta \big/ \rho R^2 \\ 12\,\eta \big/ \rho h^2 \zeta_c(\varepsilon) \\ 3\eta \big/ \rho h^2 \zeta_o(\varepsilon) \end{cases} \qquad (2.53)$$

Similarly the capillary coefficient **b** has dimensions of speed^2 (m^{2}s^{-2}) and for the circular tube, closed and open top plane channels is given as;

$$b = \begin{cases} 2\gamma_{LV}\cos\theta_e \big/ \rho R \\ 2\gamma_{LV}\cos\theta_e (1+\varepsilon) \big/ \rho h \\ \gamma_{LV}\left[\cos\theta_e (1+2\varepsilon) - 1\right] \big/ \rho h \end{cases} \qquad (2.54)$$

If the two side walls have the same Wenzel contact angles on the left hand side and right hand side walls (due to same roughness and surface chemistry), i.e. $\cos\theta_w^L = \cos\theta_w^R = \cos\theta_w^S$, then this alters the definition of the *b* parameter in the formula given by eq. (2.52). This makes the capillary co-efficient for closed and open top rough channel as;

$$b = \begin{cases} \dfrac{2\gamma_{LV}}{\rho h}\left[\cos\theta_e + \varepsilon\cos\theta_w^S\right] \\[4mm] \dfrac{\gamma_{LV}}{\rho h}\left[-1 + \cos\theta_e^B + 2\varepsilon\cos\theta_w^S\right] \end{cases} \tag{2.55}$$

2.9.8 Cross-Over Timescales

Numerically, the initial rise height is best described by the Bousanquet solution (eq. 2.20) until it crosses over with the visco-gravitational solution (eq. 2.52). Above this cross-over time, the visco-gravitational solution ever more closely agrees with the exact numerical solution as the rise height tends to its equilibrium value (Ouali et al., 2013). The cross-over time, T_C, can be calculated numerically as a function of $G\sin\varphi$ by equating the Bousanquet solution (eq. 2.20) to the visco-gravitational solution (eq. 2.52) and is given by the formula $T_C \approx \left(\dfrac{3X_e}{2}\right)^{2/3}$ in which X_e is proportional to equilibrium rise height, i.e. $x_e = \dfrac{b}{g}$. Hence, capillary rise can be described best by Bousanquet solution for time $T_C < \dfrac{1}{a}$ and for time $T_C \gg \dfrac{1}{a}$, visco-gravitational solution is best analytical approximation to the data that agrees very well with exact numerical solution. The data can be fitted accurately (to within 5%) using both solutions. For capillary rise heights significantly below the equilibrium height, this cross-over time is

$$T_C \approx \left(\frac{3X_e}{2}\right)^{2/3} \tag{2.56}$$

and has an associated dimensionless crossover rise height

$$X_C \approx \left(\frac{3X_e}{2}\right)^{1/3} \tag{2.57}$$

where $X_e = \dfrac{1}{G}$ is the dimensionless equilibrium rise height and G is a dimensionless form of the acceleration due to gravity.

Fig. 2.19 shows the behaviour of $X(T)$ as a fraction of the equilibrium height, X_e, for $G = 0.1$ and $\varphi = 90^o$ together with the, Bousanquet, Lucas-Washburn and inertial approximations.
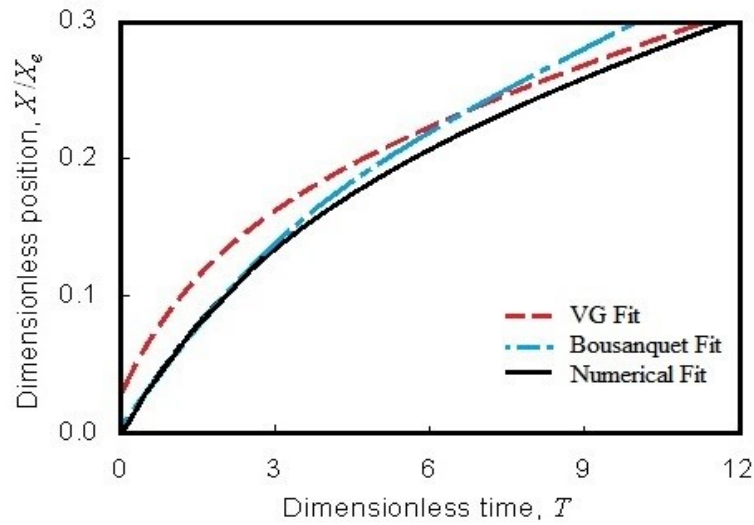
Fig. 2.19   *Comparison of approximate analytical solutions for Bousanquet [Blue line (- ---- -)] and visco-gravitational [Red line (-- --)] to the exact numerical solution (Black solid line) for G = 0.1 and $\varphi = 90^{o}$. The capillary rise height X is shown as a fraction of the equilibrium rise height, X_e (Ouali et al., 2013).*

2.10   Fitting Procedure in Excel and Mathematica®

Visco-gravitational fitting in Excel:

The visco-gravitational equation gives the analytical solution. Assuming the data is described by the visco-gravitational equation for vertical capillaries, (recalling eq. 2.52)

$$t = -\frac{ab}{g^2}\left(\frac{x}{x_e} + \ln\left(1 - \frac{x}{x_e}\right)\right) \tag{2.52}$$

Using $x_e = \frac{b}{g}$, the above equation becomes,

$$t = -\frac{ab}{g^2}\left(\frac{xg}{b} + \ln\left(1 - \frac{xg}{b}\right)\right) \tag{2.58}$$

Although this equation cannot be easily inverted to give position as a function of measured time, however, it does allow fitting of data by fitting time as a function of measured position. It can be fitted in principal using two fitting parameters *a* (the viscous term) and *b* (the capillary term), however, fitting the data at the very early

34

stages of imbibition was found to be sensitive to the initial time offset parameter t_o which was, in practice, found to be less than one to, occasionally, two measurement time intervals. For each measurement, the variation of the position of the meniscus with time was fitted to the analytical solution (eq. 2.52) within Microsoft Excel's add in 'Solver' using three fitting parameters, (a, b and t_o). The above eq. (2.58) can be written in the form of fitting parameters as,

$$t_{fit}(x) = -\frac{ab}{g^2}\left(\frac{xg}{b} + \ln\left(1 - \frac{xg}{b}\right)\right) - t_o \tag{2.59}$$

The fitting has to take a table of data for *(x, t)* and find the three parameters, which best allow eq. (2.38) to fit the data. The objective error function that is minimised is,

$$S_e = \frac{1}{N}\sum_{all\ pts}\left(t(x) - t_{fit}(x)\right)^2 \tag{2.60}$$

where N= number of points. For each value of measured position *x*, the $t_{fit}(x)$ values are calculated from eq. (2.57). In all fits, a constant contact angle $\theta_e = 0°$ for PDMS was assumed, and for the open rectangular channels data analysis was restricted to the part of the experiment during which the wetting fingers remained in the channels.

Numerical Fitting in Mathematica®:

In a similar way as in Excel, for each measurement, the variation of the position of the meniscus with time was fitted to the exact numerical solution (eq. 2.20) within Mathematica® (Wolfram research) using three fitting parameters, (a, b and t_o), where the viscous coefficient *a* and the capillary coefficient *b* are defined by Eq. (2.53) and Eq. (2.55), respectively.

2.11 Capillary Fingers

In hemi-wicking, the simplest viewpoint remains a capillary-driven penetration with a leading edge meniscus advancing in a tube/slab-like manner. However, the actual solid-liquid-vapor interface at the leading meniscus can be far more complicated as is known for capillary rise in square cross-section tubes, where the rise of a central

meniscus is preceded by liquid fingers rising up the four internal edges. This reduces the equilibrium meniscus height by a factor of $\frac{\left(2 + \pi^{1/2}\right)}{4}$ (Dong and Chatzis, 1995; Bico and Quéré, 2002). These effects are due to the wetting effects in corners and edges (Concus and Finn, 1969; Ransohoff and Radke, 1988; Ramé and Weislogel, 2009, Girardo et al., 2009, 2012). Most recently, Ponomarenko et al. (2011) have studied the capillary rise of wetting liquids in the corners of different geometries and shown that in the viscous dominated regime the meniscus of these fingers rises without limit following a universal time$^{1/3}$ law, in contrast to the Lucas-Washburn time$^{1/2}$ law which eventually saturates at an equilibrium height. These geometry induced wetting effects can be expected to impact both on capillary rise and imbibition in microfluidic channels with non-circular cross-sections. There is therefore a need to study capillary-driven imbibition and rise within rectangular cross-section channels and with open and closed boundaries.

In the next section 2.11.1, the sensitivity of imbibition for open rectangular channels to the value of contact angle and the limitations of this approach is discussed when corner filling along edges between walls due to wetting is taken into account.

It has been observed that capillary rise in rectangular channels using PDMS oils involves a rising central meniscus, but with thin fingers spreading in advance of this main rise along the inside corner edges qualitatively consistent with the type of behaviour described in Ponomarenko et al. (2011). The extent of advance of the fingers is sufficient to completely exit the channels in the experimental setup described in section 3.6.

2.11.1 Filling Conditions and Capillary Fingers:

According to the approach in section 2.9, for capillary-driven imbibition to commence it has to be energetically favourable for the liquid to enter the channel, i.e. the capillary force in eq. (2.31) must satisfy $f_{cap} > 0$ and the b parameter in eq. (2.42) must be positive. Thus, for an open or closed rectangular channel,

$$\cos \theta_e^B + \cos \theta_e^T + \varepsilon\left(\cos \theta_e^L + \cos \theta_e^R\right) > 0 \qquad (2.61)$$

For a closed channel with smooth surfaces and the same contact angle on all surfaces this simply means the contact angle must be less than 90°. However, for an open rectangular channel $\theta_e^T = 180°$ and so the condition becomes,

$$\cos \theta_e > \frac{1}{1 + 2\varepsilon} \qquad (2.62)$$

as noted by previous authors (Dong and Chatzis, 1995; Bico and Quéré, 2002). Therefore as the aspect ratio of a rectangular channel reduces imbibition becomes increasingly difficult and lower contact angles corresponding to more wetting liquids are required. For example, aspect ratios of $\varepsilon = 10$, 0.6, 0.3 and 0.2 require contact angles below 78.5°, 63.0°, 51.3° and 44.4°. Effectively the capillary pull required is principally from the wall area which becomes relatively less as the width of channel increases.
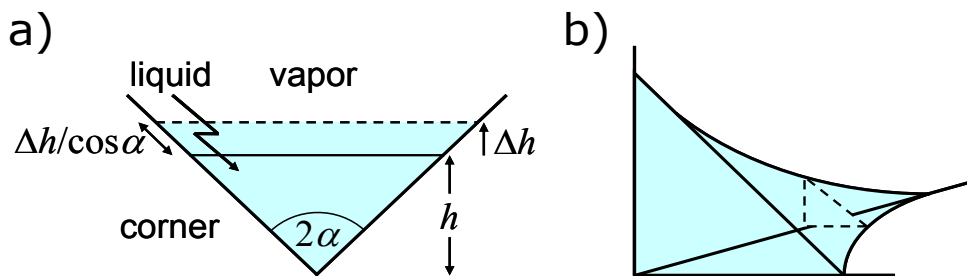

Fig. 2.20.   *Surface free energy changes as a tube/slab of liquid penetrates into a channel resulting in new solid-liquid and liquid-vapor interfaces. a) Two-dimensional corner viewpoint, and b) an edge viewed as a sequence of two dimensional corners.*

Rectangular and many other cross-sectional shape channels differ in their wetting properties from flat and smoothly circular surfaces, precisely because two walls meet at an angle. This effect, the corner filling condition, can be understood by a simple two-dimensional model. Consider two walls joining at an angle 2α with a liquid initially partially filling the corner to a depth h (Fig. 2.20a). When the corner fills with liquid by an additional amount Δh, the surface free energy change is given by,

$$\Delta F = 2\Delta h \left[\frac{(\gamma_{SL} - \gamma_{SV})}{\cos \alpha} + \gamma_{LV} \tan \alpha \right] = \frac{2\Delta h \gamma_{LV}}{\cos \alpha} [\sin \alpha - \cos \theta_e] \qquad (2.63)$$

where Young's law has been used to replace the combination of interfacial tensions by $\cos \theta_e$. Thus, the change in surface free energy is zero or negative whenever $\cos \theta_e \geq \sin \alpha$, which gives,

$$\alpha + \theta_e \leq 90^{\,o} \qquad (2.64)$$

as the corner filling condition. In the case of a flat surface, $\alpha = 90^{o}$ and a surface wets when the contact angle vanishes, and, in the case of parallel plates, $\alpha = 0^{o}$ and the surface wets between the plates whenever $\theta_e \leq 90^{\,o}$. Thus, eq. (2.61), which is the condition for imbibition assuming a tube of liquid advancing in a channel, must be considered alongside eq. (2.64).

Whilst this was a two-dimensional argument, an edge can be viewed as a sequence of two-dimensional corners (Fig. 2.20b) and so the same condition, eq. (2.64), will apply. For example, for the open rectangular channel the side walls meet the bottom surface at 90° so that the corner filling condition is $\theta_e \leq 45^{\,o}$, whereas eq. (2.62) suggests imbibition will only occur for channel aspect ratios, ε, larger than 0.207. Thus, fingers of liquid can imbibe into open channels at aspect ratios lower than might otherwise be expected. Bico and Quéré (2002) have shown that corner filling leads in square cross-section capillary tubes to fingers of liquid rising along the internal edges against gravity in advance of the central meniscus, which itself rises to an equilibrium height which is a factor $\dfrac{(2 + \pi^{1/2})}{4}$ less than would be the case without the fingers. Moreover, Ponomarenko et al. (2011) have recently used scaling arguments to show that in the viscous regime of capillary rise against gravity and independent of specifics

of the geometry the fingers spread faster than the main meniscus which follows a Lucas-Washburn law.

Thus, for good capillary-driven imbibition in open and closed rectangular channels with reduced sensitivity to the precise value of contact angle, eq. (2.61) implies it is better to use low contact angle liquids. However, doing so is likely to lead to increasingly stronger effects from liquid fingers spreading along the edges between walls at lower contact angles and higher intrusion rates. From the point of view of microfluidics and lab-on-a-chip, the consequences of this are potentially serious with fingers of liquid spontaneously spreading in advance of the bulk liquid and potentially causing contamination. An interesting question is whether the capillary-drive imbibition/rise in open and closed rectangular channels of the main meniscus can still be accurately described by eq. (2.48) and (2.51). The experimental consideration of this case is given in chapter 5.

3   Experimental Techniques

3.1 Introduction

Capillarity in circular and rectangular cross section closed glass tubes is studied. This phenomenon is also investigated in SU8 open top micro channels with various liquids having different viscosities. In order to perform these experiments open top micro channels are fabricated using photolithography. A photo mask is designed on AutoCAD and then ordered from JD Photo Tools Company. This photo mask has a specific design and its features can be transferred onto a SU8 layer to fabricate the desired patterned micro channels. In this chapter the experimental techniques are described; from designing photo masks to fabrication of open top SU8 micro channels using a photolithography. The experimental steps including cleaning process of samples, video microscopy setup, and the overview of how the videos are processed and data is collected to perform the analysis is also explained. This chapter also includes methods to measure viscosity, stylus profilometry to measure the exact dimensions of micro channels and scanning electron microscopy to get the detailed micro images of samples. Finally, the experimental design details are included to have an overview of the experiments being conducted.

3.2 Selection of Liquids and Substrate

Liquid: Polydimethylsiloxane (PDMS) Oils

PDMS oil is selected as a rising liquid in closed and open micro channels as it is very suitable liquid for well-controlled experiments due to the following reasons;
It is inert, non-toxic, non-polar and non-flammable. Its vapor pressure is quite low that is why it is non-volatile. Its viscosity depends very strongly on its molecular weight and decreases slowly with increasing temperature. Its surface tension is independent of its molecular weight. It is considered to be suitable due to its great thermal stability and optical transparency. PDMS makes very low contact angle with SU8 surface that makes it hydrophilic (de Gennes, Brochard-Wyart, & Que're, 2004).

Substrate: SU8

SU8 is a negative epoxy type photoresist. Its chemical resistance is quite excellent. Once it is cross-linked, it is very hard to reflow. It is suitable to make channels of desired aspect ratio (Chollet, 2013).

3.3   Designing the Photo Lithographic Masks on AutoCAD

In order to fabricate open top SU8 micro-channels, a number of photolithographic masks were designed on AutoCAD (v2011). These were in 2D AutoCAD design. The micro channels prepared from these photo masks have various widths and differently patterned or smooth walls. A plane walled channel has a roughness factor of 1. In order to create the "roughness" (i.e. additional surface area) effect, the walls of the channels may have different shapes or patterns. A roughness effect on the walls was created in the form of triangular and saw-tooth shapes.

3.2.1   Average Channel Width

Channel width is taken from the middle of the triangular or saw-tooth step to the plane wall if it has one patterned and one smooth wall. If both walls of the channels are patterned, then the average width for the shaped walled channel is taken to be the distance between the middle of the steps of both walls. The average width ensures average cross-section for a constant flow of liquid into micro channels. The following Fig. 3.1 indicates how to take the width of channels having one or both walls patterned and also for the plane channel.
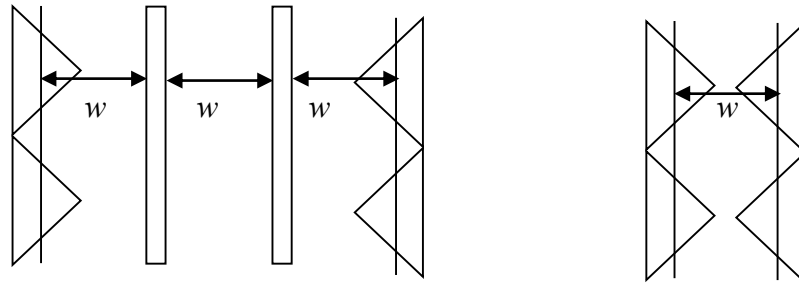
Fig. 3.1   *Average width for the shaped walled channel is taken from the middle of the steps as shown above*

3.2.2   Roughness Factor

The channel walls fabricated from the photo mask were shaped to achieve variable roughness factors and the shape of these steps was kept to be symmetric (Fig. 3.2). By symmetry it is meant that in all the steps, say in a triangular patterned walled channel, the length of the base of the triangle ℓ_B is kept the same in all the steps

in all channels and the walls of a particular channel have identical triangular or saw-tooth steps. The other two side lengths ℓ_L and ℓ_R were kept the same to get one particular roughness factor i.e. $\ell_L = \ell_R = \ell$. In order to achieve different roughness factors, ℓ can be changed accordingly. The roughness factor is calculated using the following relation;

$$r = (\ell_L + \ell_R) / \ell_B$$

$$= 2\ell / \ell_B$$

Fig. 3.2   *Steps of one of the walls of the sample channel*

Similar formula are used to achieve various roughness factors in saw-toothed walled channels. The roughness factors of the channels were changed by altering the length of the sides ℓ_L and $\ell_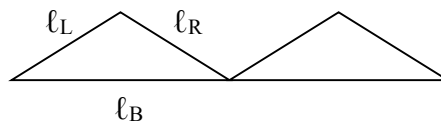L$ (or simply ℓ) of the steps in different walls. The photo masks were prepared by JD Photo Tools Company. These were quartz chrome and soda lime chrome with super high resolution and the size of the masks was 5" x 0.090". These were prepared after CAD processing from DXF data. The following are the brief description of the photo masks to prepare micro-channels of various widths, lengths and roughness factors.

3.4   Photo Masks

A number of photo masks were designed to fabricate various types of SU8 open top micro channels having varying widths and features

3.4.1   Photo Mask 1

A photo lithographic mask was designed on AutoCAD for making open top plane SU8 micro-channels having width from 150 to 400µm. It contained different sets of parallel channels design. One set of these plane parallel channels had all parallel channels of same width, while the other set contained parallel channels with gradually increasing width. An overview of the mask is shown in Fig. 3.3
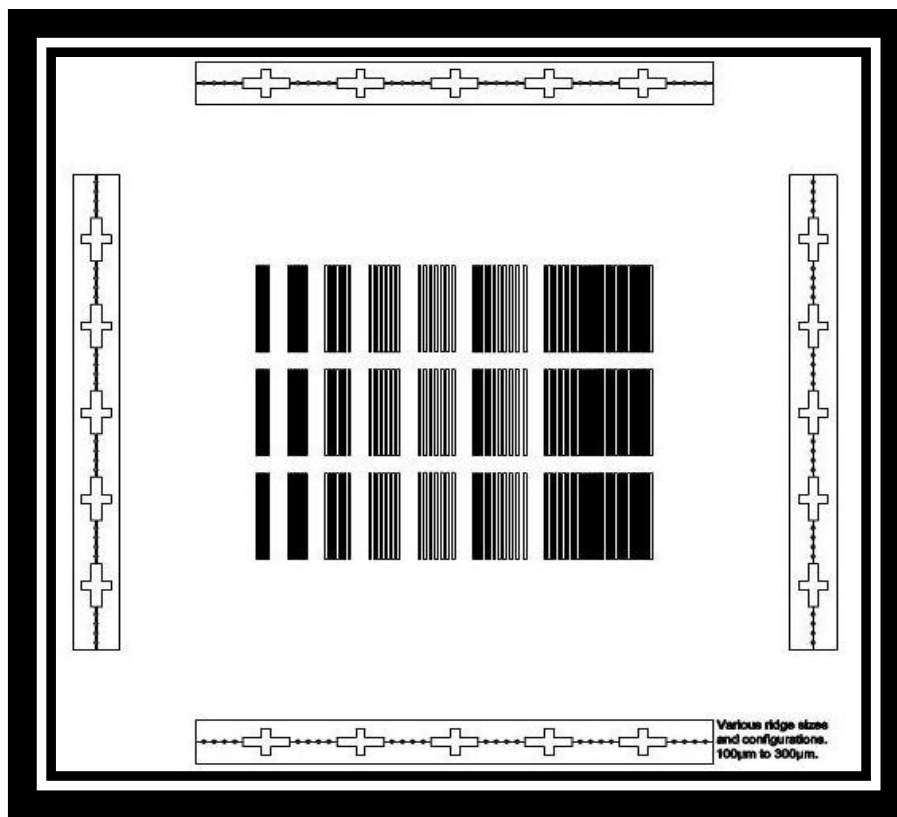
Fig. 3.3   *An overview of photo mask 1*

The channels prepared from the above mask were plane parallel channels of various widths (150 to 400µm). The AutoCAD design is shown in Fig. 3.4
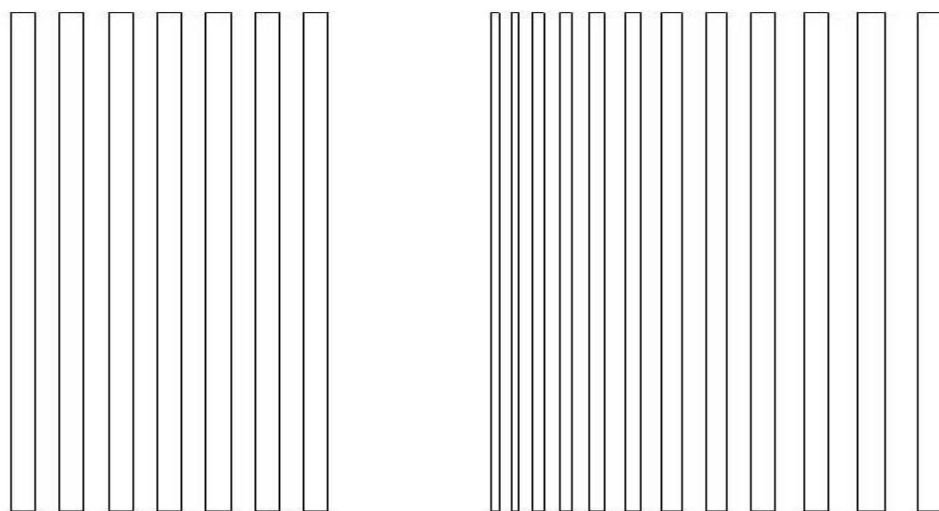

Fig. 3.4   *Plane SU8 Channel design having same and gradually increasing width*

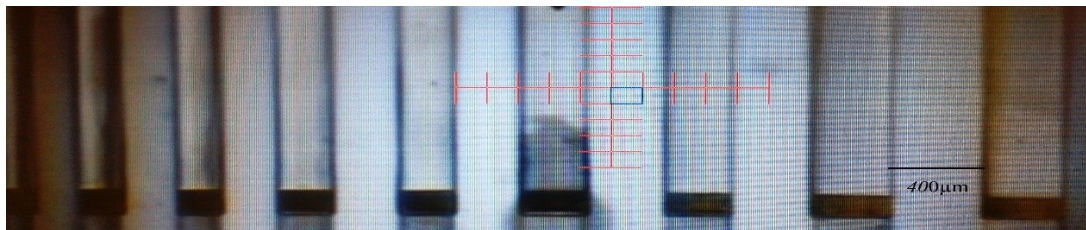Micro channels when fabricated using this mask are shown in fig. 3.5

Fig. 3.5   *Image of sample having plane channels with gradually increasing width*

3.4.2   Photo Mask 2

Another photolithographic mask was designed on AutoCAD for making open top SU8 micro-channels having width from 80 to 320μm. It contained different sets of parallel channels design. One of such sets had the following features; It is designed to get parallel channels such that one channel which is in the middle has both walls plane the other channels at the either sides of this channel has one plane and one shaped wall. The shape of the wall consisted of triangular steps which gradually varied in different channels such that the vertex angle of the triangle was changed. Another type of the set of parallel channels fabricated by this mask was such that the other channels at the either sides of the plane channel have both walls shaped. The design of the mask was such that it can be used to fabricate SU8 open channels which consist of a set of parallel channels. The middle one had two plane walls. The other channels at either side of middle channel had one plane and one shaped wall. But the shaped sides of both channels were different from each other. One of the sample channels made by this mask is shown below in Fig. 3.6.
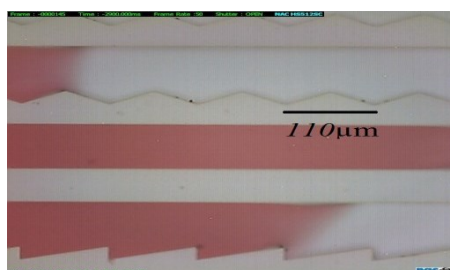

Fig. 3.6   *Open channels viewed from above. Three parallel micro-channels fabricated by using mask 2. Ethylene glycol with red food dye (2-naphthalenesulfonic acid disodium 0.1ml in 50ml ethylene glycol) is flowing in the channels.*

The average width of the channels within one set of parallel channels was kept the same.

3.4.3   Photo Mask 3

A photo mask was designed such that the parallel channels fabricated by it have similar shape but different width, and same average width but different shape. It needs to be the exact copy of the features required to be fabricated on the micro channels. There are two variables in the shape and geometry of the micro-channels fabricated by this mask, which are; <u>width of the channels</u>, and <u>roughness factors</u> of the walls. Three parallel channels are designed for comparison: one of these has both walls plane, and the other two channels at either side of the plane channel have one plane and one zigzag (saw tooth) shaped wall having different roughness factors. One set of parallel channels is shown in Fig. 3.7 below. The average width of these three channels was kept the same. One set of the parallel channels are as shown below. Two channels having only one shaped wall at either side of a plane channel (the one having both walls plane). Five sets in this pattern are designed having gradually increasing roughness factors.
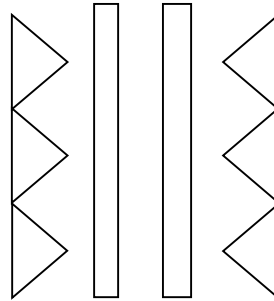
Fig. 3.7   *Three Parallel Channels having same width with roughness factor of 1.4*

Another type of set of the parallel channels has two channels having both walls shaped at either side of a plane channel (the one having both walls plane). Five sets in this pattern are designed having gradually increasing roughness factors.

Shown in Fig. 3.8 is an example of in-phase channels in which vertex of one step faces the vertex of opposite wall's step.
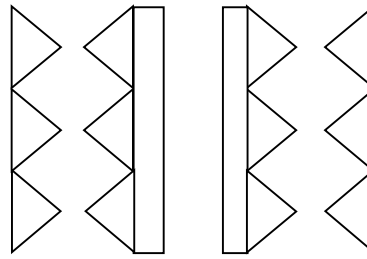
Fig. 3.8   *One plane channel in between two in-phase channels*

And the example of out of phase channels are shown in Fig. 3.9 arranged in the same pattern as in Fig. 3.8
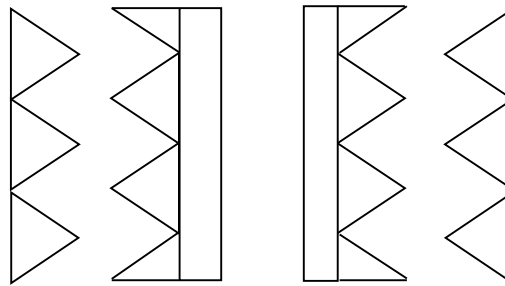
Fig. 3.9 *One plane channel in between two out of phase channels*

Again, the average width of all the channels in a single set is kept the same. An overview of mask 3 is shown in Fig 3.10
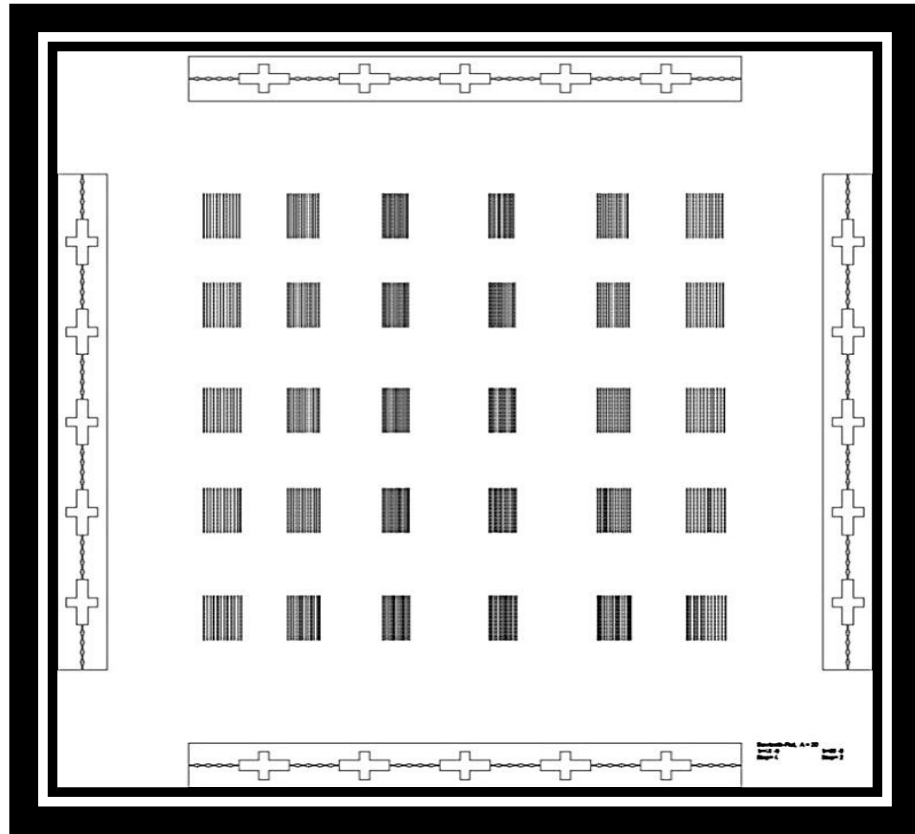
Fig. 3.10 *A (5″ x 0.090″) Chrome mask with super high resolution prepared after CAD processing from DXF data*

One of the sample channels fabricated from mask 3 is shown in Fig. 3.11
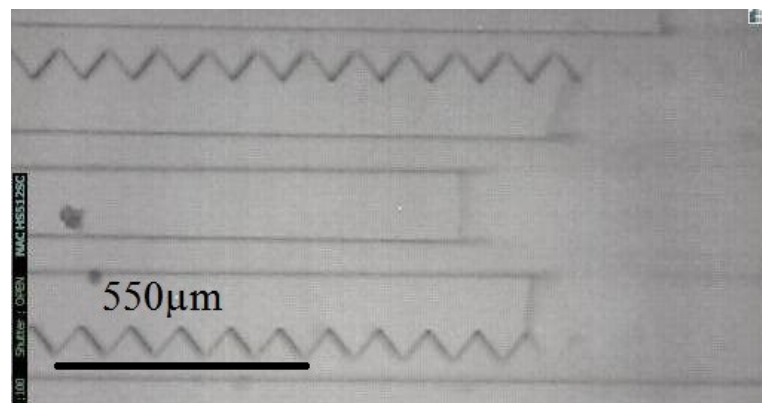
Fig. 3.11 *Sample channels prepared using mask 3*

3.4.4 Photo Masks 4 and 5

These were designed for fabricating SU8 open top micro-channels having the length L of 10mm, Roughness factors r = 1, 1.2, 1.4, 1.6 & 3, and the width, w = 400 and 600μm. These photo masks were designed to prepare the channels having in-phase and out-of-phase triangular steps and saw-tooth steps to create roughness effect on both walls of the channels. A closer look to the features of (a) triangular in-phase, (b) triangular out-of-phase and (c) saw-tooth steps is shown below in Fig 3.12
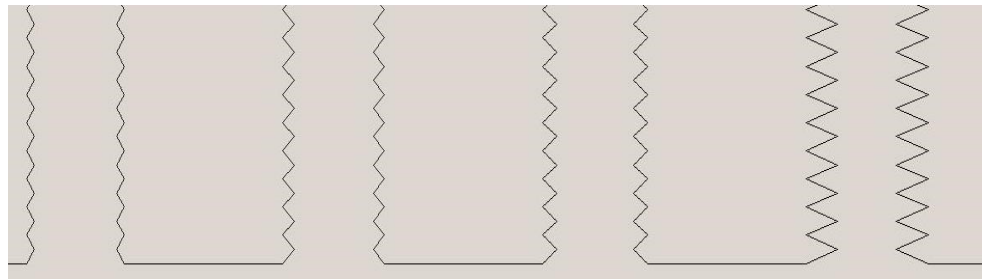
(a)
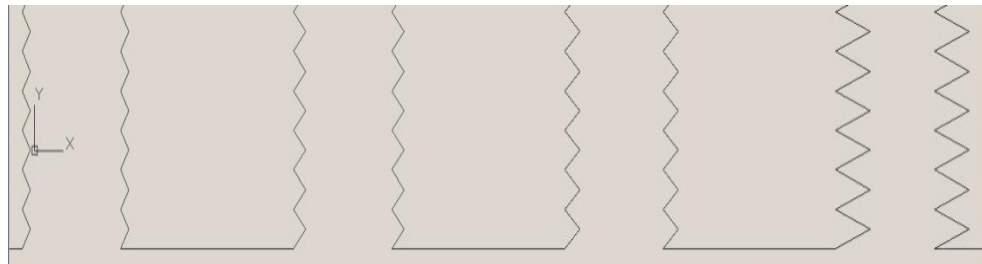
(b)
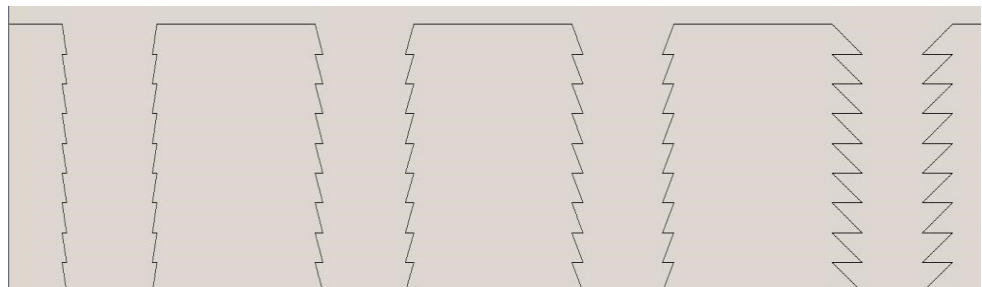
(c)

Fig. 3.12 *Roughness features (a) triangular in-phase, (b) triangular out-of-phase and (c) saw-tooth steps*

An overview of photo mask to prepare 400µm wide rough channels is shown in Fig. 3.13
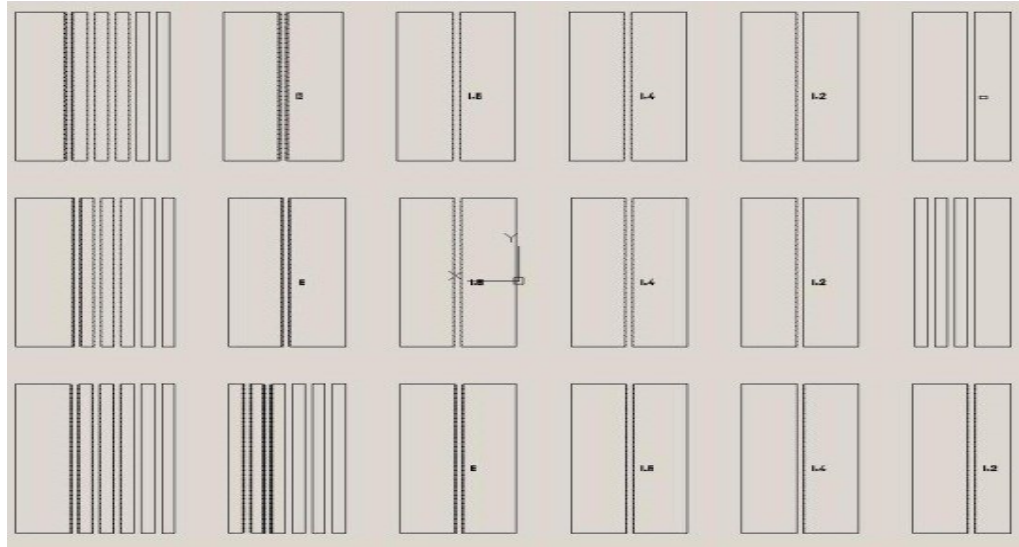
Fig. 3.13   *Overview of masks to prepare 400µm wide rough channels*

3.4.5   Photo Mask 6

To have longer micro channels, this photo mask was designed to fabricate SU8 open top micro-channels having the length, $L = 50mm$, the roughness factors, $r = 1, 1.5, 2 \& 2.5$, and the width, $w = 400 \& 600µm$. This photo mask was designed to prepare the channels having in-phase triangular steps to create roughness effect on both walls of the channels. An overview of this photo mask is shown in Fig. 3.14
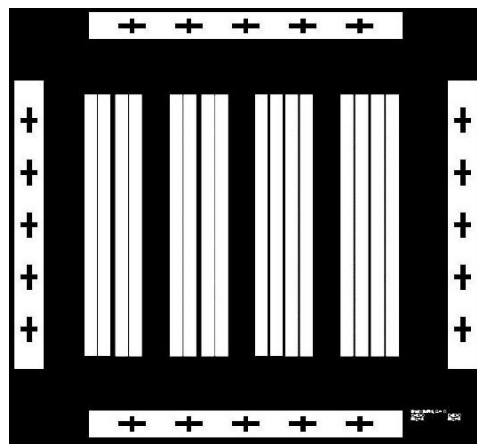
Fig. 3.14   *An overview of mask 6 to prepare 400 and 600µm wide rough open top micro channels*

3.4.6 Photo Masks 7 and 8

Photo masks 7 and 8 were designed for fabricating 400μm and 600μm wide SU8 open top micro-channels respectively having Length L = 10mm and the roughness factors r = 1.0, 1.2, 1.4, 1.6, 1.8, 2.0, 2.2, 2.4. 2.6, 2.8 and 3.0. These masks were designed to prepare the channels having in-phase triangular steps to create roughness effect on both walls of the channels. An overview of one of the photo masks (mask 8) is shown in Fig. 3.15 below which is used to prepare 600μm wide rough channels.
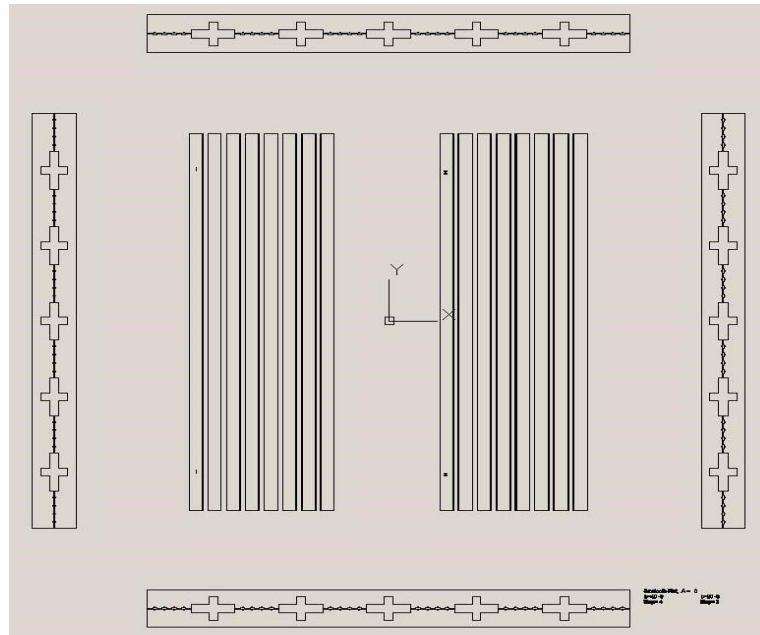
Fig. 3.15   *An overview of mask 7 to prepare 600μm wide rough channels*

Fig. 3.16 shows the image of sample channels prepared using mask 8
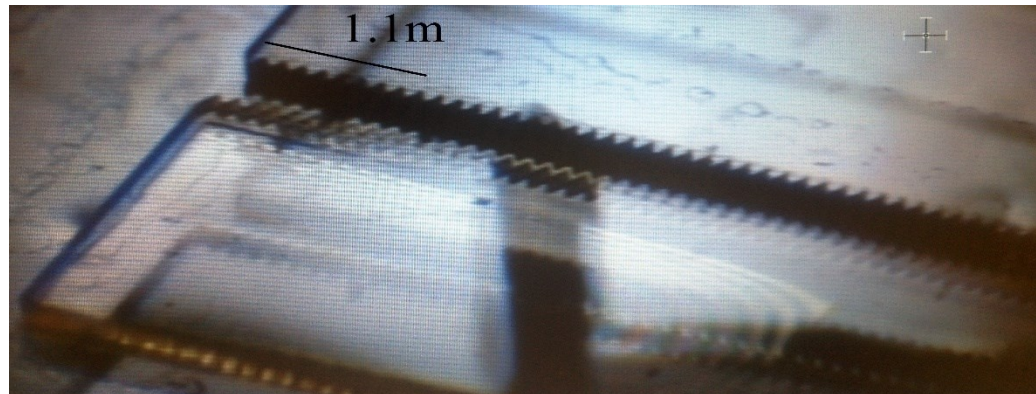
Fig. 3.16   *Image of sample channel with both walls patterned*

3.5   Fabrication of Sample Micro-Channels

A number of sample micro channels were prepared using photo masks by photolithography to transfer the pattern from a mask to SU-8 coated glass. The dimensions of the glass slide serving as substrate taken depends on the size of the desired micro-channels. A 10 to 20 micron thick bottom layer of SU8-10 (SU8-10 MicroChem) is formed first, and then 70 to 350 microns thick layer of SU8-50 (SU8-50 MicroChem) or SU8-100 (SU8-100 MicroChem) is formed for the patterns of channels. The photo resist used were SU8-50, SU8-25 and SU8-10 on a glass slide to achieve different thickness. The apparatus used was ultrasonic bath, hot plate, spin coater and mask aligner all available in the clean room.

SU8 is an epoxy based negative photo resist. When it is exposed to UV rays and developed, its molecules are strongly cross-linked and insoluble to the liquid developers providing the desired structure of the channels. The developer used was 1-Methoxy-2-propyl acetate.

The process of fabrication of sample micro channels includes a number of steps (Fig. 3.17) namely;

I.   Cleaning Sample Glass Slides

II. Spin Coating

III. Pre-baking

IV. UV Exposure

V.   Post-exposure Baking

VI. Developing

VII. Rinsing & Drying
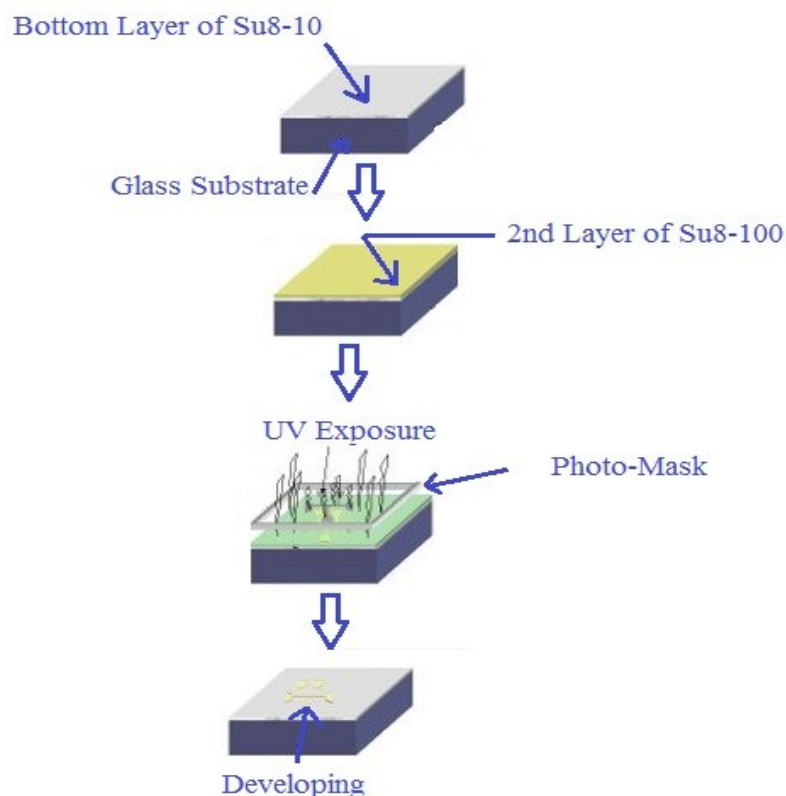
Fig. 3.17   *Schematic diagram to demonstrate photolithography*

These steps are briefly described below;

I.   Cleaning Sample Glass Slides

In the cleaning process, glass slides of various sizes were immersed in warm solutions of decreasing detergent (Decon R90 from Decon Laboratories Limited) concentrations from 5% to 0.5% in de-ionised water and were heated up to 60 $^{\circ}$C one after another and then placed into an ultrasonic bath for 10 minutes to remove dust and greasy particles. After taking out the glass sample from ultrasonic bath, it was dipped into isopropyl alcohol (IPA) at 40 $^{\circ}$C and then blow dried with N_2 to remove any traces of water.

II.   Spin Coating

The dried slides were subjected to spin coating with the negative photo resist polymer SU8. The speed and duration of rotation of the spin coater was varied in order

to get different thickness of the layer. The spin coater used was *WS-6505-6NPP/A2/AR2 from Laurell Technologies Corporation*. The coating procedure consisted of two stages;

Firstly, spun for 10 seconds at 500 rpm to remove any excess of negative photo resist, secondly, it was spun for 30 seconds at various rpm to get uniform layers of desired thickness of negative photo resist.

III.   Pre Baking

After spin coating, the sample was subjected to pre-heating on a hot plate in order to remove any part of the solvent contained in photo resist SU-8 at;

65 ^{O}C for 15-30 minutes, and

95 ^{O}C for 15-30 minutes

The sample was allowed to cool down for about half an hour before being exposed to UV radiation

IV.   UV Exposure

The sample was then exposed to a mask under UV radiation for various durations depending on what height of the channels is desired, in the mask aligner (Model MJ 54 from SUSS Microtec) using soft contact, e.g. for making the micro-channels having thickness of almost 140-350 microns, exposure is done from 45 to 90 seconds using filter when SU8-50 or SU8-100 is used for making layers on the glass substrate.

Similarly to get about 70 microns thickness exposure time is reduced to 30 to 35 seconds using a filter. The exposed energy of the aligner is 300 mJ/cm^2. The excessive radiations were filtered out to get better imaging results, i.e. straightest possible walls, which reduces the intensity of the radiation by 35% to 45%. In order to achieve more thickness, exposure time was increased accordingly.

V.   Post-exposure Baking

To cross-link the exposed parts of the SU8 layer, the sample is post-baked on a hot plate at 65 ^{O}C for 15-25 minutes, and at 95 ^{O}C for 30-90 minutes, and 110 ^{O}C for

15 minutes. The duration and range of temperatures of post-exposed baking (PEB) depends on the desired thickness of channel. The sample was allowed to cool down slowly on the same hot plate to avoid cracking and minimizing stress by turning it off.

VI.   Developing

After cooling down the samples for about two hours, these were immersed in the SU8 developer from 20 to 45 minutes (again depending on the desired thickness of the channel walls). It will reveal only the exposed features on the layer by cross linking those regions. All other regions are soluble to the developer.

VII.   Rinsing & Drying

The samples were then washed with isopropyl alcohol or acetone and blow dried with N_2 gas

In order to make the bottom layer of SU8 same process above is repeated except for two steps: the layer does not need to be exposed for so long and the use of the filter and the mask are not required as this should be very thin layer with no pattern. Also, it does not need to be developed separately. Then the whole process is repeated on the same sample to produce the shaped walls of the channels.

The following Table 3.1 gives the exact parameters used to achieve various thickness on the glass substrate.

Product	Thickness	Spin Speed	Pre-bake Time (min)		Post-bake Time (min)		UV Exposure Time	Developing Time
	(μm)	rpm	65 ^{O}C	95 ^{O}C	65 ^{O}C	95 ^{O}C	(sec)	(min)
SU8-10	20	6000	3	3	30	0	5	N/A
	45	3000	10	15	15	20	30	20
	100	2000	15	20	20	25	45	30
	300	1600	20	30	25	35	80	40
	350	1500	30	45	30	45	90	50

Table 3.1   Exact Parameters used for achieving various thickness of the channels.

3.6   Video Microscopy

Experiments were performed keeping the samples oriented vertically using polydimethylsiloxane (PDMS) oils (Dow Corning Xiameter PMX-200) of viscosities

55

η = 96.0, 48.0, 19.2 and 4.8 mPa s (±5%) and corresponding densities of 960, 950, 930 and 913 kg m^{-3} (DOW Corning Xiameter PMX-200 Data sheet) as the flowing liquid in micro channels. The sample was held vertically in front of the back light LCD. A high speed camera (NAC Hotshot 512SC) was placed horizontally to setup a video-microscope system capable of monitoring capillary flow at high speed from 50 to 1000 frames per second. The arrangement of experimental setup is shown in Fig. 3.18 below.
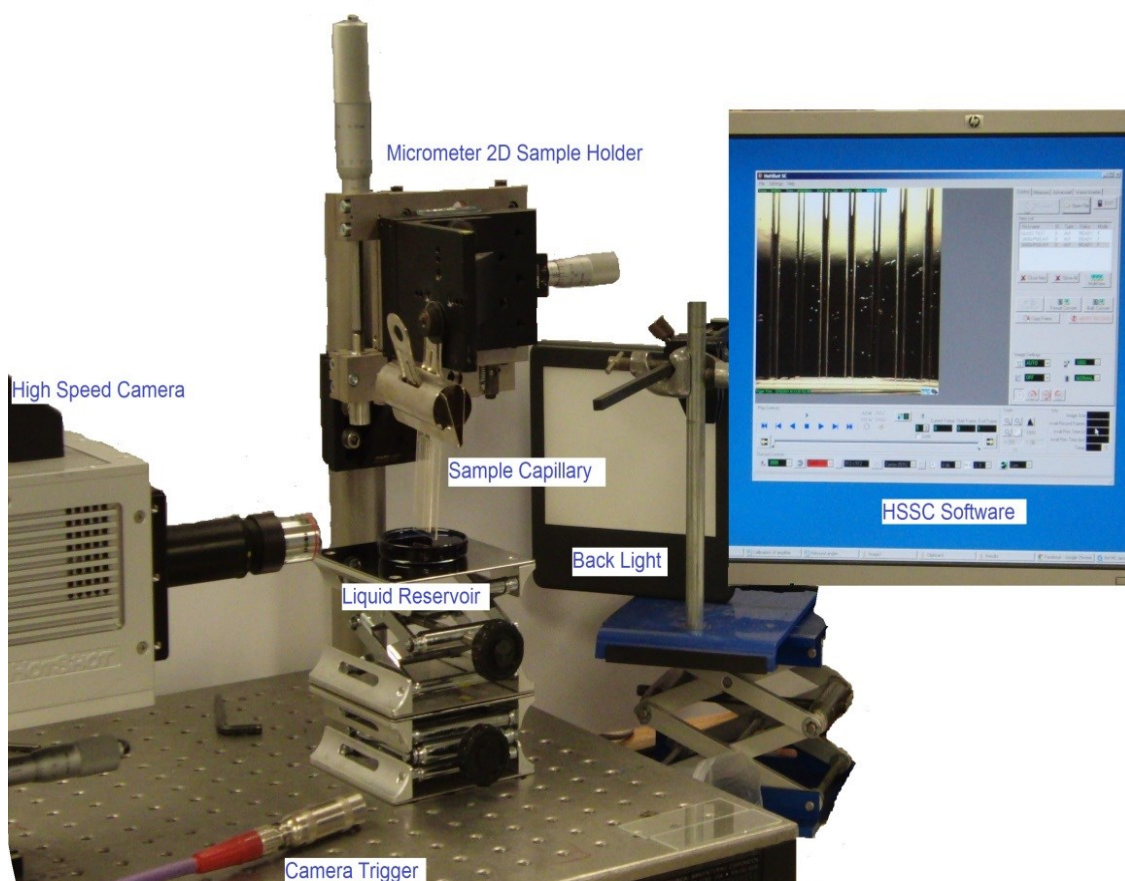
Fig. 3.18   *Experimental setup for vertically held samples*

A high resolution (X10) lens was used in the high speed camera. After getting the videos in hsf format, JPEG pictures were extracted from it using the software HSSC Link. These pictures were processed in *ImageJ* to make note of the position of interface of the liquid flowing at regular time intervals. In some of the experiments, red food colour is used as a dye to improve the visibility of the flowing liquid interface. The data is exported to Microsoft Excel work sheets for analysis of the results obtained.

3.7   Drop Shape Analysis (DSA)

In order to determine various parameters related to contact angle analysis such as equilibrium contact angle of liquid with the SU8 surface, advancing and receding contact angles while it spreads over the surface using its pure as well as dyed state, drop shape analysis (DSA) was used to approximate advancing and receding contact angles using tilt method. Fig. 3.19 shows (a) the approximate advancing and receding contact angles and (b) equilibrium angle while a drop of PDMS oil of viscosity 96 cSt is in contact with the surface of SU8. The range of the equilibrium contact angles was found to be 2º (±0.5º) on SU8.

(a)

(b)
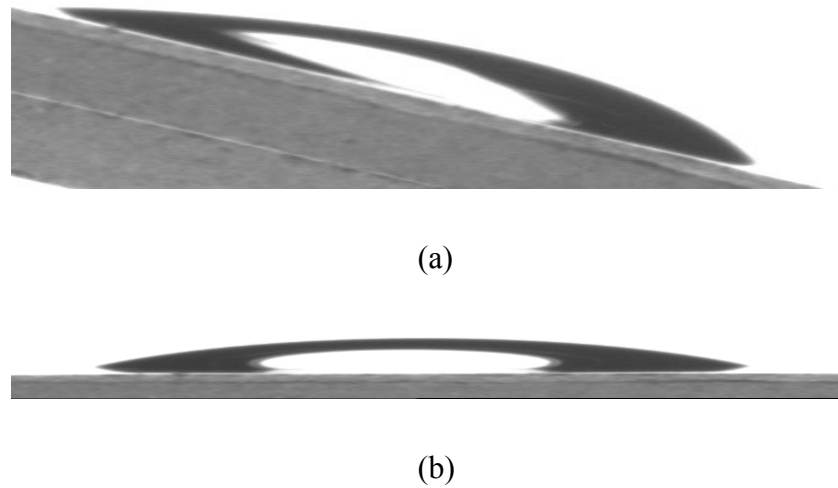
Fig. 3.19   *(a) Tilt method to approximate advancing and receding contact angles and (b) equilibrium contact angle of 96 cSt PDMS oil on SU8 using DSA*

3.8   Physical Properties of PDMS

The table below shows the properties of PDMS oil used as a rising liquid in SU8 microchannels.

Density (Kg/m^3)	960
Viscosity (mPas)	96, 48, 19.2 and 4.8
Surface Tension (N/m)	0.0198
Contact Angle	0º

Table 3.2   *Physical parameters of PDMS oil used*

3.9   Scanning Electron Microscope (SEM)

After performing experiments, the samples are scanned using a scanning electron microscope (SEM). Before scanning, the samples were gold coated in the gold coater to improve visibility of the pictures obtained by the SEM. The software used with the SEM is INCA and the resolution of picture is usually set at 512 x 400 pixels.

Fig. 3.20 shows the scanning results of rough open top micro channels with (a) 400μm and (b) shows a cross-sectional view of a round glass tube of diameter 1.33 (±0.03) mm.
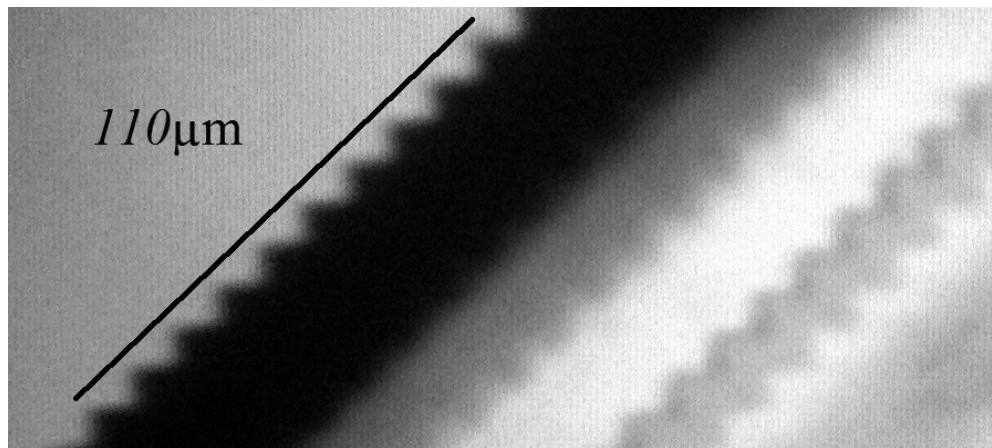
(a)
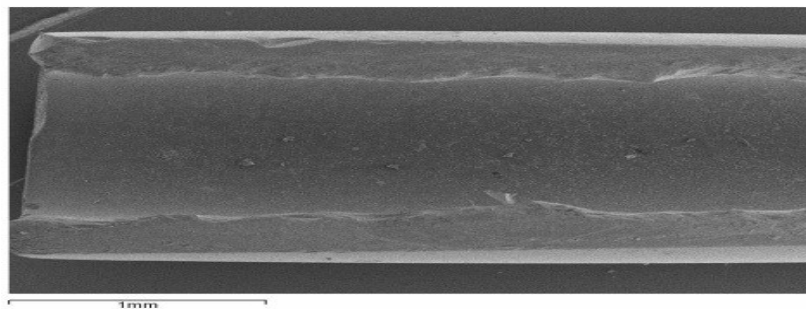
(b)

Fig. 3.20   *(a) Image of 400μm wide sample channel and (d) cross-sectional view of round glass tube of diameter 1.33mm from SEM at resolution 512 x 400 pixels using INCA software*

3.10   Profilometry

Two types of profilometer are used to determine various physical dimensions of the sample channels. The width and height of the channels were determined by *Stylus Profilometer* and *Optical Profilometer* is used to obtain 3D image of the channels. DEKTEK software is used with the stylus profilometer to measure width and thickness of the walls of the channels.

Fig. 3.21 shows the plot obtained from the DEKTEK software while using stylus profilometer to measure width and thickness of an open top micro channel of thickness 135μm and width 250μm.
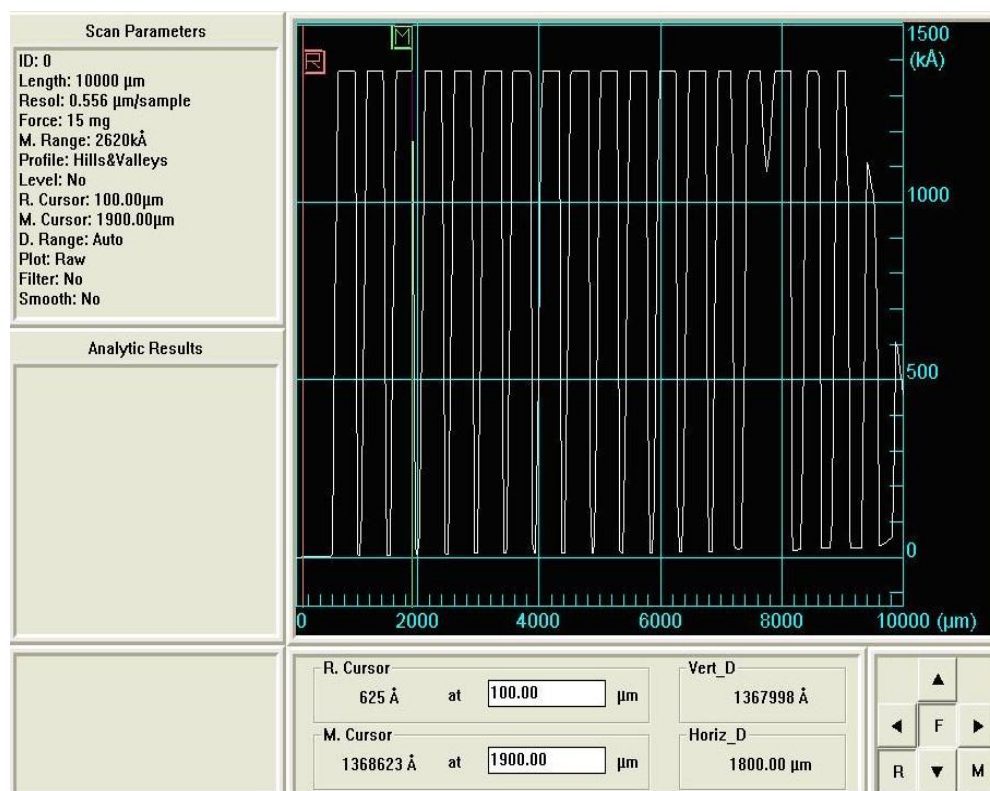
Fig. 3.21   *Thickness and width of a sample channel determined by DEKTEK stylus profilometer*

3.11   Measurement of Surface Tension of Liquids

Surface tension of ethylene glycol in pure state as well as with dye was determined using K6 Tensiometer (KRÜSS) (as shown in Fig. 3.22) which uses the ring method.

Ring Method:

The liquid is moved up until the ring comes in contact with the liquid surface. Then the liquid is moved down so that the liquid film produced under the ring is stretched. As the film is stretched a maximum force is experienced; this is recorded in the measurement. At the maximum the force vector is exactly parallel to the direction of motion; at this moment the contact angle θ is 0°.

The calculation is made according to the following equation:

$$\gamma = \frac{F_{max} - F_V}{L \cos \theta} \tag{3.1}$$

Here,

γ = surface or interfacial tension, F_{max} = maximum force,

F_V = weight of volume of liquid lifted, L = wetted length and

θ = contact angle

The contact angle θ decreases as the extension increases and has the value 0° at the point of maximum force.

Fig. 3.22   *K6 Tensiometer[www.kruss.de]*

3.11   Measurement of Viscosity of Liquids

A rotational viscometer was used to measure the viscosity of rising liquids. Its working is based on the fact that viscosity of a fluid is dependent on the torque needed to rotate an object in the fluid. Therefore, a disc at a constant speed is rotated in the fluid and the torque is measured. The gradient of the graph of shear stress (torque) against shear rate (angular velocity) is the measure of viscosity according to the following formula (recalling eq. 2.4a);

$$Shear\ Stress = \eta\ (Shear\ Rate) \tag{2.4a}$$

Fig. 3.25 is an example of measuring viscosity of pure PDMS and is given by the slope of the Shear Stress vs. Shear Rate graph which came out to be 19.16 ($\pm$1.5) mPas.

Fig. 3.25 *Slope of the shear stress vs. shear rate graph gives the viscosity of PDMS oil*

4   *Capillarity in Glass Tubes and Smooth Rectangular Channels*
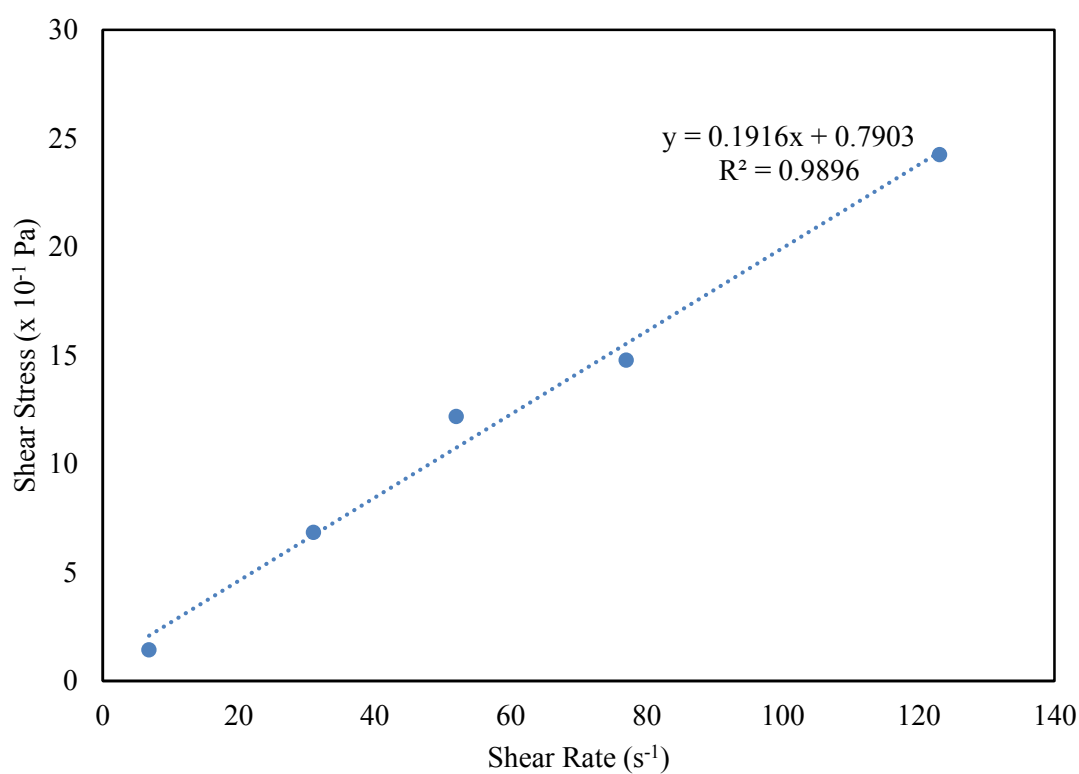
4.1 Introduction

Capillarity is very important for wide range of many applications; the examples are printing [Schoelkopf J et al., 2002], lab-on-chip [Brody et al., 1996; Squires and Quake, 2005], porous media [e.g. Marmur and Cohen, 1997; Siebold, 2000] and soil water repellency [Shirtcliffe et al, 2006]. The capillaries may be of any shape and size, e.g. in the form of circular or square glass tubes or micro-channels (usually of rectangular cross-section). These may be open top or closed top channels that are mounted either vertically or horizontally or at any angle to the horizontal.

In this chapter, a theory for capillary rise is tested experimentally in round and square glass tubes and rectangular cross-section open top plane micro-channels. The theory considers rigidified and non-rigidified boundary conditions for the liquid-vapour interfaces and the effects of surface topography assuming Wenzel and Cassie-Baxter states. This theory [Ouali et al., 2013] provides a relationship for the viscous friction associated with the rise in rectangular cross-section open top micro-channels as a function of aspect ratio. A cross-over time T_c was derived, and it was shown that below this cross-over time the Bousanquet solution was the best approximation and above this time the visco-gravitational solution provided the best approximation for capillary imbibition in the tubes and micro-channels with the dimensions being used in experiments; it also agrees very well with its exact numerical solution. The expression for this cross-over time for the rise height below equilibrium height is found to be $T_c \approx (3X_e/2)^{2/3}$ and that for dimensionless rise height $X_c \approx (3X_e/2)^{1/3}$, where $X_e = 1/G$ is the dimensionless equilibrium rise height and G is a dimensionless form of the acceleration due to gravity. The data can be fitted using the visco-gravitational solution and the exact numerical solution with the accuracy of within 5%, although small disagreement occurred at the very initial stages of flow. This discrepancy may be justified as in our analysis, we assumed a constant contact angle $= 0^o$ and we did not take into account the dynamic contact angle changes which is effective at very early stages of imbibition when the liquid just touches the edges of a capillary.

It is also found that liquid fingers imbibe in advance of the main meniscus in open top rectangular cross-section micro-channels along the corners of channel walls. This theory was tested by the experiments in which polydimethylsiloxane (PDMS) oils of viscosities 96, 48, 19.2 and 4.8 mPas were allowed to flow in circular and closed

square glass tubes and also in SU8 open top rectangular cross-section micro-channels. For the dimensions of capillaries we have used, it seems that the presence of these liquid fingers do not prevent both fits to describe their capillary dynamics.

It is shown that the analytical visco-gravitational solution is the best approximation for the capillarity in the tubes and channels and it is similar to its numerical fits for capillary rise height. The fitting was found to be very sensitive to offset time t_0 at very initial stages of the flow which was less than two measurement time intervals.

The viscous contribution was found to be slightly greater than predicted by the theory assuming a non-rigidified liquid-air boundary, but far below that for a rigidified boundary, which was recently reported for imbibition into horizontally mounted open top micro-channels (Yang et al. 2011). In all measurements for fitting we assume Young's equilibrium angle $\theta_e = 0^\circ$. Consistent with wetting expectations, liquid fingers were found to imbibe along the internal corners of channel walls far above the main liquid meniscus. These have many implications for a microfluidic system design.

The viscous co-efficient 'a' and capillary term 'b' was found to be in very good agreement with the parameters from the fits using both solutions. For the value of 'a' it is within 5% and that for 'b' it is 2% for all the capillaries used in our experimental setup. Therefore, for our capillaries, capillary rise height can be fitted either visco-gravitational solution or the exact numerical solution.

4.2   Glass Tubes

4.2.1   Tube Dimensions

For this section of experiments, commercially available 400 and 600µm square glass tubes and round tube of diameter 1.3mm were selected. Circular tube was used for the calibration and comparison. To make sure that the internal surface of the glass tubes are plane and free from any ridges or marks, we performed full SEM scan for the internal surfaces of the glass tubes. The following Fig. 4.1 shows the cross sectional view of circular glass tube of diameter 1.3mm and 600µm square glass tube.
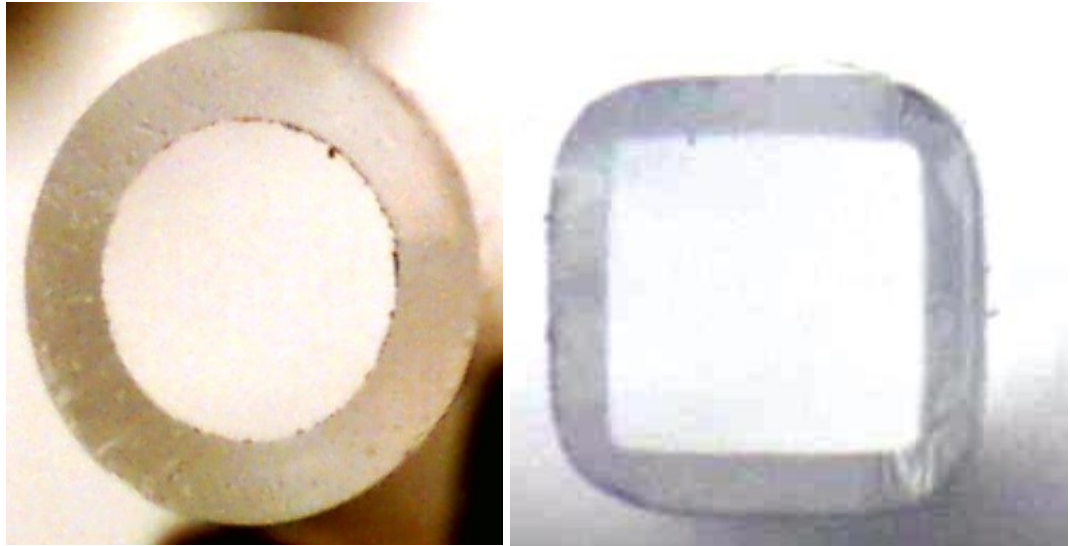
Fig. 4.1   *Cross sectional view of 1.3mm diameter circular and 600µm square glass tubes*

3.2.2   Cleaning Process

The tubes were dipped in IPA and were put in ultrasonic bath for 30 minutes. These were then taken out from IPA and were baked in an oven at 100ºC for 45 minutes. The tubes were cooled down for an hour and were ready to do experiments with.

4.2.3   Microscopy

The tubes were held vertically against a millimetre scale for length calibration. Imbibition of polydimethylsiloxane (PDMS) oils (Dow Corning Xiameter PMX-200) of

viscosities η = 96.0, 48.0, 19.2 and 4.8 mPas (±5%) and corresponding densities of 960, 950, 930 and 913 kg m^{-3} by bringing the reservoir into contact with the vertically held capillaries (round tubes of diameter 1.3mm and 400 and 600μm square glass tubes) was captured using a high speed camera (NAC Hotshot 512SC) at the rate of 50 to 250fps. The videos were saved in .hsf format using the "HSSC Link" software.

The .hsf format video was then converted into pictures of every frame in the format of JPEG using 'HSSC Link software'. These pictures were used to extract data points after equal intervals using 'Image J' software. The position of main meniscus at the central point and the corresponding time interval was extracted. The videos were analyzed after the experiment and the position of the central meniscus measured in ImageJ from the corresponding frames at a set of pre-determined time intervals. The initial time t = 0 was defined as the time the liquid first appeared to enter the tube/channel; this was determined to within one frame (i.e., 20 ms). The spatial resolution can be estimated from the field of view of the camera and the pixel resolution and was 0.02 mm. Each capillary sample was used only once but experiments were repeated with the other samples of same physical dimensions to ensure data reproducibility.

The experimental setup is shown in Fig. 4.2 which includes high speed camera which uses high resolution lens(x4), liquid reservoir, white back light that could be raised and lowered according to the position of the capillary sample and a micrometer 2D adjustable sample holder.
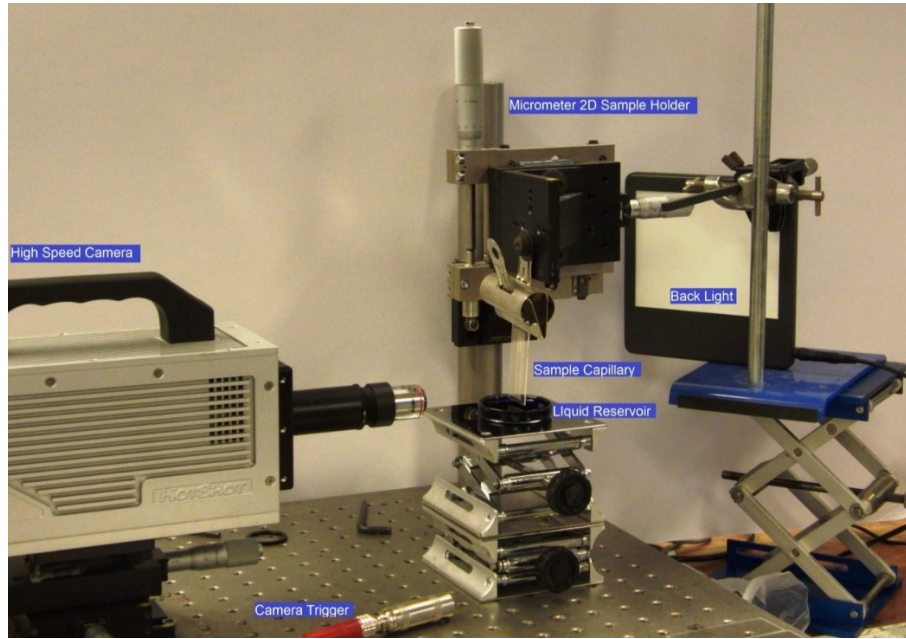
Fig. 4.2 *Experimental setup for capillarity in micro channels*

4.2.4 Results and Discussions for Round Tube Experiments

Fig. 4.3 below shows capillary rise of PDMS oil of viscosity 96mPas in a circular tube of diameter 1.3mm. 0.1ml of dye (Tetramethylrosamine) is mixed in the 500ml oil to enhance the video contrast for rising meniscus; control experiments were carried out to establish that mixing of dye in PDMS makes no noticeable difference to the capillary dynamics. The data was found to have very good reproducibility to within 20 ms.
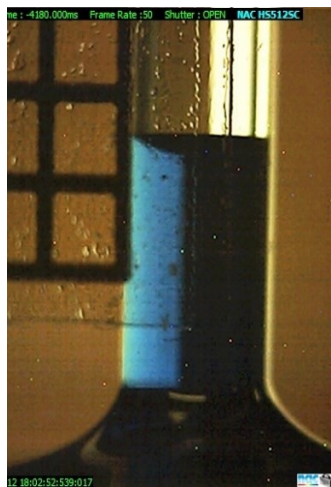
Fig. 4.3 *Rise of 96mPas PDMS (with blue dye) in a circular tube of radius 0.65mm*

The data extracted from *ImageJ* gives the variation of rise height corresponding to increasing time intervals. This data is fitted using the exact numerical solution (eq. 2.20) as well as the analytical solution (eq. 2.52). In this case as the tube is mounted vertically therefore the angle φ is taken to be 90°. Mathematica® (Wolfram research) was used to fit the data and viscous co-efficient '*a*', capillary term '*b*' and offset time t_o were the three parameters used as fitting parameters. The value of equilibrium contact angle θ_e was taken to be 0° in both fits.

In these experimental conditions, it was found that the best analytical approximation is visco-gravitational solution (already discussed in section 2.9.6) which is in agreement with the relationship derived for cross-over time $T_C \approx \left(\dfrac{3 X_e}{2} \right)^{2/3}$ below which Bousanquet solution agrees very well with the numerical fits to the data but above this cross-over time the best agreement with numerical fits to the experimental data is visco-gravitational solution [Ouali et al., 2013]. Here $T_C = a t_c$ is dimensionless cross-over time and $X_e = 1/G$ is the dimensionless equilibrium rise height where $G = \dfrac{g}{a} \sqrt{\dfrac{2}{b}}$ is a dimensionless form of the acceleration due to gravity. This cross-over time *Tc* occurs within first 20ms of the rise time when liquid just enters the glass tube, which is during the first time interval to be measured. Therefore, under these experimental conditions, the time intervals measured for the flow are always greater than the cross-over time, for which visco-gravitational fits were found to be the best agreement with the numerical fits to the data.
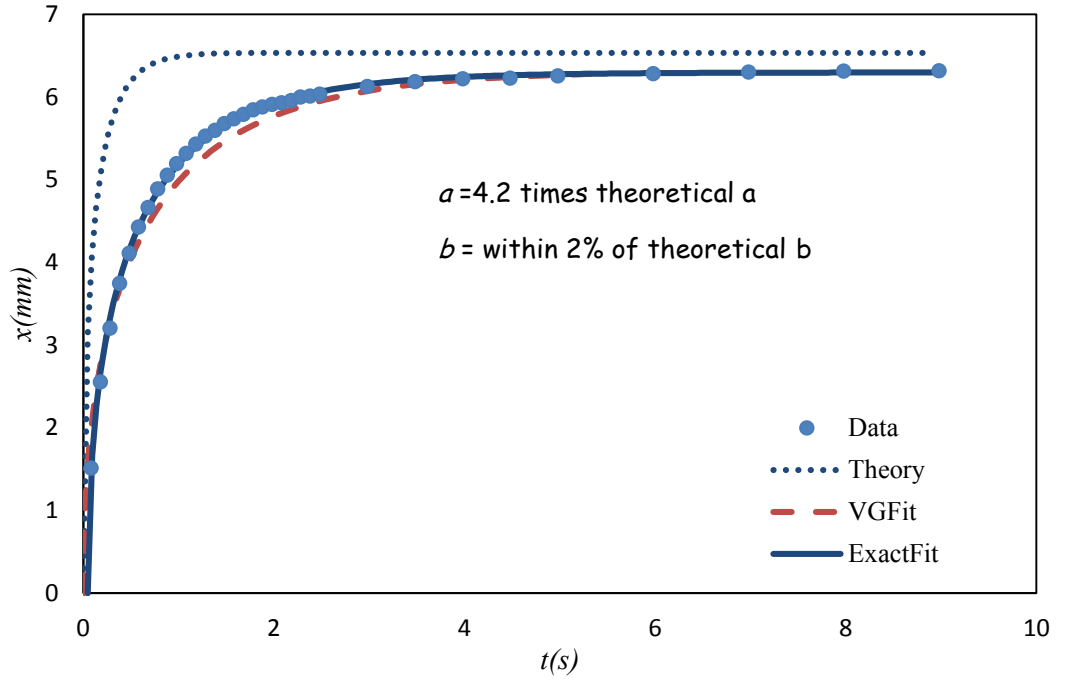
Fig. 4.4   *The experimental data of 96 mPas PDMS in 0.65mm radius circular tube is shown using solid symbols, analytical fit by red dashed lines and numerical fit by using blue solid line. The expected rise is indicated by dotted lines*

The variation of meniscus position of 19.2mPas PDMS oil in 1.3mm diameter circular glass tube is shown in Fig. 4.4. The data points indicating the rise height with time are represented by solid symbols. The blue solid line shows exact numerical fit eq. (2.20) and dashed line represents the visco-gravitational solution eq. (2.52). The dotted line represents the expected rise using the nominal device parameters. The reproducibility for the experiments using circular glass tube was found to be within 2%.

The value of viscous co-efficient 'a' was found to be larger than the corresponding theoretical value for all viscosities of PDMS in circular cross-section glass tube while the value of capillary term 'b' was found to be in very good agreement with the theoretical 'b'. The value of viscous co-efficient 'a' for round tube was found to be 4.2 ($\pm$0.2) times larger than the theoretical 'a' and the capillary term 'b' was observed to be within 2% of the theoretical 'b', therefore, for round tubes, the equilibrium height x_e was obtained to be within 2% of the value predicted by theory as

$$x_e = \frac{b}{g}.$$

Fig. 4.5 shows rate of rise height of PDMS oils of viscosities η = 96.0, 48.0, 19.2 and 4.8 mPas (±5%) in round glass tube of diameter 1.3mm with corresponding visco-gravitational fits. For higher viscosity oil, the rise is slower and it is faster for less viscous oils but in all cases, the same equilibrium height was achieved which shows that equilibrium height is independent of viscosity of the liquid. Table 4.1 lists the ratio of fitted values of '*a*' and '*b*' to their corresponding predicted values for various viscosities of PDMS.
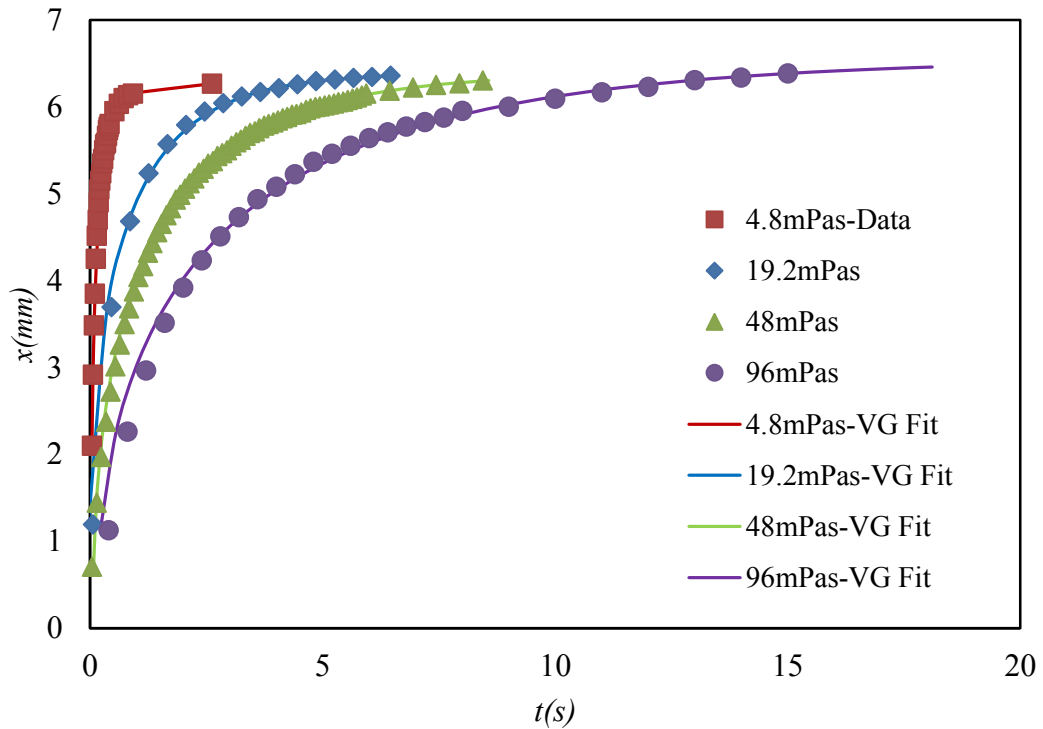
Fig. 4.5 *The effect of various PDMS oil viscosities on capillary rise rate in 650μm radius circular tube. Solid lines show VG fits to the corresponding data.*

Viscosity (mPas)	Predicted a	Fitted a	Fitted a / Predicted a	Predicted b	Fitted b	Fitted b / Predicted b
(±0.5%)	(s⁻¹)	(s⁻¹)		(mm/s)²	(mm/s)²	
4.8	94.67	383(±76)	4.05	63.462	61.60(±1.2)	0.97
19.2	378.70	1550(±310)	4.1	63.462	62.20(±1.2)	0.98
48	946.75	3860(±770)	4.08	63.462	62.20(±1.2)	0.98
96	1893.49	7800(±1600)	4.1	63.462	62.80(±1.2)	0.99

Table 4.1 *The ratio of fitted values of 'a' and 'b' to their corresponding predicted values for various viscosities of PDMS in 0.65mm circular tube.*

The rate of rise of PDMS oils in capillary to reach the equilibrium position was found to be slower than expected. Many people [Siebold et al., 2000; Hamdaoui and Nylander; 2002; Chebbi 2007; Xiao et al.; 2006; Xue et al 2006] found the slower flow in capillaries than predicted rate and they have suggested various possible reasons for this liquid retardation. One of the possible reasons maybe the effect of dynamic contact angle, that liquid interface makes with the capillary walls as soon as it comes into contact with the capillary. Increasing frictional dissipation of the rising liquid gives rise to a possible retardation co-efficient [Hamdaoui and Nylander, 2002].

4.2.5 Results and Discussions for Square Tubes Experiments

A number of experiments were performed with four different viscosities of PDMS oils to observe their effect on the capillary rise. Fig. 4.6 (a) shows imbibition of PDMS oil of viscosity η=48 mPas (±5%) and corresponding density of 950kgm^{-3} in 400μm square glass tube captured by high speed camera at the rate of 50fps.

Fig. 4.6 (b) shows rate of rise height of PDMS oils of viscosities η=96.0, 48.0, 19.2 and 4.8 mPas (±5%) in 400μm square glass tube. For higher viscosity oil, the rise is slower and it is faster for less viscous oils but in all cases the same equilibrium height was achieved which demonstrates that equilibrium height is independent of viscosity of the liquid.

(a)   (b)
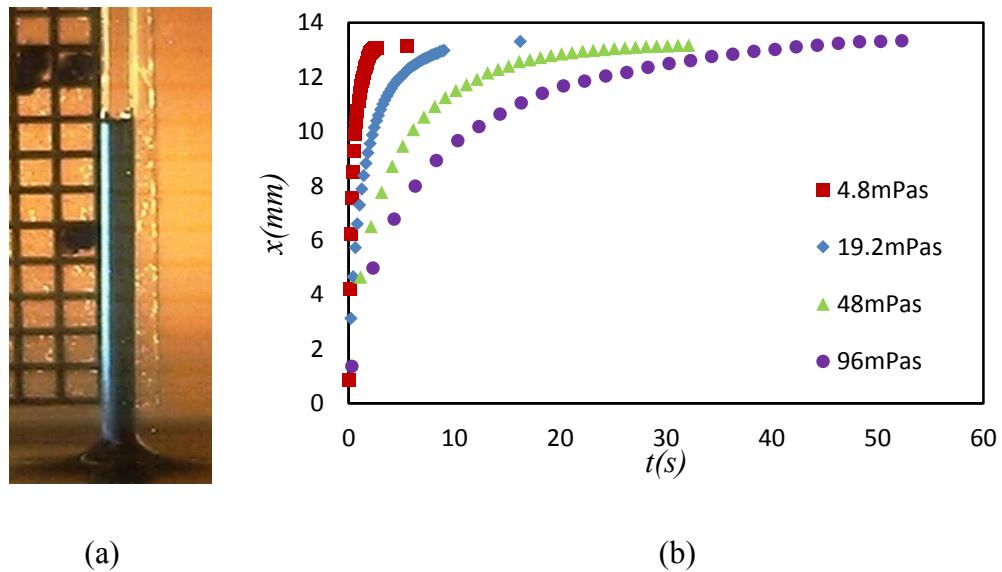
Fig. 4.6   *(a) Rise of PDMS 48mPas (with blue dye) and (b) The effect of various PDMS oil viscosities on capillary rise rate in 400μm square tube*

The variation of meniscus position of 19.2mPas PDMS oil in 400μm and 600μm diameter square glass tube is shown in the following Fig. 4.7 and 4.8
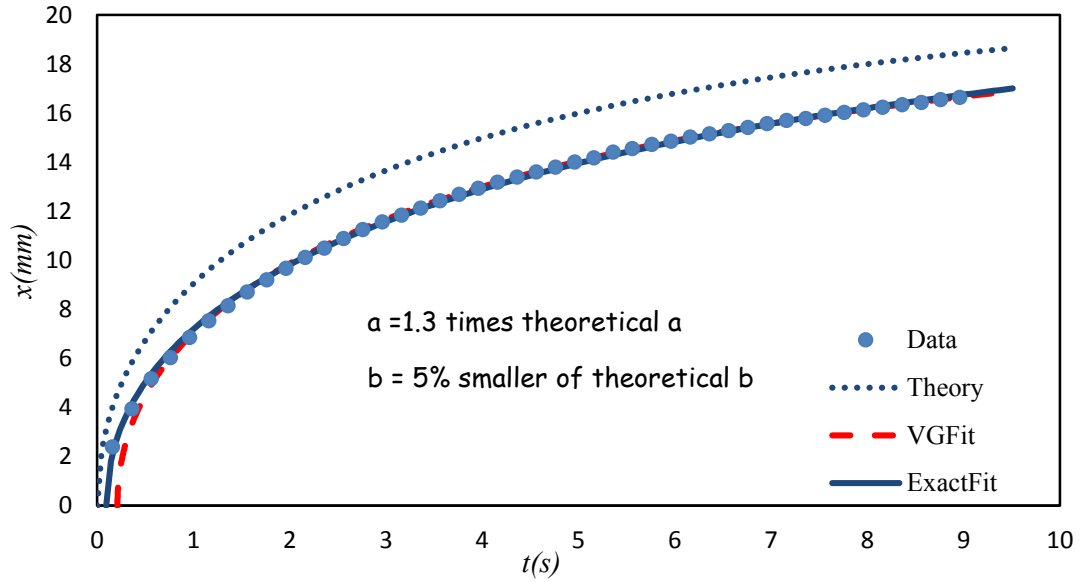
Fig. 4.7 *The experimental data is shown for 400μm square glass tube using solid symbols, analytical fit by red dashed lines and numerical fit by using blue solid line. The expected rise is indicated by dotted lines*
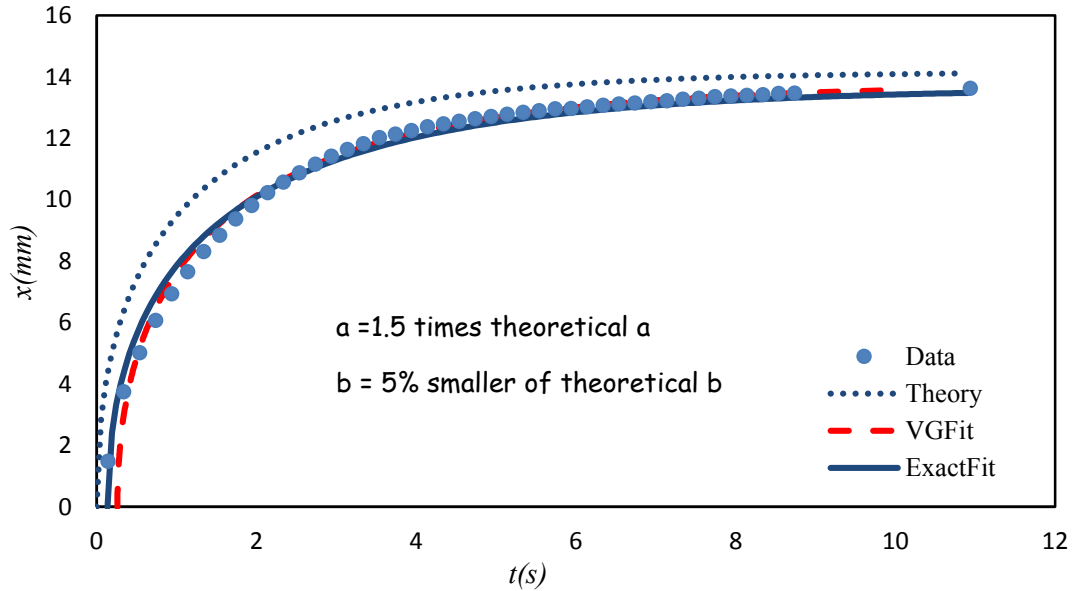
Fig. 4.8 *The experimental data is shown for 600μm square glass tube using solid symbols, analytical fit by red dashed lines and numerical fit by using blue solid line. The expected rise is indicated by dotted lines.*

Similar to the case of circular tube, the value of viscous co-efficient '*a*' was found to be larger than the corresponding theoretical value for all viscosities of PDMS in square tubes. The rate of rise of PDMS oils in capillary to reach the equilibrium position was found to be slower than expected which is shown by the dotted curve. The value of capillary term '*b*' was found to be smaller than the theoretical '*b*'. This indicates that the agreement between fitted parameters and respective predicted values becomes better for smaller dimensions of the capillaries. The value of viscous co-efficient '*a*' for 400μm closed square tubes was found to be 1.3 (±0.1) times and for 600μm closed square tube it was 1.5 (±0.1) larger than the theoretical value of '*a*'. The capillary term '*b*' was observed to be 5% smaller than the theoretical '*b*'.

The measured equilibrium height values are found to be 5% smaller than the theoretical value in the case of 400 μm and 600μm closed square capillaries. This reduction in equilibrium height is most likely due to the presence of liquid fingers which propagate ahead of main meniscus along the four internal edges of the square glass tubes (discussed in details in chapter 5). Bico and Quéré (2002) suggested that in square tubes, equilibrium rise height is reduced by a factor of $(2+\pi^{1/2})/4 = 0.943$ consistent with the observations presented here. Table 4.2 gives the values of predicted and their corresponding fitted values of the viscous co-efficient '*a*' and the capillary term '*b*' for various viscosities. Each experiment was repeated 5 times.

Viscosity (mPas)	Predicted a	Fitted a	Fitted a / Predicted a	Predicted b	Fitted b	Fitted b / Predicted b
(±0.5%)	(s^{-1})	(s^{-1})		$(mm/s)^2$	$(mm/s)^2$	
4.8	893.77	1170.00(±120)	1.31	206.25	195.90(±3.6)	0.95
19.2	3575.06	5110.00(±460)	1.43	206.25	193.90(±1.2)	0.94
48	8937.65	11400(±1200)	1.28	206.25	195.90(±2.7)	0.95
96	17875.31	24300(±2300)	1.36	206.25	195.40(±3.8)	0.95

Table 4.2   *The ratio of fitted values of 'a' and 'b' to their corresponding predicted values for various viscosities of PDMS in 400μm square tube.*

4.3   Open Top Plane Walled Micro Channels

4.3.1   Micro Channel Dimensions

For this section of experiments SU8 open top plane micro channels of rectangular cross-section were used. The bottom layer is fabricated using SU8-10 while the side walls were made of SU8-100 and the top was open to air. The fabrication of these plane channels are already discussed in detail in sec. 3.5. These micro channels were 400 (±5) μm and 600 (±5) μm wide and 135 (±5) μm thick. Although the variation in thickness is unavoidable during the process of fabrication but exact measurements for thickness and depths are taken into account while the data was being compared with theory. Fig 4.9 and 4.10 show view from above and cross sectional view of plane parallel SU8 micro channels of varying widths.
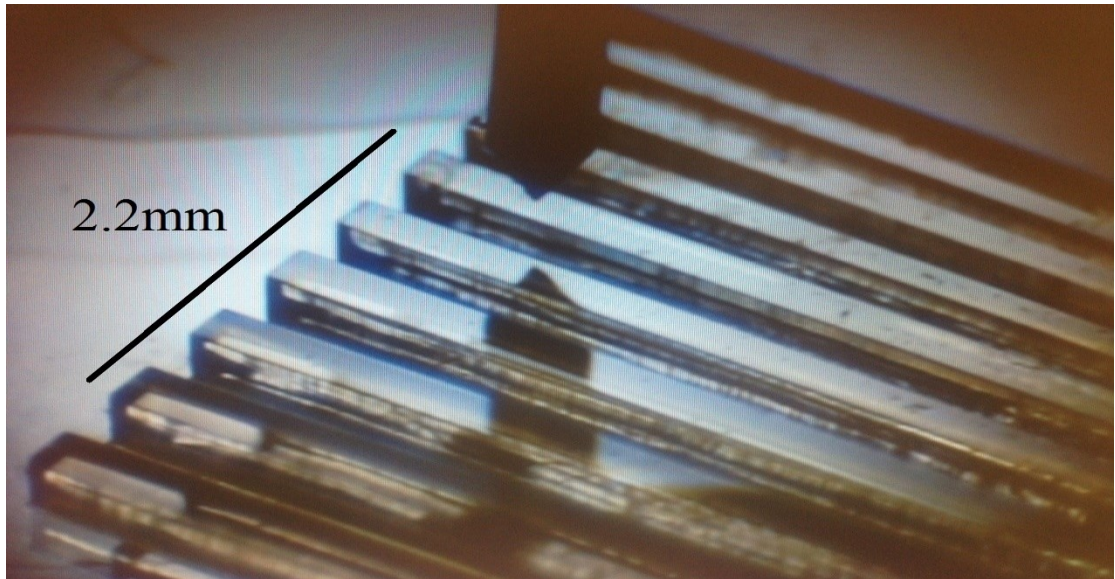

Fig. 4.9   *View from above of SU8 open top plane parallel micro channels of varying widths*
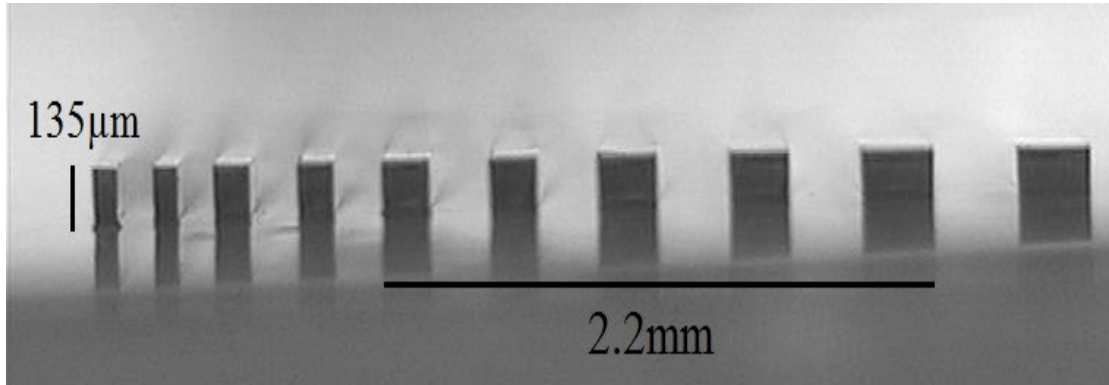
Fig. 4.10   *Cross sectional view of SU8 open top plane parallel micro channels of varying widths*

To ensure complete wetting, a strongly wetting liquid such as PDMS oil was used with contact angle $\theta_e = 0^o$, as for open top micro channels, the liquid vapour interface is completely hydrophobic (oleophobic, when liquid is an oil). The contact angle of many liquids is sensitive to the precise exposure and baking condition of lithographically produced SU8 structures so PDMS was chosen to avoid this. (Section 3.2). The thickness of these channels was measured using a stylus profilometer.

4.3.2   Cleaning Process

The open top micro channels were dipped in IPA and were put in ultrasonic bath for 30 minutes. These were then taken out from IPA and were baked in oven at 80°C for 20 minutes. The channels were cooled down for an hour and then were ready to do experiments with.

4.3.3   Microscopy

The experimental setup used to study capillary rise in SU8 open top smooth walled micro channels was the same as described in section 4.2.3. Each sample channel was used only once but experiments were repeated with the other samples of same physical dimensions to ensure data reproducibility.

4.3.4   Results and Discussions

PDMS oils of viscosities η=96.0, 48.0, 19.2 and 4.8 mPas (±5%) were made to rise in 135µm deep SU8 open top smooth walled micro channels of width 400 and

600µm. The following Fig. 4.11 shows the effect of PDMS viscosity on the capillary rise height in open top plane SU8 micro channels. This graph indicated that equilibrium rise height is independent of viscosity but rate of rise depends on viscosity of liquid. Each experiment was run 5 times to check for reproducibility.
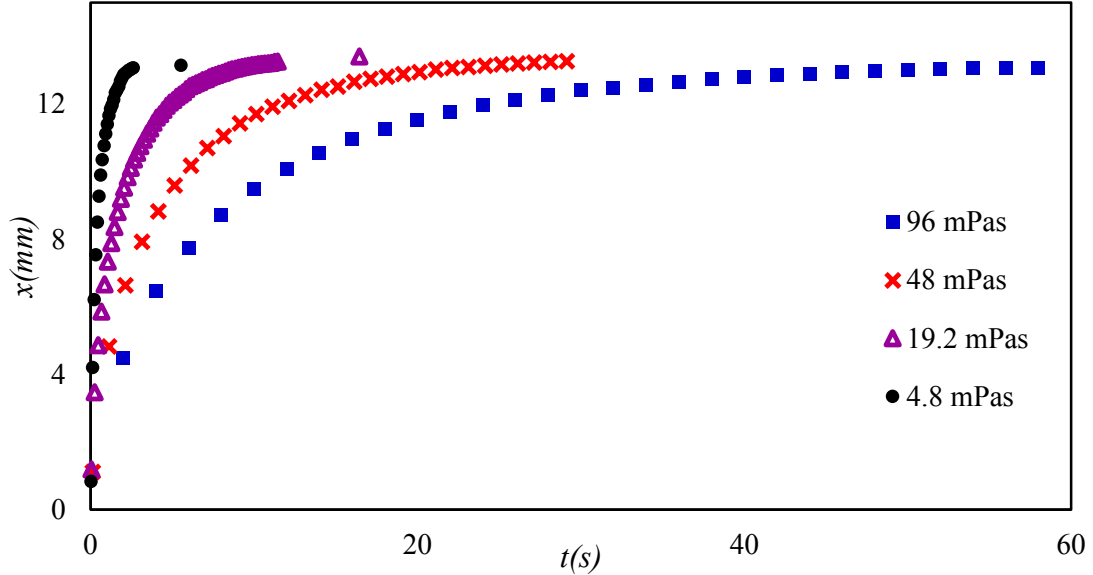
Fig. 4.11 *Effect of PDMS viscosity in 600µm wide and 135µm deep open top plane micro-channel*

The data from open top plane SU8 micro-channels was analysed and fitted using exact numerical solution and visco-gravitational solution. It is of note that only data from the part of experiment during which liquid fingers are propagating within the open channel just before they leave the other edge of the channel walls were analysed.

Fig. 4.12 and 4.13 show the data fitting for rise of PDMS 19.2 mPas in 400µm and 600µm wide open top micro channels respectively. The data can be fitted using visco-gravitational solution and exact numerical solution with the accuracy of within 5%, although small disagreement at the very initial stages of flow. This discrepancy may be justified, as in the analysis, it was assumed a constant contact angle = 0° and dynamic contact angle changes which is effective at very early stages of imbibition when liquid just touches the edges of micro channels were not taken into account. When a vertical tube first comes into contact with the horizontal meniscus of the reservoir the instantaneous contact angle is likely to be 90° and must relax towards the equilibrium value as imbibition commences [Popescu et al., 2008].

Fig. 4.12 *Exact numerical solution (solid blue line) and visco-gravitational solution (dashed line) to the experimental data (solid symbols) in 400μm open top plane SU8 micro channels using PDMS 19.2 mPas. The dotted line represents expected flow.*

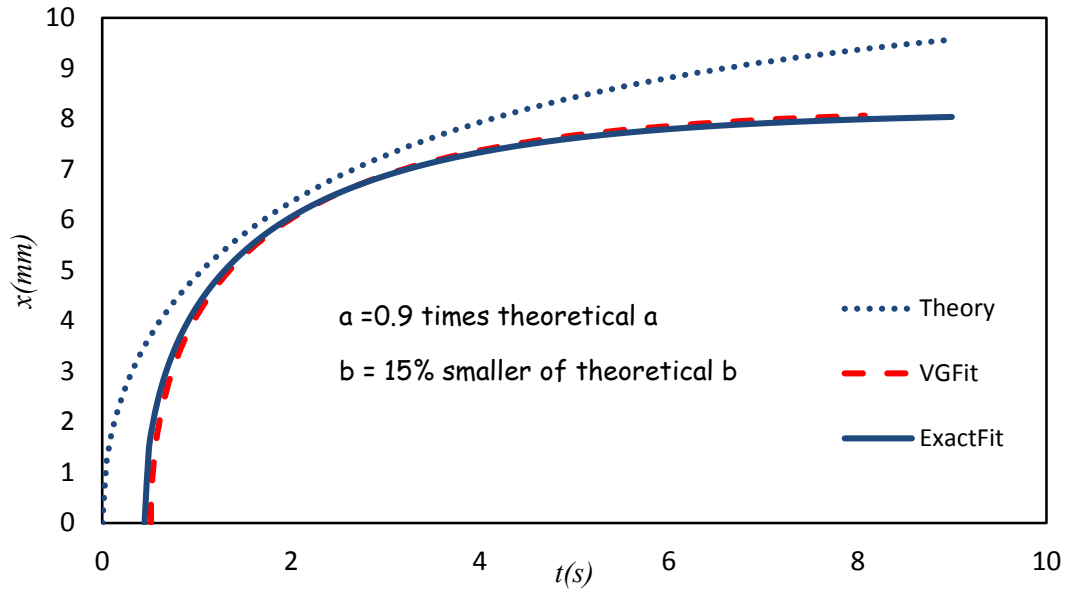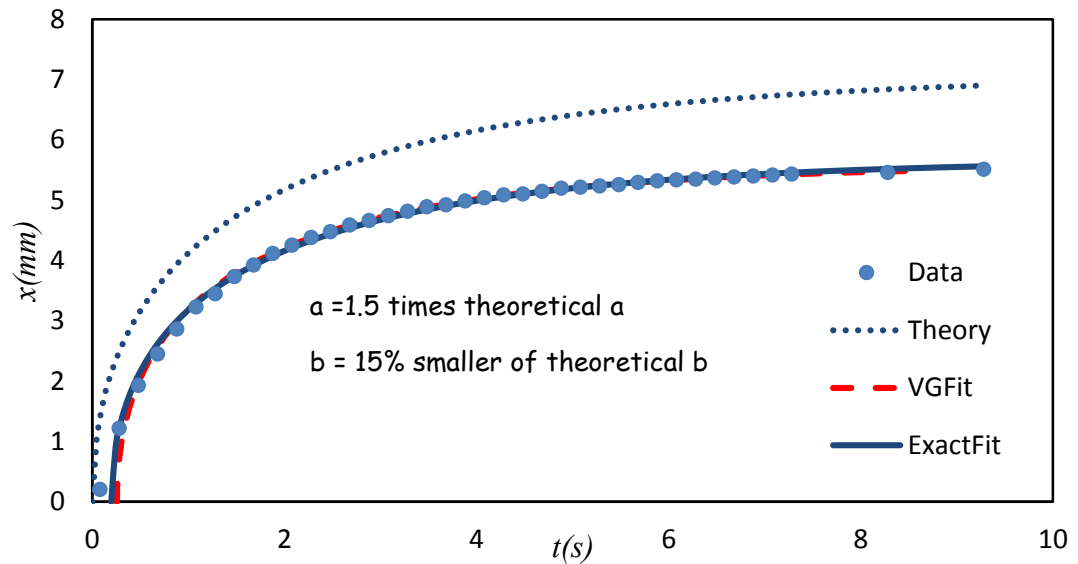**Fig. 4.13** *19.2 mPas PDMS in 600μm open top plane SU8 micro channels. Exact numerical solution (solid blue line) and visco-gravitational solution (dashed line) to the experimental data (solid symbols). The dotted line represents expected flow.*

The solid symbols are actual data points that give variation in rise height with time, the solid line is the exact numerical fit, the dashed lines show visco-gravitational solution and dotted lines show the expected dynamics of capillary flow. It can be seen from Fig. 4.12 and 4.13 that capillary rise is slower than the expected rate for both widths and fitted value of viscous co-efficient 'a' is 1.5 (±0.1) times its theoretical value for 600μm wide micro channel but it is 0.9 (±0.1) times the theoretical value of 'a' for 400μm wide micro channel (Fig. 4.9). Better agreement was observed for the fitted value of 'a' with the value predicted by theory for smaller dimensions of capillaries used, that is why for 400μm open channels fitted 'a' is in better agreement with theoretical 'a' than in the case of 600μm wide open channels. The preliminary measurements suggests that the agreement gets better if the capillary radius is less than 0.1 times the capillary length of the liquid given by:

$$L_C = \sqrt{\frac{\gamma_{LV}}{\rho g}} \tag{4.1}$$

where γ is surface tension and ρ is density of liquid and g is acceleration due to gravity. For PDMS capillary length is 1.45mm. The data for the square tubes and rectangular channels also indicate a better agreement for smaller dimensions with a reasonable agreement for the 400 μm wide open channels.

The deviation of fitted value of 'a' from the theoretical value of 'a' indicates the actual rise of liquid is slower than the rate predicted by theory. The fitted value of capillary term 'b' in both cases is 15% smaller than its predicted value. The reason for this deviation may be attributed to the dynamic contact angle effect at the very early stages of flow when liquid just enters the channel. Increasing frictional dissipation of the rising liquid gives rise to a possible retardation co-efficient [Hamdaoui and Nylander, 2002].

The equilibrium rise height x_e is proportional to b ($x_e = \frac{b}{g}$) already discussed in

section 2.9.4. Therefore the equilibrium height achieved is lower than the expected value. The possible reason for the reduced equilibrium height may be due to the presence of liquid fingers that imbibe along the internal edges of the channel much faster and far ahead of the main meniscus (discussed in chapter 5).

Unlike glass tube experiments, it was observed that up to 10% variation in data reproducibility was found in open channels as shown in Fig. 4.14. This deviation is most likely due to the channel thickness being more variable from sample to sample (±20μm) which is unavoidable during the fabrication process.
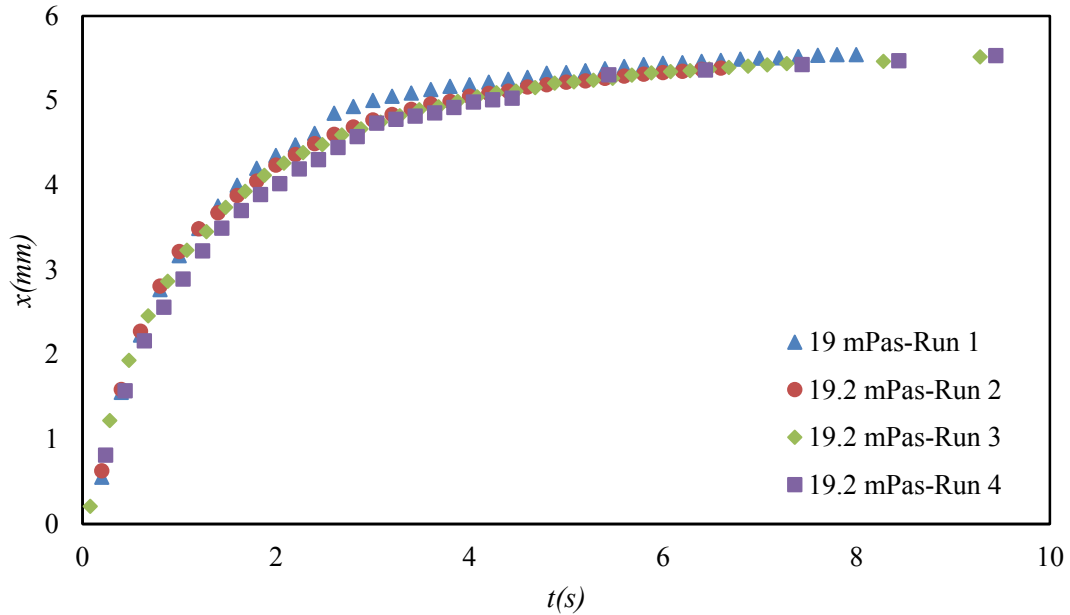
Fig. 4.14   *Reproducibility in 600μm open top plane SU8 micro channels when 19.2 mPas PDMS rises in four different samples.*

In this section, the effect of viscosity of liquid used is already described and in the next section, experimental results are given to show the effect of channel dimensions, e.g. thickness and width on capillary flow.

4.3.5   Effect of Depth on Capillary Rise in Plane Walled Micro Channels

Various depths of open top plane micro channels can be achieved by altering spin speed and baking times during lithography process. To investigate the effect of depth on capillary rise, 150, 300 and 400μm wide SU8 open top plane micro channels of depths 40, 132.5 and 300μm were fabricated. PDMS oils of viscosity 48 mPas was made to flow in these channels. It was observed that deeper the channels, higher were the equilibrium heights gained by the liquid.

It was not possible to get all the data points of liquid flow, reason being the short length of fabricated micro channels (10mm) which is less than the actual equilibrium rise height for PDMS, therefore, the recorded final height does not represent the

equilibrium rise height. Furthermore, the points were taken within the time duration in which the liquid fingers remained within the channels before leaving at the other side of the channels. In Table 4.3 the table gives the expected equilibrium rise height for various dimensions of micro channels.

Width (μm)	Depth (μm)	Expected x_e (mm)
150	100	27.29
	132.5	27.23
	300	27.5
300	100	13.48
	132.5	13.56
	300	13.7
400	100	10.03
	132.5	10.11
	300	10.25

Table. 4.3   *Expected equilibrium rise height of 48 mPas PDMS oil in micro channels of various dimensions*

The following Fig. 4.15, 4.16 and 4.17 show how the thickness of 150, 300 and 400μm wide open top plane micro channels affect the dynamics of 48 mPas PDMS oil.
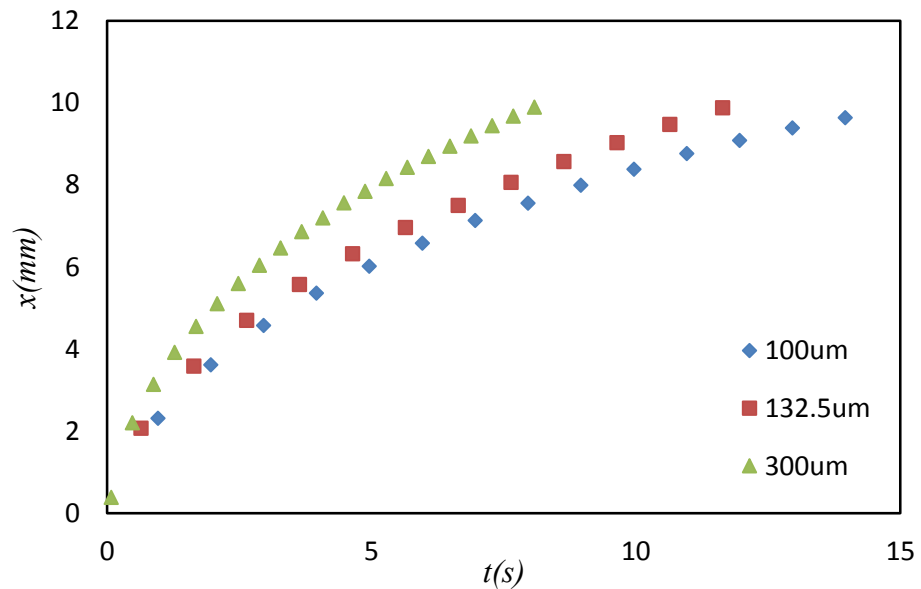
Fig. 4.15   *48 mPas PDMS oil in 150μm wide open top plane micro channels with three different depth values*
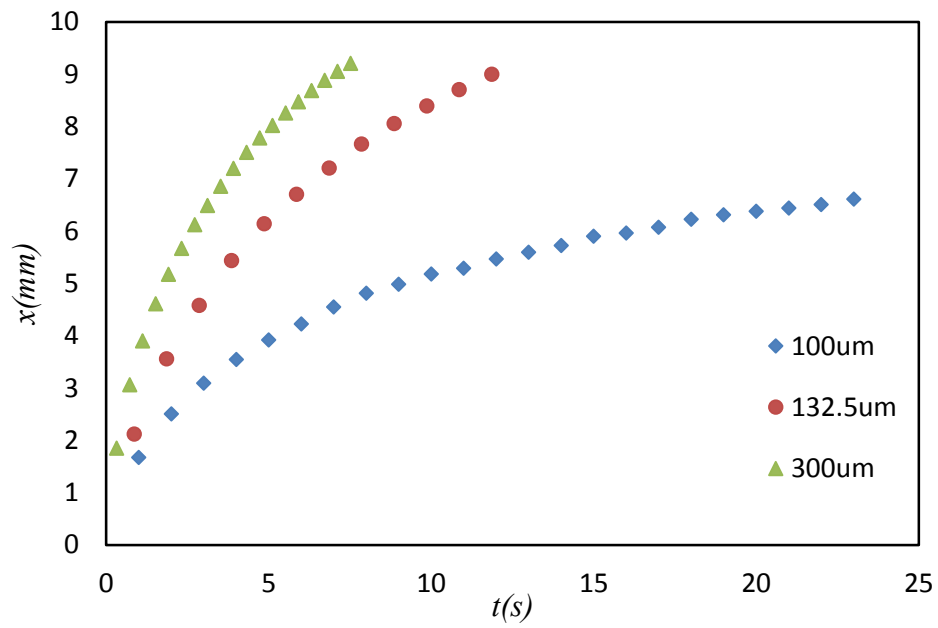
Fig. 4.16   *48 mPas PDMS oil in 300μm wide open top plane micro channels with three different depth values*
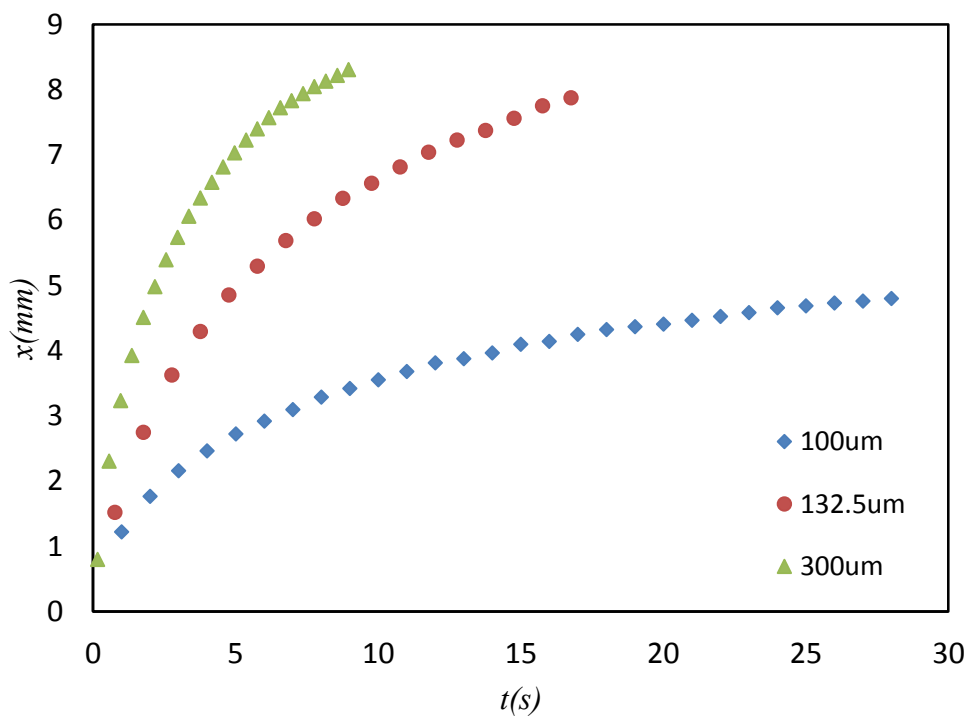
Fig. 4.17   *48 mPas PDMS oil in 400μm wide open top plane micro channels with three different depth values*

4.3.6 Effect of Width on Capillary Rise in Plane Walled Micro Channels

The capillary rise in channels having different widths was investigated, keeping the viscosity of the liquid and thickness of the channels the same. Re-plotting the data from the Fig. 4.15 to Fig. 4.17, the effect of varying widths is shown in the following Fig. 4.18 which represents the capillary rise of PDMS of viscosity 48 mPAS in 100μm thick open top micro channels of widths 150, 300 and 400μm. Again, the final height does not represent the equilibrium rise height due to the fabricated length of micro channels (10mm) being shorter than the expected final height (already explained in Table 4.3).

These experimental results can also be predicted by using the data scaling method, which is explained in detail in the next section 4.4.
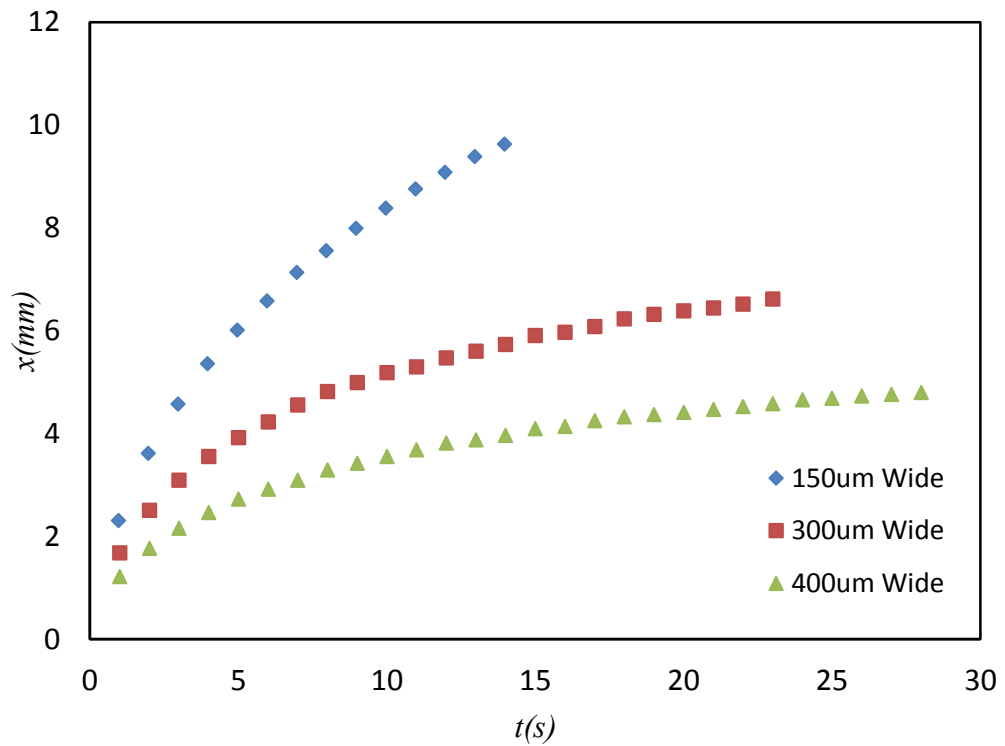
Fig. 4.18   *48mPas PDMS oil in 100μm thick and 150, 300 and 400μm wide open top plane micro channels*

4.4   Scaling of Data to Predict Capillary Dynamics for 135μm Deep Channels

4.4.1   Scaling of the Data for Viscosity

According to visco-gravitational solution, for the same physical dimensions of capillaries at a given rise height;

$$t \propto a\, b \propto \eta \qquad\qquad \text{(eq. 2.52, 2.53 and 2.54)}$$

where η is viscosity of liquid used, t is the time of rise height, '*a*' and '*b*' are viscous co-efficient and capillary term respectively.

This expression enables the data of one particular viscosity to be used to scale the data using a capillary of given dimensions to the other viscosity value if the density and surface tension of the liquid are independent of viscosity which for these experiments was within 5%.

This is shown experimentally by re-plotting the data from the sample with PDMS 96 mPas as rising liquid for various other viscosities. The scaled time t* for any other viscosity η is calculated by using the relation,

$$t^* = t \times 96/\eta \qquad\qquad (4.2)$$

Thus capillary dynamics can be predicted for other viscosities using one viscosity data having same physical dimensions. The results are shown in the Fig. 4.19, 4.20 and 4.21 for 650μm circular tube, 400μm and 600μm square tubes respectively, which show that data can be scaled for viscosity.
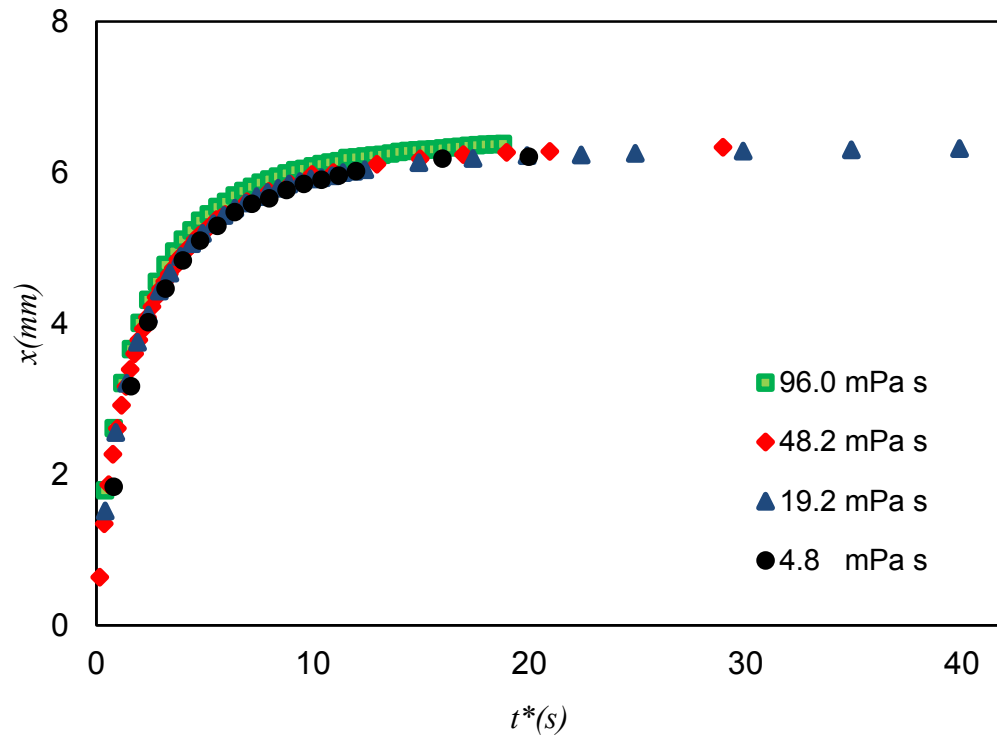
Fig. 4.19 *Scaling of 96 mPas PDMS oil data for 48.2, 19.2 and 4.8 mPas PDMS oils in 650μm round tube*
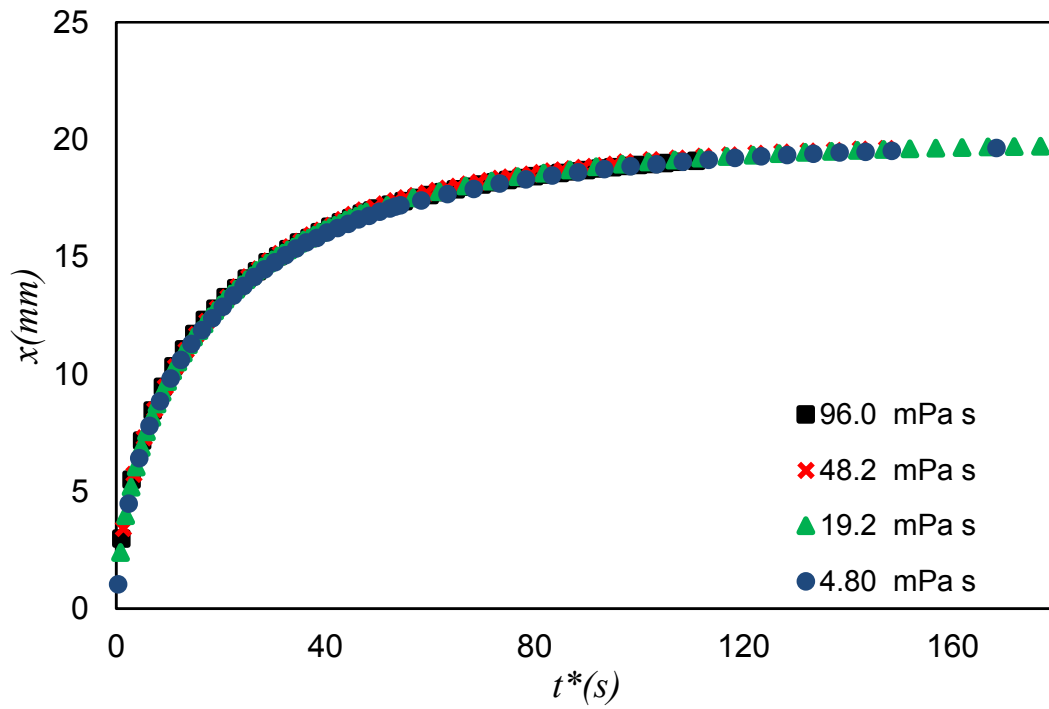
Fig. 4.20 *Scaling of 96 mPas PDMS oil data for 48.2, 19.2 and 4.8 mPas PDMS oils in 400μm square tube*
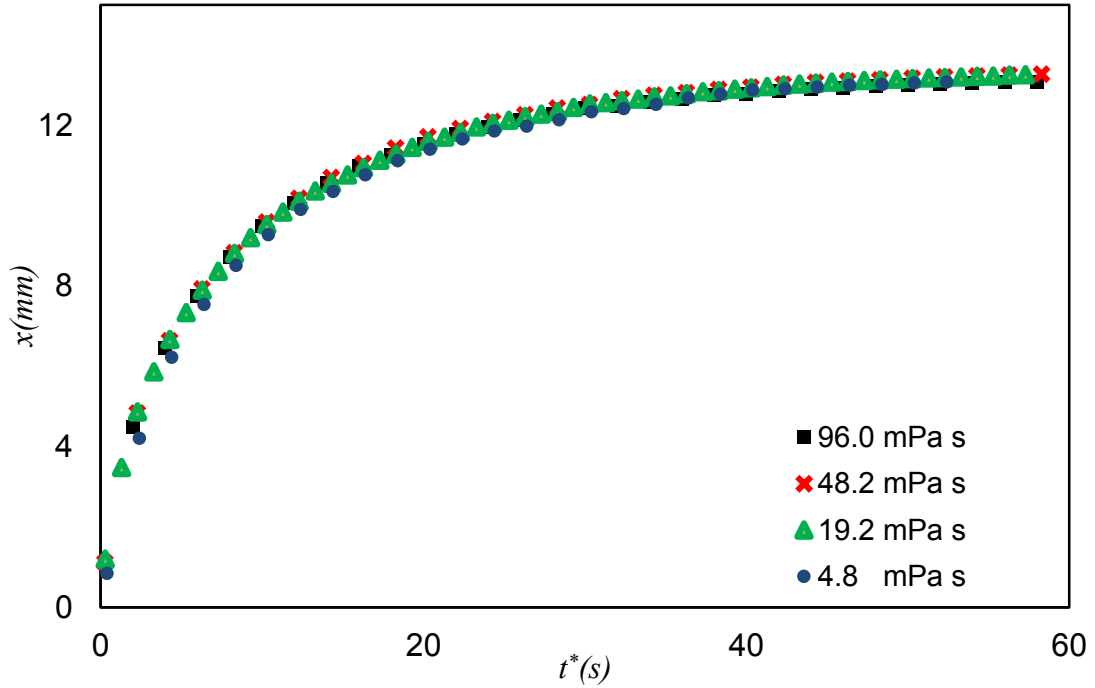
Fig. 4.21 *Scaling of 96 mPas PDMS oil data for 48.2, 19.2 and 4.8 mPas PDMS oils in 600μm square tube*

It is of note that the scaling for viscosity for open top rectangular channels did not show such good agreement (as shown by Fig. 4.22 and 4.24). This may be due to variations in channel depth between samples (130-140 (±5) μm) which was unavoidable during their fabrication. By taking into consideration the variations in the channel depths between samples at a given channel width, the scaling method gives the improved results (will be discussed later in section 4.4.3) as shown by Fig. 4.23 and 4.25. It can be seen that the data cannot be scaled for as good for channels in the same way as for closed square capillaries, the reason for this is that the theory underestimates the viscous dissipation by an amount that is dependent on the sample dimension.
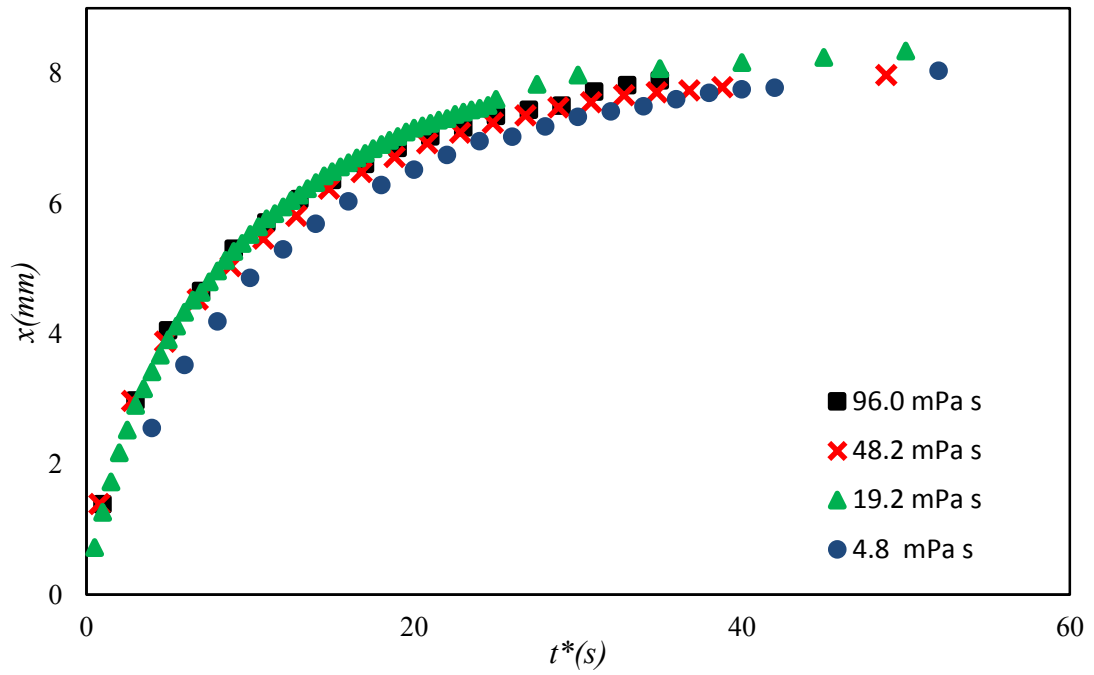
Fig. 4.22   *The data of 96 mPas PDMS experiment scaled for other viscosities in 400µm open top rectangular micro channels*
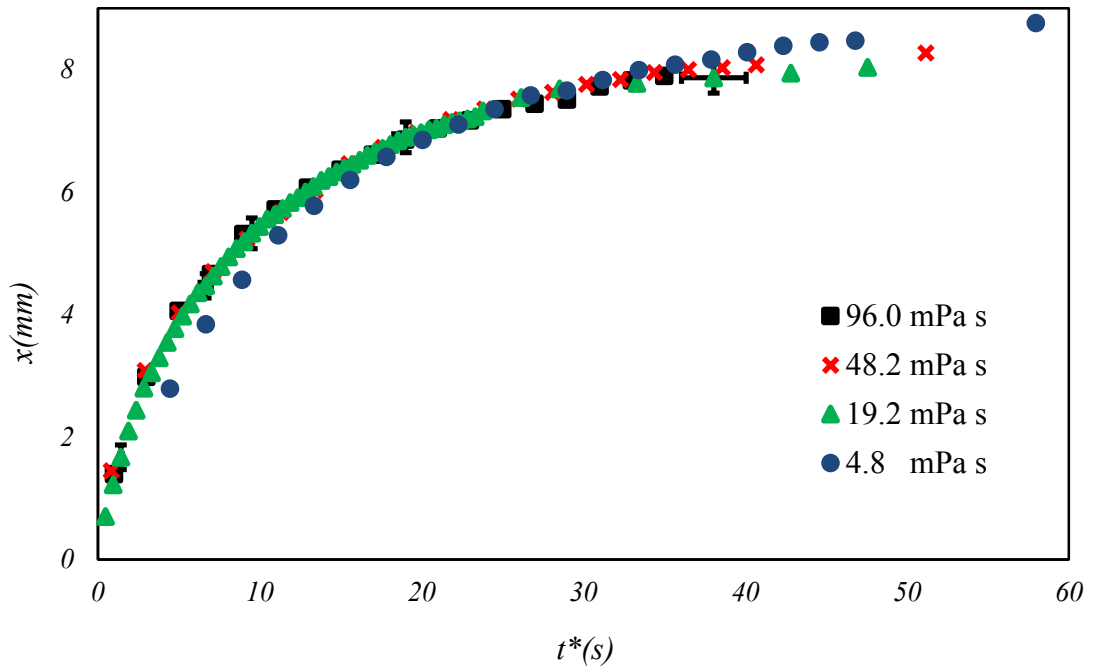
Fig. 4.23   *The data of 96 mPas PDMS experiment scaled for other viscosities in 400µm open top rectangular micro channels when exact channel depths were taken into account*
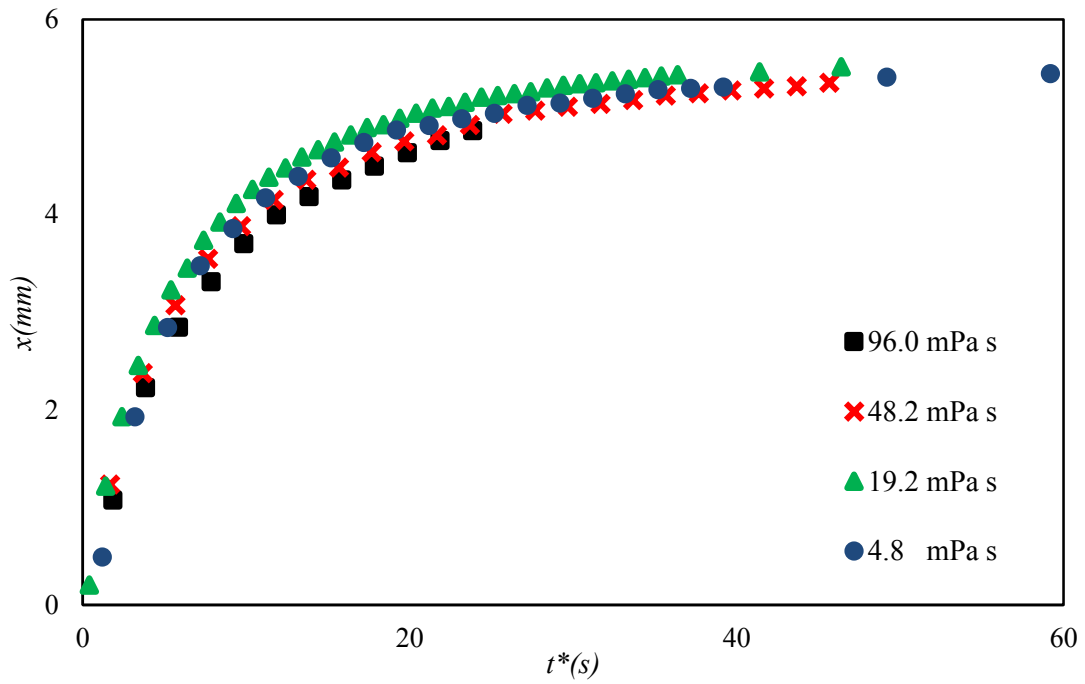
Fig. 4.24 *The data of 96 mPas PDMS experiment scaled for other viscosities in 600μm open top rectangular micro channels*
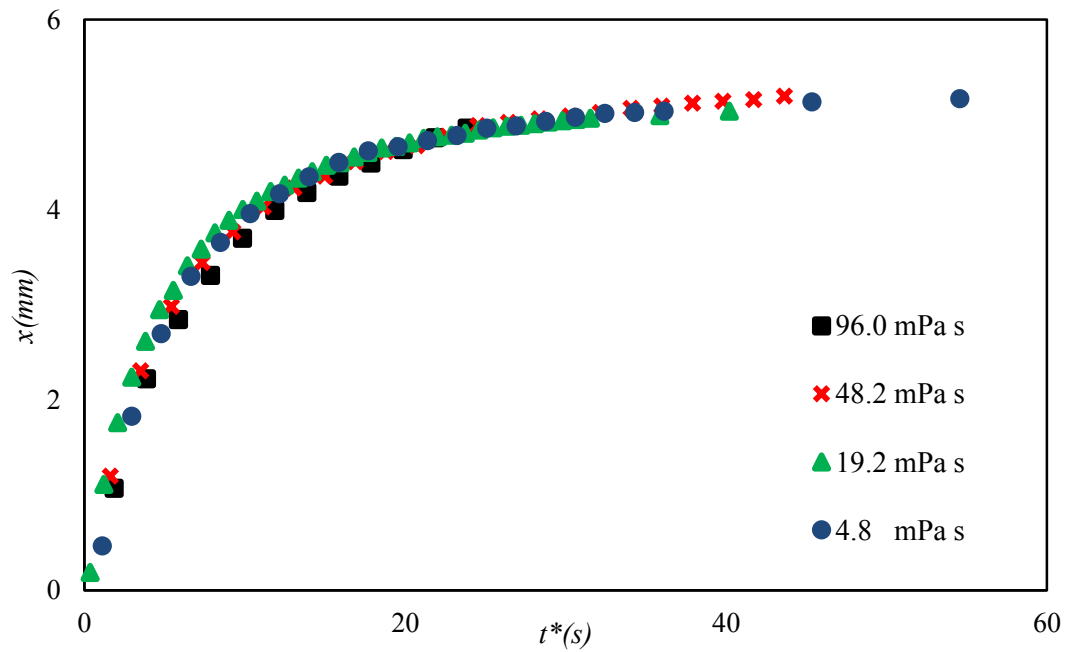
Fig. 4.25 *The data of 96 mPas PDMS experiment scaled for other viscosities in 600μm open top rectangular micro channels when exact channel depths were taken into account*

4.4.2   Scaling of Data for the Fitted Value of '*a*'

The data of a given viscosity is scaled to other viscosities by using the fitted value of the viscous co-efficient '*a*' according to the relation $t \propto ab \propto \eta$ as discussed earlier in section 4.4.1. This shows that if the experimental data of one given viscosity is fitted for visco-gravitational solution, the fitted value of '*a*' can be used to predict the capillary dynamics for other viscosities of liquid for the same known physical dimensions of capillaries. The results are shown in the following Fig. 4.26 which shows the data from the sample using 96 mPas viscosity is scaled by taking the fitted value of '*a*' for 48, 20.6 and 4.8 mPas PDMS.
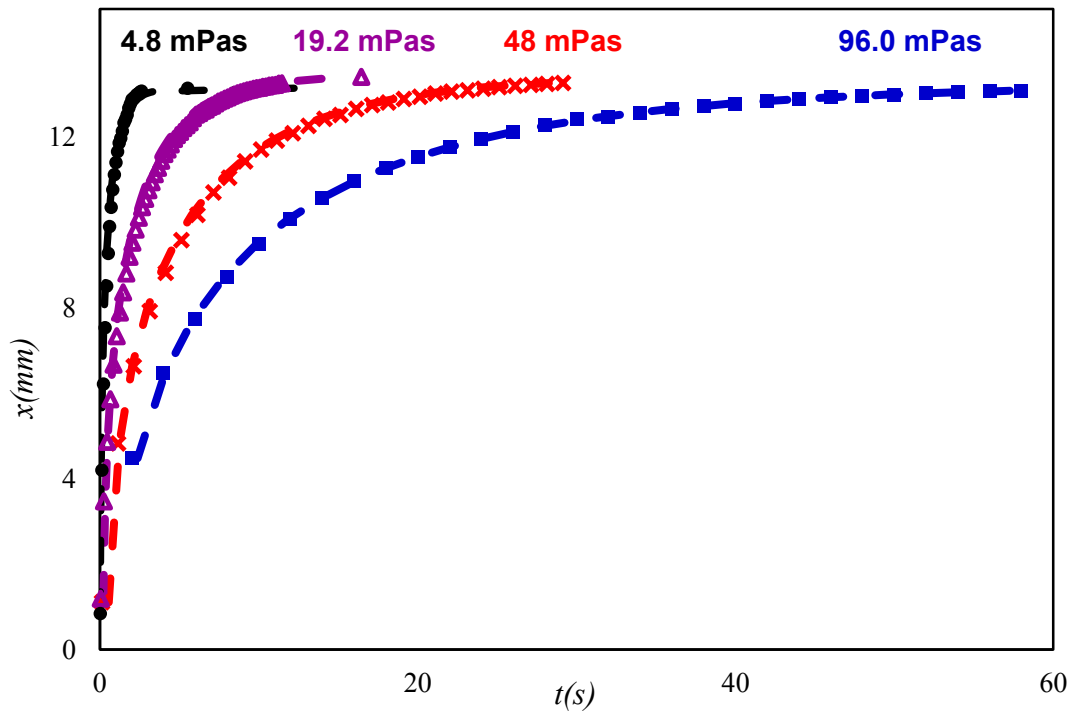
Fig. 4.26   *Scaling of 96 mPas data by using the fitted value of 'a' for 48.2, 19.2 and 4.8 mPas PDMS in the same physical dimension capillaries*

4.4.3   Scaling of Data for Physical Dimensions

According to visco-gravitational solution, for the given $\dfrac{x}{x_e}$,

$$t \propto ab \propto \eta \left/ \left(H^{3} \xi_{c}(\varepsilon) \right) \right. \propto \eta \, H^{-3} \qquad (4.3)$$

Where $\zeta_{c}(\varepsilon) = \zeta_{c}(1)$ is independent of dimension for square tubes.

As $b = x_{e}g$, that indicates that equilibrium rise height x_{e} is inversely proportional to depth of the capillary (eq. 2.54). Therefore, the data can be scaled from a capillary of a given dimension H for any other sample dimension $H^{'}$ both for rise height and time by using the following relations;

$$\text{The scaled rise height, } x* = \left(\frac{H'}{H} \right) x \qquad (4.4)$$

and,

$$\text{The scaled time, } t* = \left(\frac{H'}{H} \right)^{3} t \qquad (4.5)$$

The following Fig. 4.27 shows the effect of tube dimensions on PDMS 96 mPas oil while Fig. 4.28 shows the scaling for tube dimensions and viscosity for 400µm and 600µm square tubes.
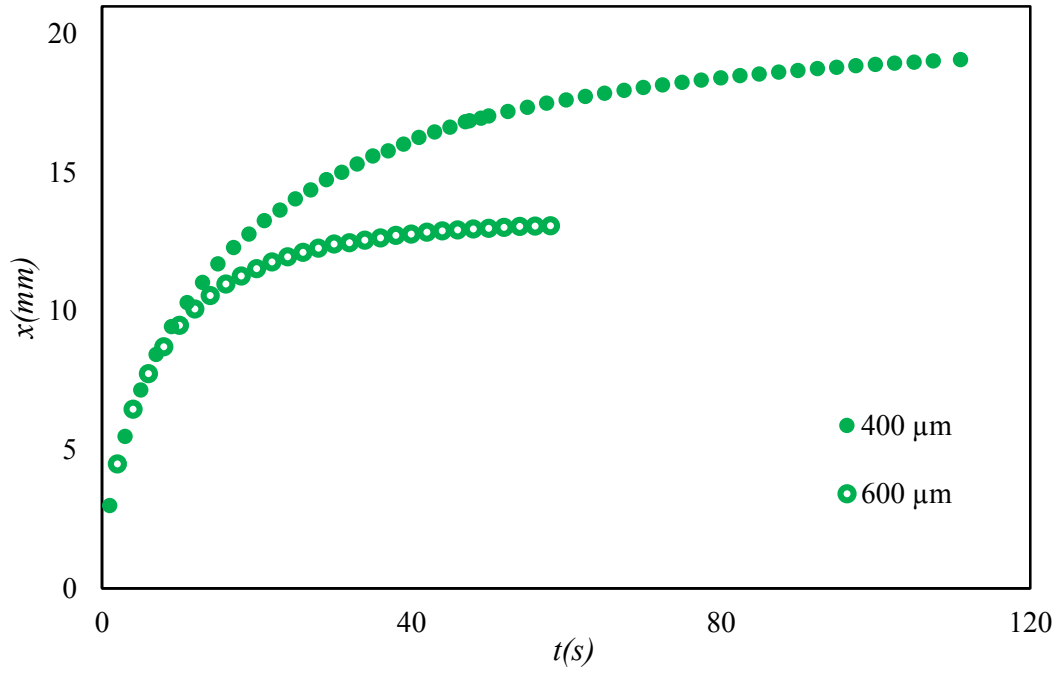
Fig. 4.27   *The effect of square glass tube dimensions on PDMS 96 mPas rise height*
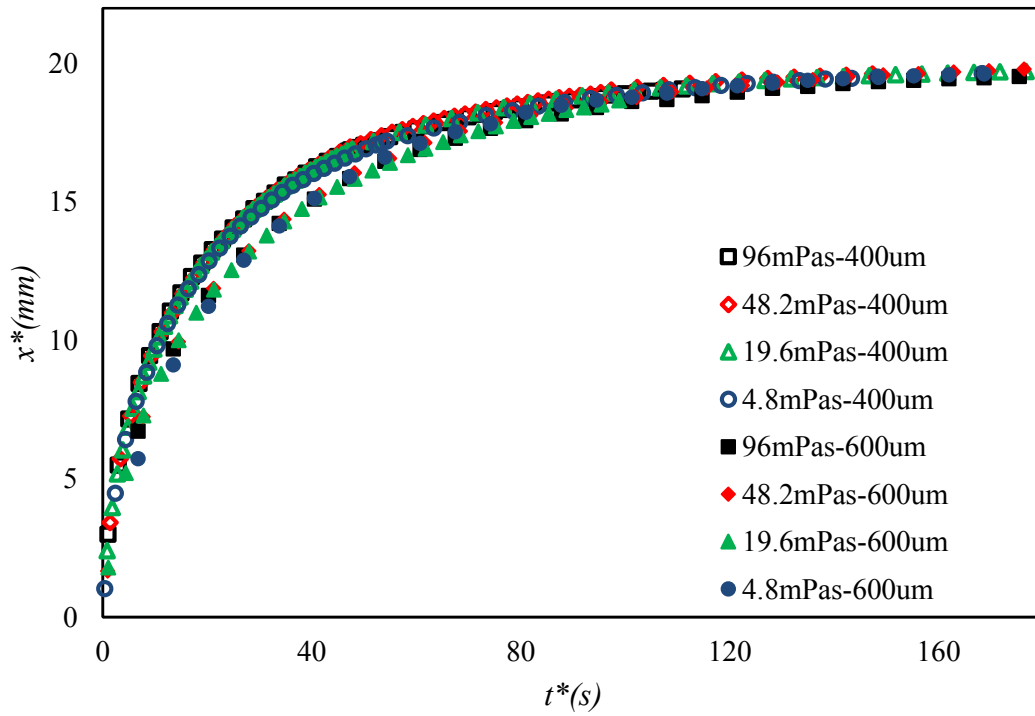
Fig. 4.28   *Scaling for tube dimensions and viscosity for 400μm and 600μm square tubes*

For open channels of varying depths and with $\theta_e = 0^o$,

$$t \propto a\,b \propto \eta / \left(H^3 \zeta_o(\varepsilon) \right) \propto \eta / \left(WH^2 \zeta_o(\varepsilon) \right) \tag{4.6}$$

where $\zeta_o(\varepsilon)$ can be determined using eq. (2.39). Therefore it is possible to scale the rise for any sample of known width W, height H (hence ε) and viscosity η relative to any other sample with given dimensions and viscosity following the same procedure as for square capillaries. The data of 96 mPas PDMS was scaled for viscosity in 400μm and 600μm open top rectangular micro channels as shown by the Fig. 4.19 and 4.21, and small variations in channel depths at fixed channel widths as shown by Fig. 4.20 and 4.22. It can be seen, however, that the data cannot be fully scaled for channel width, in the same way as for closed square capillaries, the reason for this is that the theory underestimates the viscous dissipation by an amount that is dependent on the sample dimension.

4.5   Summary

A number of experiments were performed to investigate the capillary rise in vertically held closed plane glass tubes and open top SU8 plane micro channels using various viscosities of PDMS oils as rising liquid. The data was fitted numerically as well as analytically using visco-gravitational solution.

It was observed that visco-gravitational model is adequate to describe the dynamics for the specific dimensions used in these experiments above a particular cross over time below which Bosanquet model is the best approximation to describe the capillary rise dynamics. In these experimental conditions the cross over time lies between the first two time intervals of the measurements, hence it is shown that visco-gravitational model is the best approximation.

It has been shown through scaling method that given the data for one viscosity it is possible to predict accurately what will happen for other viscosities for the same physical dimensions. A number of experiments were performed in which effect of one particular parameter (e.g. viscosity of liquid or thickness and width of sample used) was observed on capillary rise keeping the other parameters constant. The results were in very good agreement with the data predicted by scaling method.

It has been observed that liquid fingers propagate ahead of the main meniscus along the edges of the corners in non-circular capillaries and are very prominent in open top SU8 micro channels.

It has also been observed that the viscous flow of meniscus is slower than predicted which is consistent with previously observed data for circular tubes. The reason for this slower flow may be attributed to viscous friction and the presence of liquid fingers. It may also be due to the possible dynamic contact angle effect during capillary rise and a possible retardation coefficient caused by increased frictional dissipation of the main meniscus. The equilibrium height attained was observed to be less than the predicted value and it is assumed that the reason for this reduction is the presence of propagating liquid fingers ahead of the main meniscus of rising liquid. Therefore, it is important to study these liquid fingers and their effect on capillary dynamics. In the next chapter, the liquid fingers observed in non-circular capillaries are discussed in detail.
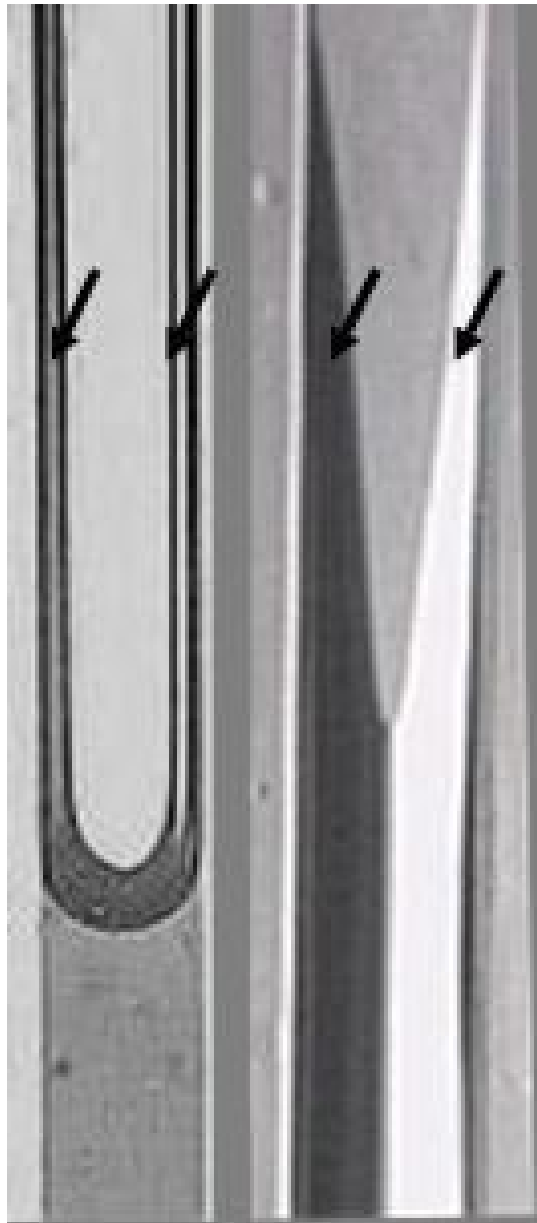
5.1   Liquid Fingers in Capillaries

It has been found that during the capillary rise in non-circular capillaries, liquid fingers propagate along the corners of capillary walls of rectangular cross section, as discussed in section 2.10. These liquid fingers become more prominent as they advance. The size of these fingers increase with time (the size of finger Δx is taken to be the difference in length from the main liquid meniscus and the edge of liquid finger as shown in Fig. 5.1). It is to be noted that he size of the fingers in the following Fig. 5.1 on both walls seems to be a bit different due to the light incident from one side of the channels. Due to the image contrast different at both walls, one finger seems higher than other. Although there was very small difference (not more than 0.01 mm) found in finger size in some of the samples at both walls, the mean of two lengths was taken for analysis.
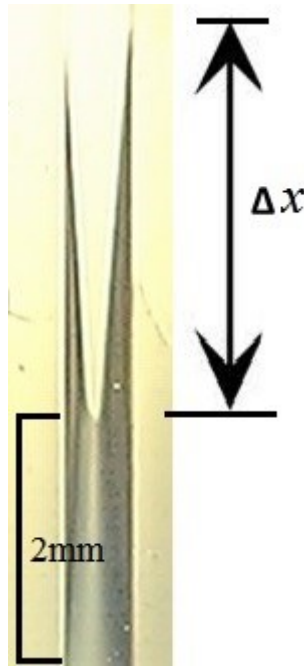
Fig. 5.1   *Liquid fingers in 400μm open top micro channel. Size of liquid finger is taken to be the length between meniscus and end of the advancing finger*

In the closed glass capillaries, these fingers were observed to be advancing along the four internal corners or edges of their walls. The aspect ratio is $\varepsilon = \dfrac{h}{w} = 1$ for closed glass tubes and the edge of the capillary is defined by where its walls meet at 90°. In

this case, the liquid fingers were very thin advancing only along the edges of the tubes and this makes it difficult to image them with good contrast in the experimental setup used in Fig. 3.18. These fingers are shown in Fig. 5.2 in 400μm and 600μm closed glass tubes.

(a)   *(b)*
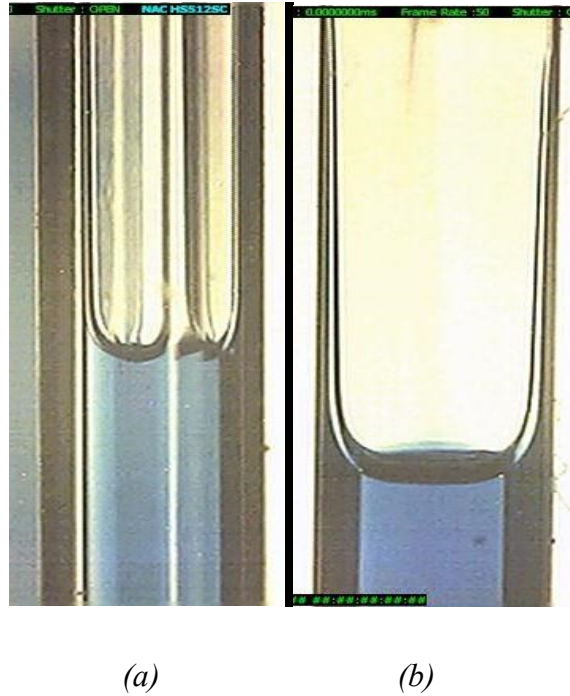
Fig. 5.2   *Liquid fingers in (a) 400μm and (b) 600μm closed glass tubes*

Girardo *et al*. (2009) also reported the same observations in the open channels for the same height to width ratio. In case of SU8 open top rectangular micro channels with aspect ratios from $\varepsilon = 0.07$ to 0.58, it was observed that the liquid fingers advanced ahead of main meniscus along the two internal edges where side walls meet the bottom side of the channel at 90° and became very prominent and gradually increasing in size as they rise with time, as shown in fig. 5.2. It was also observed that the speed with which these liquid fingers advance was much faster than the main meniscus and eventually moved out from the other end of the channels completely in experimental setup shown in Fig. 3.18.

Seemann et al. (2005) have reported that for static liquids in open rectangular channels held horizontally, the shape of these liquid fingers depends upon the height to

width ratio of the capillaries and the contact angle that liquid makes with the channel walls, and they also found that for liquids having contact angle approaching 0°, very prominent and thick liquid fingers were observed for the micro channels with smaller height as compared to their widths i.e. for aspect ratio less than 0.5. For aspect ratio greater than 0.5, the liquid fingers were confined to only the edges of the capillary walls and were very thin. The shape dependence of these fingers in the experimental setup has been found to be consistent with the above observations reported by Seemann *et al*. (2005). In this chapter, liquid fingers in SU8 open top micro channels are analysed and the data for meniscus with very prominent fingers is fitted using visco-gravitational approximation. The size speed of these fingers are also measured.

Various channel widths have been used to study liquid fingers, i.e. from 150μm to 600μm but visco-gravitational fits were performed only to 400μm and 600μm wide channels in order to have comparable results with those obtained in chapter 4. Due to this reason, the same channel dimensions are also selected for the rough channel experiments given in chapter 6. Furthermore, the data was fitted using only visco-gravitational solution in this chapter and later in chapter 6, as it is clear from the results in chapter 4 that it is the best approximation for the particular channel dimensions and is equivalent to the exact numerical fits.

5.2   Liquid Fingers: Shape and Size

The difference between liquid fingers shape and size is shown by the following snapshots taken at equivalent time intervals for three SU8 open top micro channels having the same width but different thickness when liquid of the same viscosity rises through these channels. Channel width of these samples was 600μm and PDMS oil of viscosity 48 mPas was used as rising liquid. The following Fig. 5.3, 5.4 and 5.5 show the shape and size of liquid fingers after 3.5 sec when PDMS Oil of viscosity 48 mPas enters 600μm wide and 48μm, 135μm and 350μm deep SU8 open top micro-channel and then after every 6 sec interval.

5.2.1 Finger Shape and size of 48um Deep Channels:
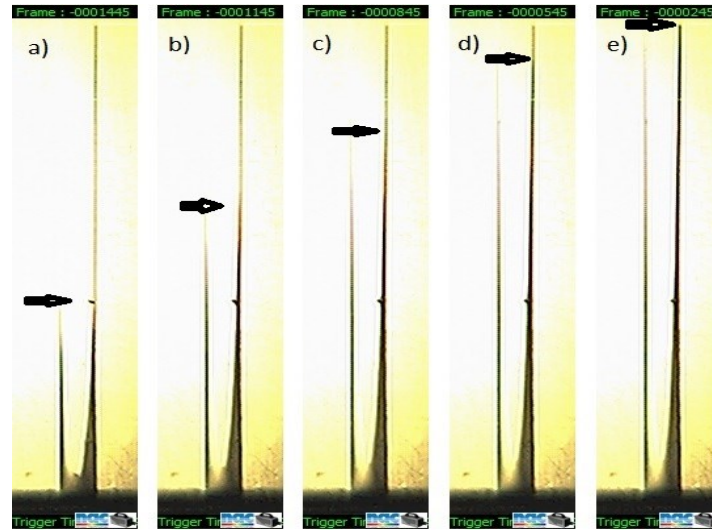
Fig. 5.3 *Liquid finger size and shape in 600µm wide and 48µm deep plane micro channel at a) 3.5 sec, b) 9.5 sec, c) 15.5 sec, c) 21.5 sec, d) 27.5 sec and e) 33.5 sec after PDMS oil of viscosity 48 mPas first enters the channel. The arrows show position of finger. The scale for this set of pictures is 44.6 pixels / mm. The length of the following channel is 10mm and the aspect ratio of the sample is 0.08.*

5.2.2 Finger Shape and Size of 135um Deep Channels:
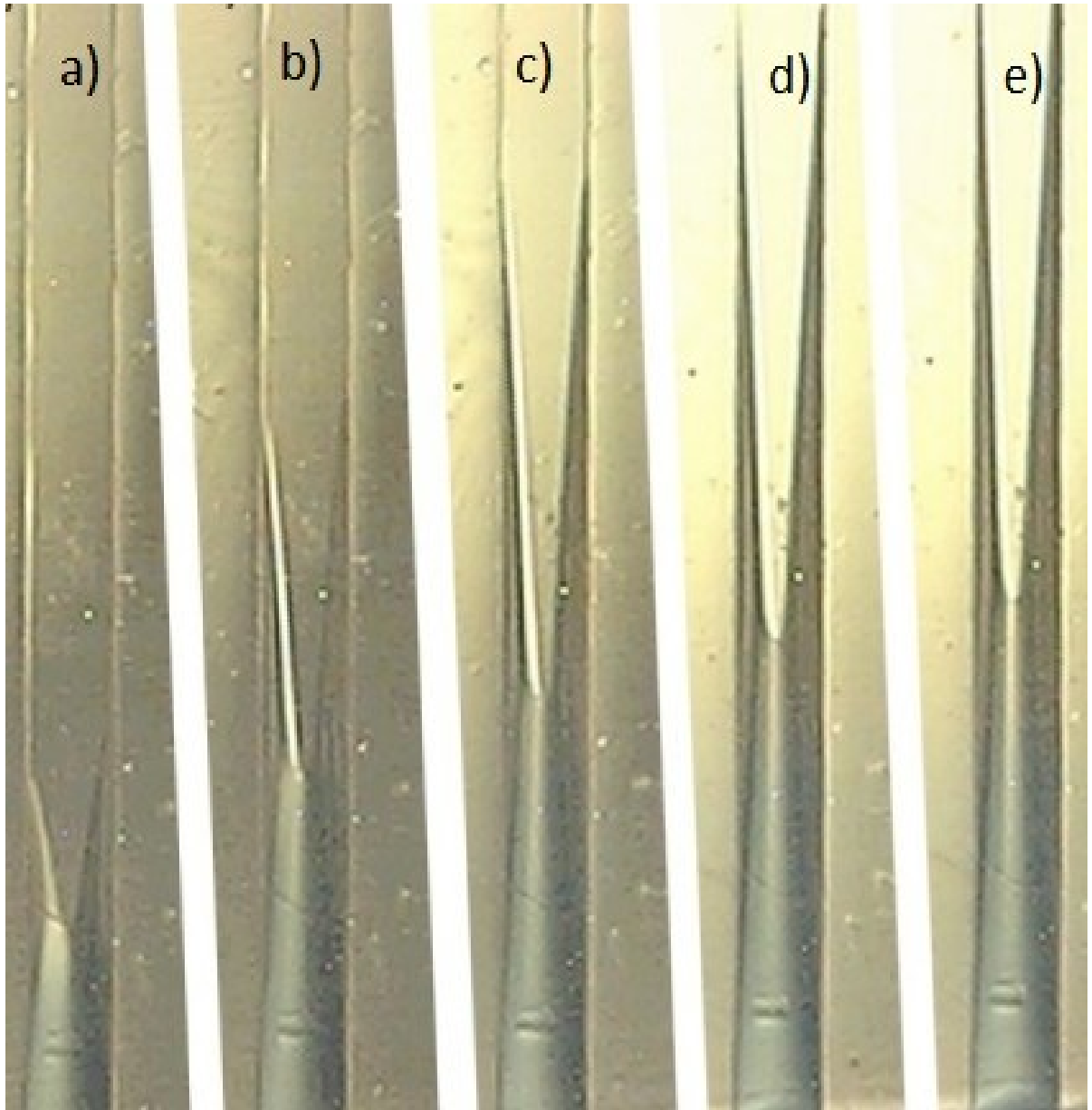
Fig. 5.4   *Liquid finger size and shape in 600μm wide and 135μm deep plane micro channel at a) 3.5 sec, b) 9.5 sec, c) 15.5 sec, c) 21.5 sec, d) 27.5 sec and e) 33.5 sec after PDMS oil of viscosity 48 mPas first enters the channel. The scale for this set of pictures is 45.6 pixels / mm. The length of the following channel is 10mm and the aspect ratio of the sample is 0.225.*

5.2.3 Finger Shape and Size of 135um Deep Channels:
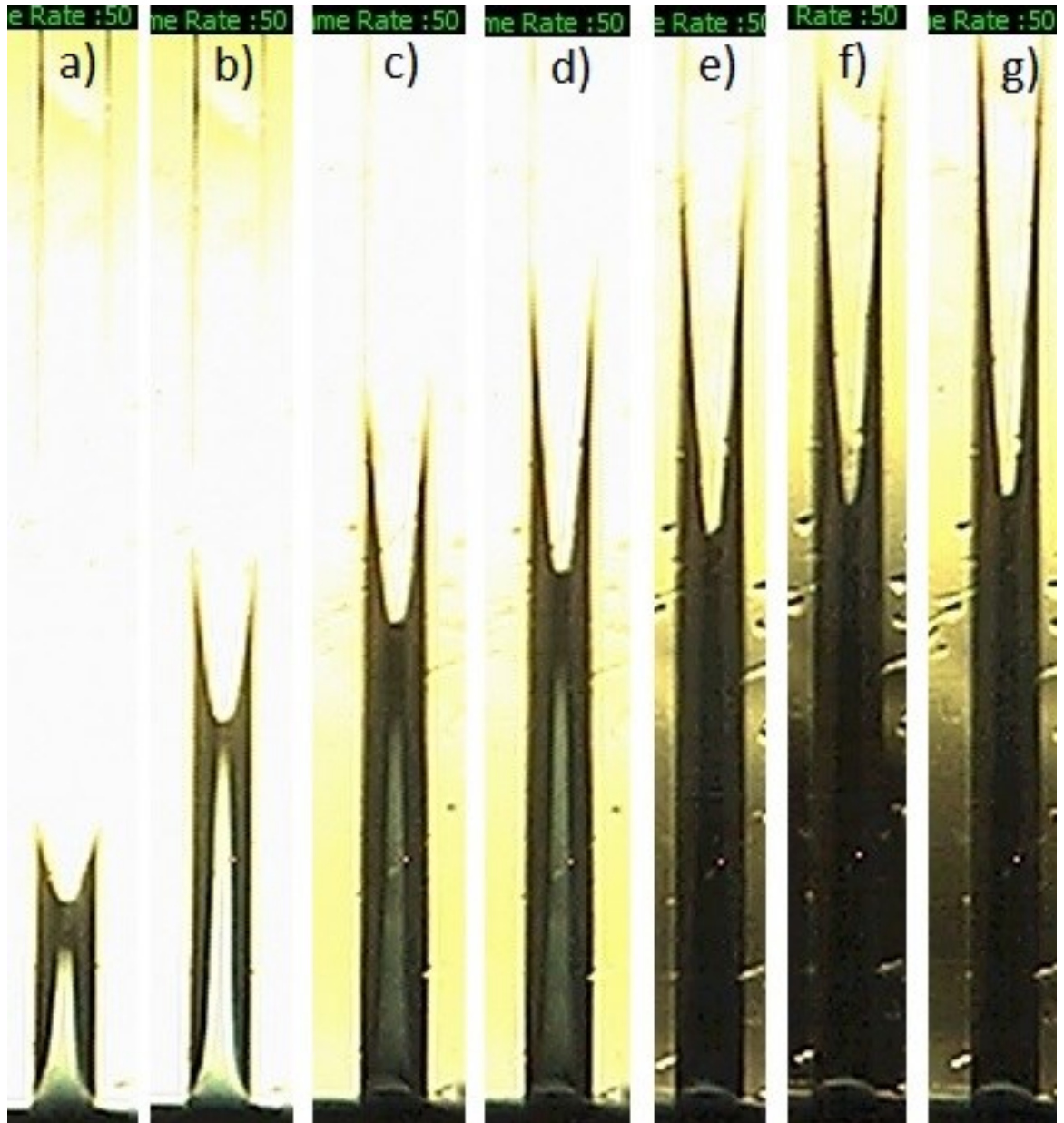
Fig. 5.5 *Liquid finger size and shape in 600μm wide and 350μm deep plane micro channel at a) 3.5 sec, b) 9.5 sec, c) 15.5 sec, c) 21.5 sec, d) 27.5 sec, e) 33.5 sec, f) 39.5 sec and g) 45.5 sec after PDMS oil of viscosity 48 mPas first enters the channel. The scale for this set of pictures is 57 pixels / mm. The length of the following channel is 50mm and the aspect ratio of the sample is 0.58.*

5.2.4   Finger Shape and size of 100um Deep Channels:

Fig. 5.6 gives the comparison of shape and size of liquid fingers in plane parallel open top SU8 micro channels of width ranging from 150 to 400µm. The depth of these channels was 100µm. It can be noted from Fig. 5.3 to 5.6 that finger size is largest in the shallowest channel with smallest aspect ratio. In deeper channels, liquid fingers become less prominent particularly at the initial stages of flow and the size of liquid fingers is negligibly small in the narrow channels with high aspect ratio.   The contrast of the image is not very good due to the light arrangement, especially setup to find the exact position of fingers.
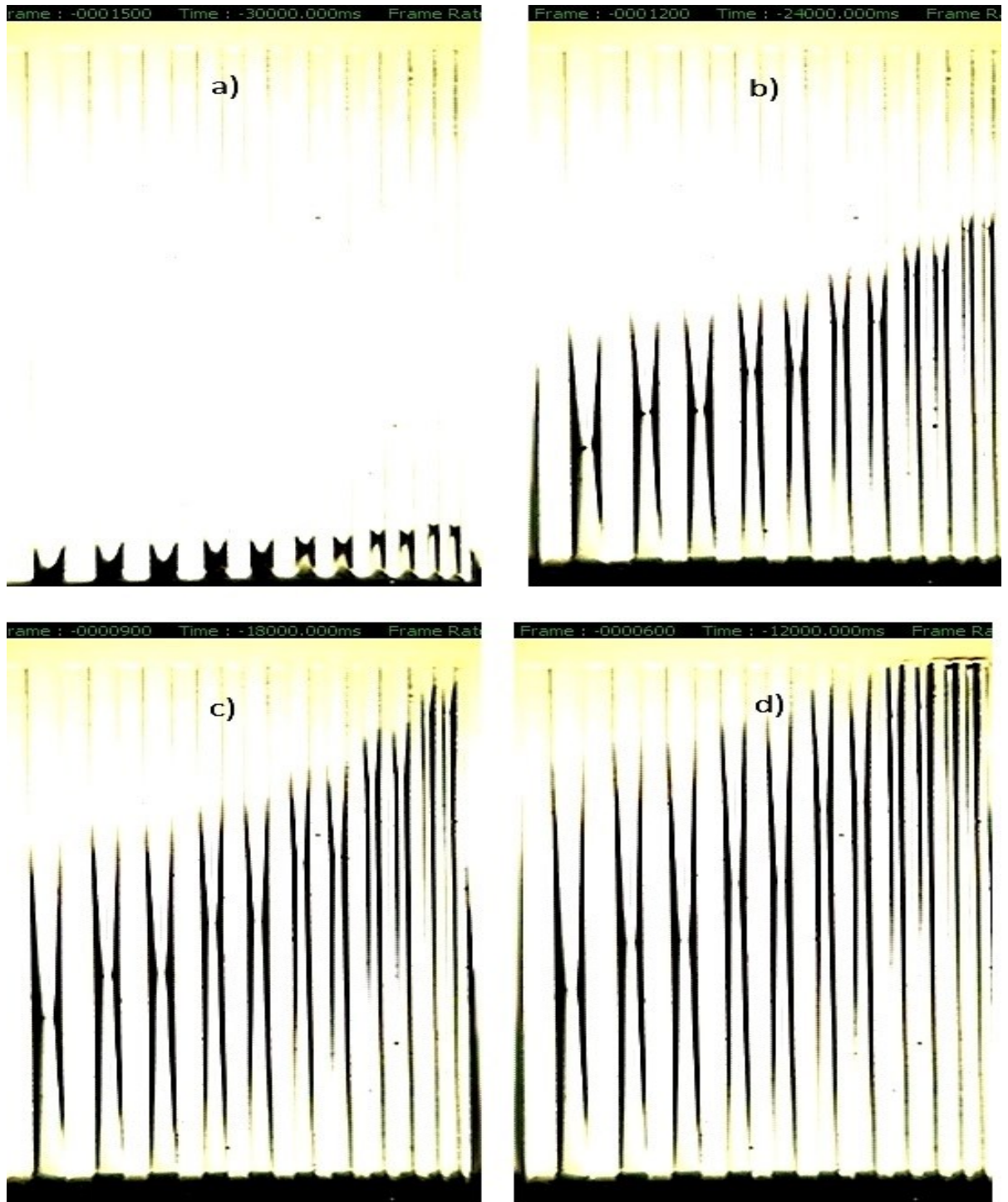
Fig. 5.6 *Liquid finger size and shape in 100μm deep having width from 150 to 400μm wide (from right to left) plane parallel micro channels at a) 0.6 sec, b) 6.6 sec, c) 12.6 sec, c) 18.6 sec and d) 24.6 sec after PDMS oil first enters the channel. The scale for this set of pictures is 46.4 pixels / mm. The length of the following channel is 10mm and the aspect ratio of the sample ranges from 0.4 to 0.67.*

5.3   Comparison of Finger and Meniscus Propagation

PDMS oil of viscosity 48 mPas was made to rise in SU8 open top plane micro channels having three different depths (100, 135 and 300μm) and three different widths of 150, 300 and 400μm. The effect of depth of channels having the same width and with the same viscosity of rising liquid was observed. It was also observed how three different widths of the micro channels having the same depth can effect on the capillary dynamics when PDMS oil of same viscosity rises in these micro channels.

Fig. 5.7 shows how capillary dynamics change when PDMS oil of viscosity 48 mPas rises in 400μm wide SU8 open top plane micro channels having three different depths of 100, 135 and 300μm.
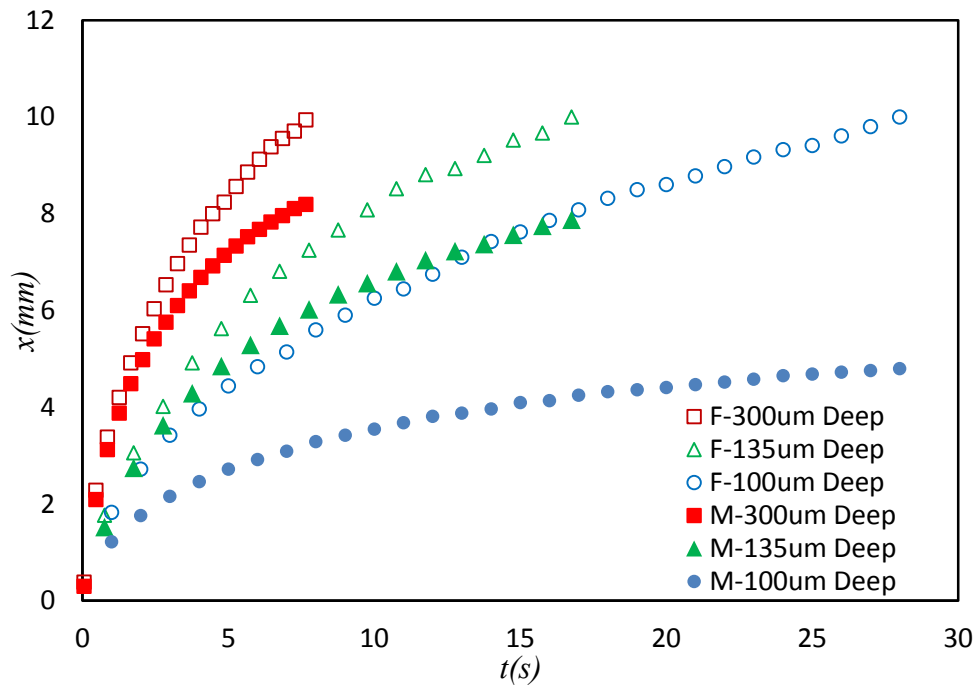
Fig. 5.7   *Effect of the channel depth on capillary rise of 48 mPas PDMS oil in 400μm wide channels. Solid filled symbols represent meniscus position and unfilled symbols indicate the finger position with time.*

It is clear from Fig. 5.7 that the liquid fingers rise in advance of main meniscus and the finger size increases with decreasing depth of micro channels. This shows that if a micro-channel of given width becomes deeper, the finger speed as compared to that of main meniscus decreases for a given viscosity of rising liquid.

Similarly, Fig. 5.8 indicates the effect of width of 100μm deep micro channels having widths of 150, 300 and 400μm and gives the comparison of liquid finger and main meniscus propagation with time.
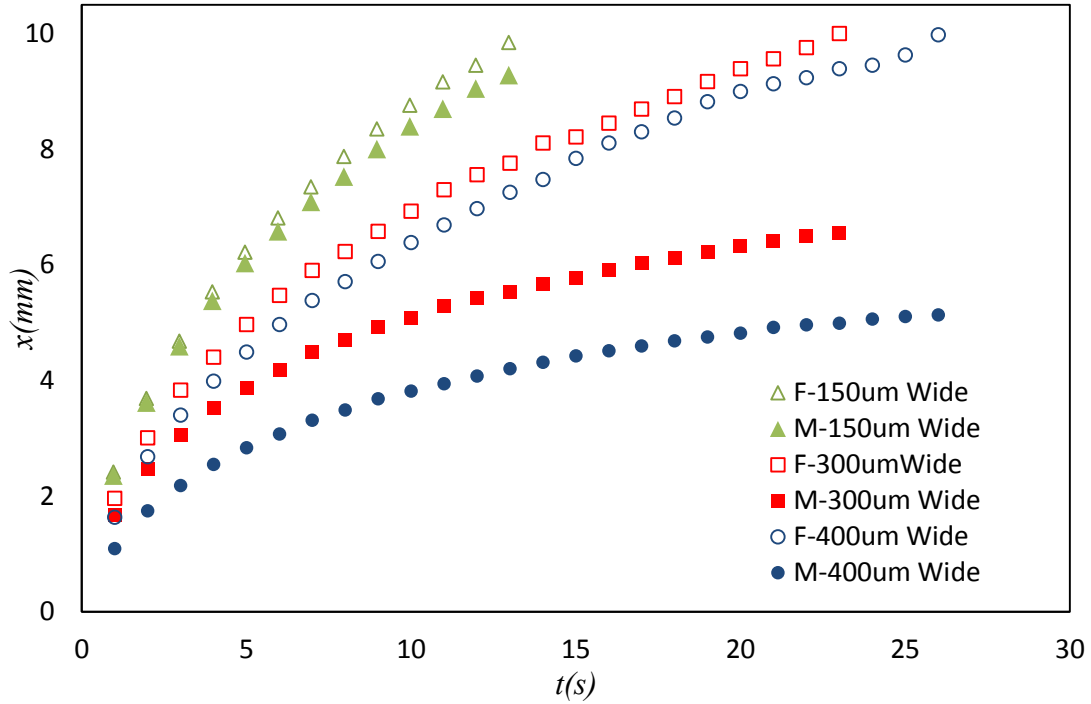
Fig. 5.8   *Effect of the channel width on capillary rise of 48 mPas PDMS oil in 100μm deep micro channels. Solid filled symbols represent meniscus position and unfilled symbols indicate the finger position with time.*

Fig. 5.8 indicates that for a given depth of a micro channel, the liquid finger speed compared to the speed of the meniscus increases with the increasing width of micro channel.

5.4   Finger Size

It has been observed that finger size Δx increases with time as the liquid rises in micro-channels. For the same experiments described by Fig. 5.7, the size of liquid fingers is indicated in Fig. 5.9, which shows that it gradually increases with time as it continues rising in plane SU8 open top micro channels. It also suggests that liquid fingers are more prominent and their size is greater in shallower micro channels, however, the size of fingers in 135μm and 300μm deep channels did not seem to follow

this trend at initial flow regime, but eventually their size is greater in 135μm deep channels at the later flow stages.
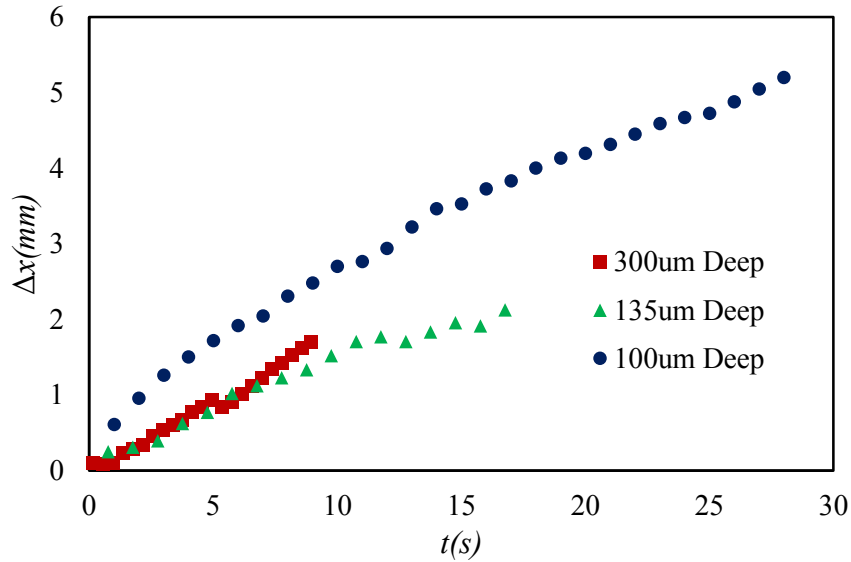
Fig. 5.9   *Effect of the channel depth on liquid finger size of 48 mPas PDMS oil in 400μm wide channels*

Similarly, for the same experiments described by Fig. 5.8, the size of liquid fingers are plotted in Fig. 5.10, which indicates that liquid fingers are more prominent and their size becomes greater when the width of micro channels increases.
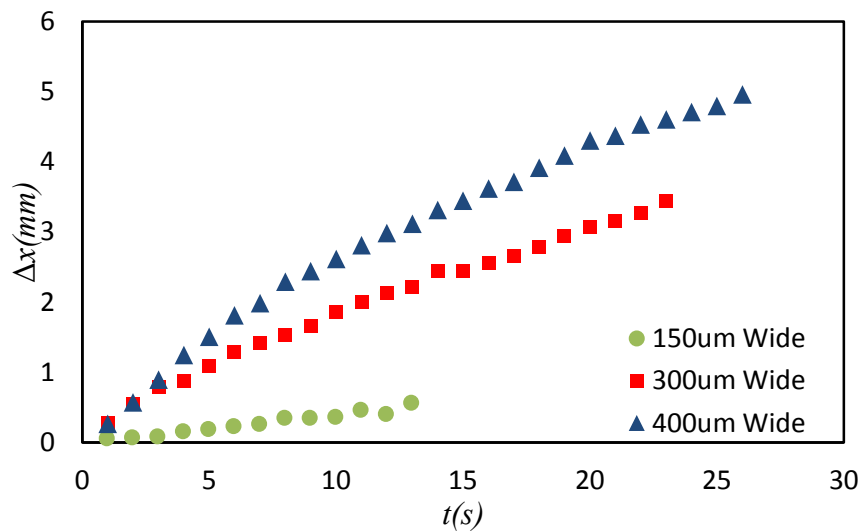
Fig. 5.10   *Effect of the channel width on finger size using 48 mPas PDMS oil in 100μm deep micro channels*

5.5 Analytical Solution of Capillary Dynamics with Prominent Fingers

A number of experiments were performed with open top rectangular plane SU8 micro channels of width 150, 300, 400 and 600μm. PDMS oil of viscosity 19.6, 48 and 96 mPas was used as rising liquid in these experiments.

It is to be noted that the channels with width 150 and 300μm were only 10mm long and the data for capillary rise was restricted to this height only. If the channels were longer than 10mm, more data could be collected for liquid fingers. The data from these experiments does not give the complete dynamics of capillary flow because of equilibrium height values are higher than 10mm for these micro channels, therefore, the analytical and numerical fitting of this data is not performed.

The data from 400 and 600μm open top micro channels with different aspect ratios responsible for variation in liquid finger shape and size, is fitted analytically to measure the deviation in fitting parameters '*a*' and '*b*'. The Table 5.1 shows the dimensions of micro-channels and the viscosity of the liquid used for the fitting of the data.

Channel Width, w (±5μm)	*PDMS Viscosity* (mPas)	*Channel Depth, h* (μm)	*Aspect Ratio* $\varepsilon = (h/w)$
400	50	100(±5)	0.250
		135(±5)	0.337
		350(±15)	0.875
600	48	100(±5)	0.167
		135(±5)	0.225
		350(±15)	0.584
	19.2	45(±5)	0.075
	48	45(±5)	0.075

Table 5.1 *Table of liquid viscosity values and micro-channel dimensions used for analytical fitting*

5.5.1 Analysis of 400µm Wide Micro Channels:

For 48 mPas PDMS in 400µm wide channels having depth of 100, 135 and 350µm, the data was fitted for meniscus propagation x using visco-gravitational solution and the viscous co-efficient 'a' (eq. 2.53) and the capillary term 'b' (eq. 2.54) (as discussed in section 2.9.2) were measured in each case.

Large deviation in the values of capillary term was observed for capillary rise in the shallower channels with prominent and larger liquid fingers. The shape and size of advancing fingers in these channels is already shown in fig. 5.6 and the comparison of meniscus and finger propagation in the same channel is shown by Fig. 5.7. The following Figs. 5.11 and 5.12 show visco-gravitaional fitting for the data when 48 mPas PDMS rises in 350µm and 100µm deep channels with aspect ratios of 0.87 and 0.25 respectively.
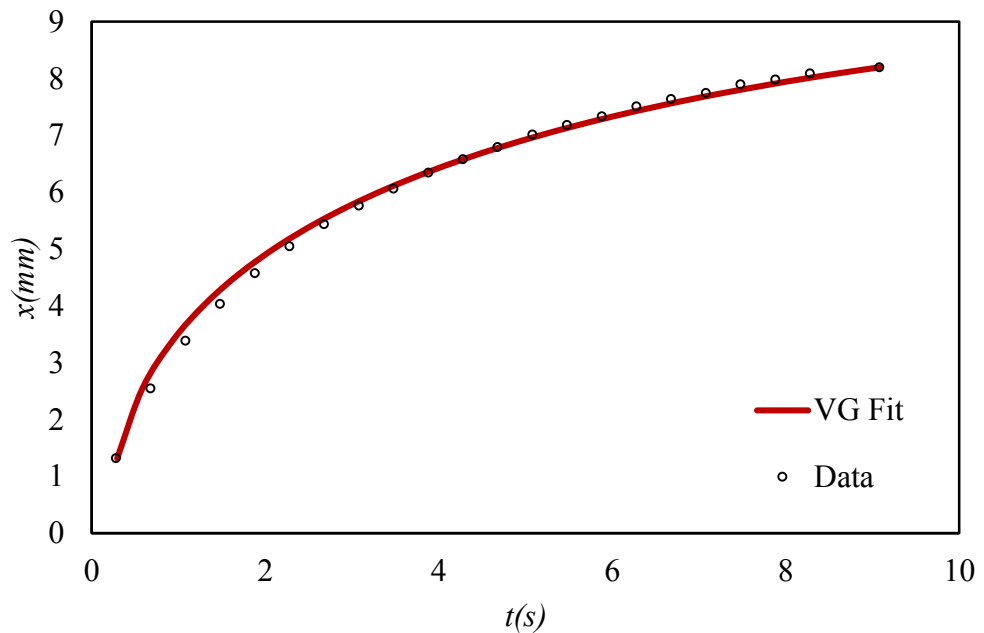
Fig. 5.11 *Red solid line represents visco-gravitational fit and black circles shows actual data points for meniscus position with time of PDMS 48 mPas rise in 400µm wide and 350µm deep plane open top micro-channel*
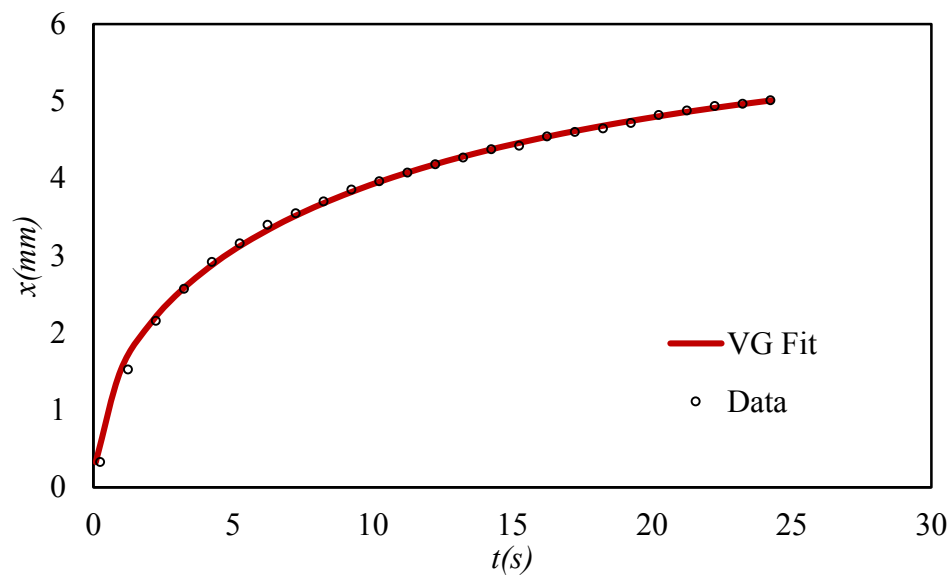
Fig. 5.12 *Red solid line represents visco-gravitational fit and black circles shows actual data points for meniscus position with time of PDMS 48 mPas rise in 400μm wide and 100μm deep plane open top micro channels*

Table 5.2 gives the results from experiments with 400μm wide open channels for three different widths using 48 mPa.s PDMS oil as rising liquid. The variation in the values of the capillary term '*b*' for different aspect ratios are given. It can be noted that for very shallow channels with small aspect ratio and very prominent liquid fingers, value of capillary term '*b*' decreases significantly, that shows very large reduction in equilibrium rise height consistent with the observation of Dong and Chatzis, 1995 and Bico and Quéré, 2002 for square capillaries.

Ch Depth (μm)	*Asp. Ratio ε*	*Predicted b (m/s)²*	*Fitted b (m/s)²*	*Fitted b / Predicted b*
350 ($\pm$ 20)	0.87($\pm$ 0.12)	10.1 x 10^{+4}	9.76 x 10^{+4}	0.97 ($\pm$ 0.08)
135 ($\pm$ 5)	0.33($\pm$ 0.03)	9.92 x 10^{+4}	9.44 x 10^{+4}	0.95 ($\pm$ 0.01)
100 ($\pm$ 5)	0.25($\pm$ 0.03)	9.84 x 10^{+4}	5.78 x 10^{+4}	0.59 ($\pm$ 0.14)

Table 5.2 *Variation in capillary term 'b' for micro channels with different aspect ratios in 400μm wide open channels shows that liquid fingers reduce the equilibrium height significantly.*

The decrease in the fitted value of '*b*' indicates the reduction in equilibrium rise height as $x_e = \dfrac{b}{g}$ (Ouali et al., 2013) where *g* is acceleration due to gravity. This deviation may be attributed to the presence of thicker and larger liquid fingers as reported by Bico and Quéré (2002) for square capillaries that liquid rising along the internal edges against gravity in advance of the central meniscus, which itself rises to an equilibrium height which is found to be less than would be the case without the fingers.

The results for the fitted values of the viscous term '*a*' are listed in Table 5.3 which indicates the deviation of the fitted values from the values predicted by visco-gravitational approximation. For 350μm deep channels, its value is found to be more than that for 135μm, which may be attributed to more viscous friction the liquid has to face during its flow due to larger surface area. Increasing frictional dissipation of the rising liquid gives rise to a possible retardation co-efficient (Hamdaoui and Nylander, 2002).

Ch Depth (μm)	*Asp. Ratio* ε	*Predicted a* (s⁻¹)	*Fitted a* (s⁻¹)	*Fitted a / Predicted a*
350 (± 20)	0.87(± 0.06)	5847	8656.40	1.48 (±0.03)
135 (± 5)	0.33(± 0.01)	21300	18538.62	0.93 (±0.03)
100 (± 5)	0.25(± 0.01)	21400	41588.22	2.03 (±0.10)

Table 5.3 *Variation in viscous term 'a' for micro channels with different aspect ratios when 48 mPas PDMS rises in 400μm wide open channels.*

It can be noted that compared to its predicted value by visco-gravitational model, the fitted value of '*a*' was found to be greater for 100μm deep channels than that for 135μm deep channels. The possible reason for the variation in '*a*' may be attributed to the critical angle effect i.e. according to eq. (2.59), the filling condition must be satisfied in order to have $f_{cap} > 0$ and the *b* parameter in eq. (2.42) must be positive. In shallower channels, the critical angle is reduced significantly. It is assumed that dynamic contact angle becomes greater than 0º and approaches the value of critical angle the moment the liquid enters the channels with small aspect ratios. This causes

reduction in the capillary pull and greater viscous retardation and it may be possible that the visco-gravitational approximation is not applicable in this case. It may be assumed that because of this reason 100µm deep channels with aspect ratio of 0.25, when equilibrium height was observed to be almost 40% less than the expected value, the fitted value of viscous co-efficient '*a*' was found to be even greater than that for 135 and 350µm deep channels. It can also be noted that for 135µm deep channels, the fitted value of '*a*' and '*b*' are in agreement with the results presented in chapter 4 (section 4.3.4).

5.5.2   Analysis of 600µm Wide Micro Channels:

For 600µm wide open top plane micro channels, visco-gravitational fitting was also performed for three different depths and three different viscosities of PDMS oil (as indicated in Table 5.2). The following Fig. 5.13 and 5.14 show visco-gravitational fitting for 350µm and 135µm deep micro channels respectively when 96 mPa.s PDMS oil was made to rise in these channels. The black circles and red solid line represent actual data points and visco-gravitational fit respectively.
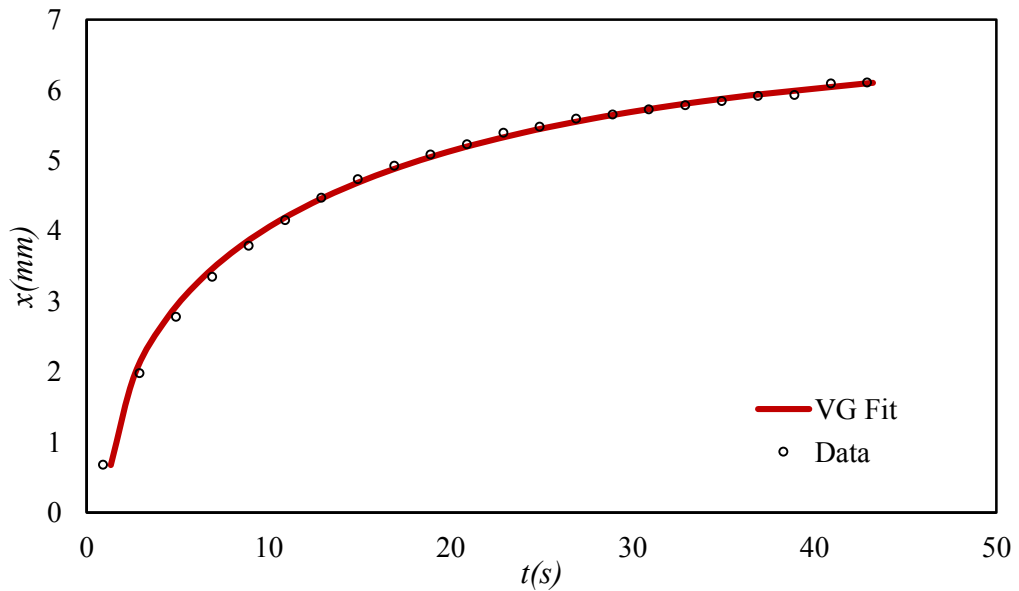
Fig. 5.13   *Capillary rise of PDMS 96 mPas in 600µm wide and 350µm deep plane open top micro channel. Red solid line represents Visco-Gravitational fit and black circles shows actual data points for meniscus position with time.*
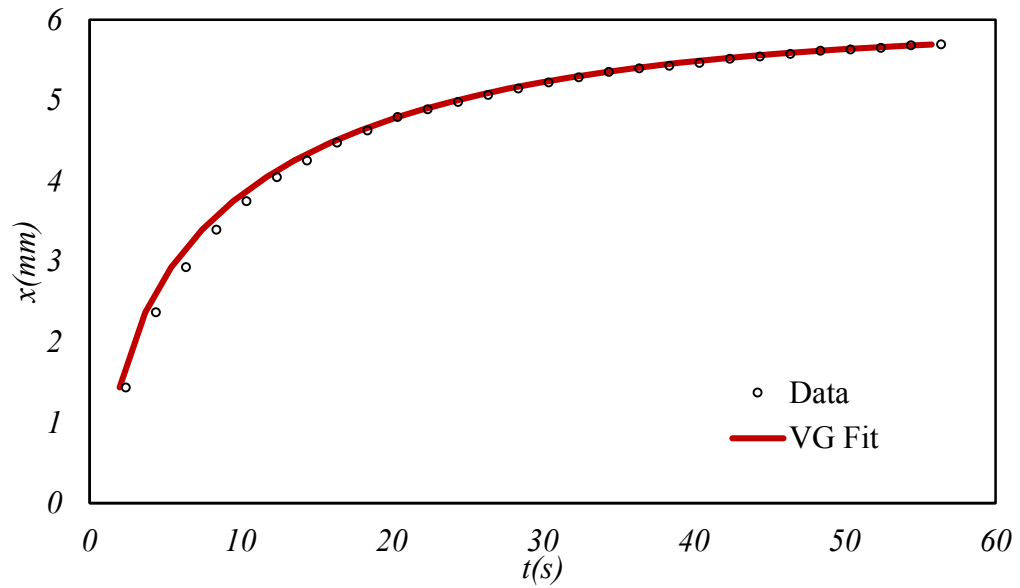
Fig. 5.14   *Capillary rise of PDMS 96 mPas in 600µm wide and 135µm deep plane open top micro channel. Red solid line represents Visco-Gravitational fit and black circles shows actual data points*

The results for other viscosities and different aspect ratios are given in Table 5.4. It is assumed that large deviation in the value of capillary term '*b*' is attributed to advancing liquid fingers, particularly when the liquid rises in wider and shallower micro channels with very small aspect ratio e.g. 0.075 where equilibrium rise height reduces to 0.16 times its predicted value. The other possible reason is critical angle effect already discussed in section 5.5.1.

Viscosity (mPas)	Ch. Depth (µm)	Asp. Ratio ε	Predicted b (mm/s)²	Fitted b b (mm/s)²	Fitted b / Predicted b
96	350 (± 20)	0.58(± 0.03)	66810.28	62210.16	0.93 (± 0.02)
96	135 (± 5)	0.23(± 0.01)	65384.50	57299.57	0.88 (± 0.01)
96	45 (± 5)	0.08(± 0.01)	9105.30	61495.3	0.15 (± 0.02)
48	45 (± 5)	0.08(± 0.01)	9910.43	60448.96	0.16 (± 0.03)
19.2	45 (± 5)	0.08(± 0.01)	9603.74	60312.01	0.16 (± 0.03)

Table 5.4   *Variation in capillary term 'b' for micro channels shows that liquid fingers reduce the equilibrium height significantly in 600µm wide plane micro channels with different aspect ratios.*

110

Similarly, the following Table 5.5 lists the results for fitted values of the viscous term compared to its value predicted by visco-gravitational model for different aspect ratios and viscosities.

Viscosity (mPas)	Ch. Depth (μm)	Asp. Ratio ε	Predicted a (s⁻¹)	Fitted a (s⁻¹)	Fitted a / Predicted a
96	350 (± 20)	0.58(± 0.03)	7300(± 270)	34600(± 2400)	4.74
96	135 (± 5)	0.23(± 0.01)	22401(± 79)	38400(± 800)	1.71
96	45 (± 5)	0.08(± 0.01)	159000(± 35000)	128000(± 7200)	0.81
48	45 (± 5)	0.08(± 0.01)	80000(± 17000)	86300(± 6700)	1.09
19.2	45 (± 5)	0.08(± 0.01)	31800(± 6900)	35800(± 2500)	1.12

Table 5.5 *Variation in capillary term 'a' for 600μm wide plane walled micro channels with different aspect ratios when PDMS of three different viscosities rises in them.*

It can be seen from Table 5.5 that the ratio of fitted 'a' to its predicted value for 350μm deep channel is greatest indicating more viscous dissipation, whereas its value for very small aspect ratio of 0.075 becomes greater than that for 0.225. The reason may be the critical angle effect (already discussed in section 5.5.1).

It is to be noted that the fitting analysis for the meniscus was performed instead of finger position as the fingers continue to rise along the channel walls and eventually exit the other end of the channel and this restricted its rising motion further along the channel walls and the complete dynamics of the fingers could not be measured.

5.6   Speed of Liquid Fingers

The speed with which liquid fingers advance along the edges of non-circular capillaries, decays with time. It has been found that it decays to $t^{1/2}$ in the long time

limit. Fig. 5.15 shows the relationship between velocity and time of 96 mPas PDMS rising in 600μm wide open top micro channels having depth of 45, 135 and 350μm.
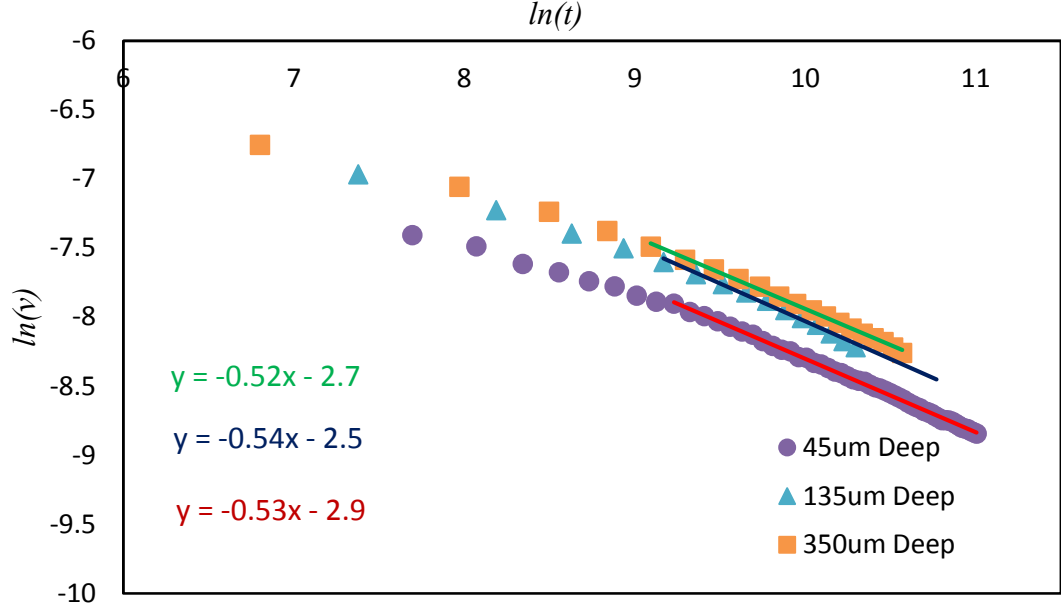
Fig. 5.15   *Finger velocity in 600 μm wide and 45, 135 and 350μm deep channels. Reduction in finger speed with time found to be proportional to $t^{1/2}$*

Linear regression was performed in MS Excel to the above data to find the relationship of finger velocity with time. For 45, 135 and 350μm deep channels, the relationship is found to be:

$$\text{ℓn}(v) = (-0.52 \pm 0.01)\text{ℓn}(t) + (-2.70 \pm 0.07) \qquad (5.1)$$

$$\text{ℓn}(v) = (-0.54 \pm 0.02)\text{ℓn}(t) + (-2.56 \pm 0.17) \qquad (5.2)$$

$$\text{ℓn}(v) = (-0.53 \pm 0.00)\text{ℓn}(t) + (-2.98 \pm 0.03) \qquad (5.3)$$

The decay in the velocity is found to be proportional to the square root of the time, which is found to be consistent with the literature [Ponomarenko *et al.*, 2011]

5.4   Summary

In non-circular capillaries, i.e. square closed glass tubes and rectangular cross-sectional SU8 open top micro channels, imbibition of wetting liquid is observed in the

form of fingers along all the corners of capillaries where its sides meet at 90° with each other. The shape and size of these liquid fingers depend upon the physical dimensions of the capillaries.

In the case of square closed glass tube, i.e. when ε = 1, liquid fingers were found to be very thin and advanced along all the four corners of the tube. It has been observed that these fingers were very prominent and very fast in speed as compared to the main meniscus propagation in SU8 open top micro channels, particularly when the aspect ratio of the channels had very small value. Finger propagation followed the same manner as that of main meniscus but with much faster speed. Their size was observed to be increased gradually with time. The effect of different factors, e.g. capillary dimensions and viscosity of liquid, on the propagation of fingers was the in a similar way as on main meniscus. Velocity of these fingers reduced with time similar to the main meniscus propagation.

The capillary dynamics of vertically held open top micro channels in which the liquid fingers were found to be very prominent was studied. The data from these channel experiments was analysed using visco-gravitational approximation and it has been found that for capillary rise in channels with very thick and larger liquid fingers, the capillary term 'b' was reduced significantly. It is assumed that these fingers may attribute to the reduction in the value of 'b' and, therefore, in the equilibrium rise height.
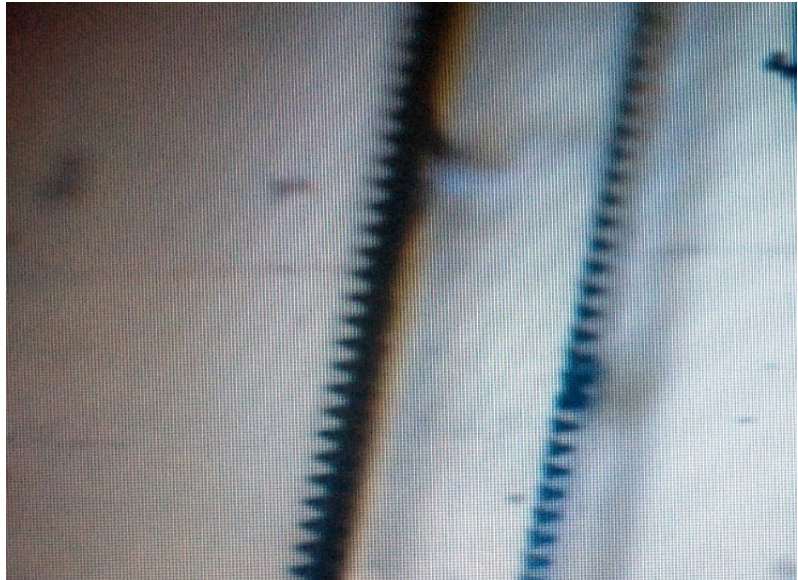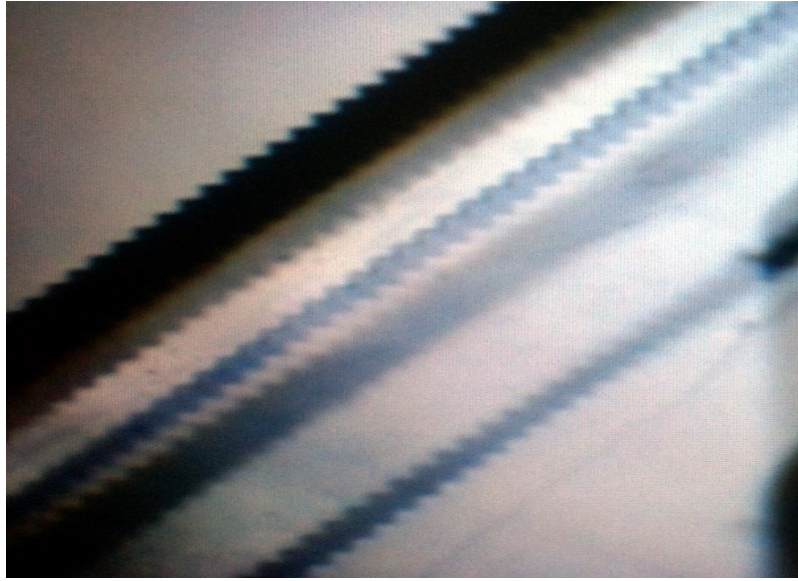
6   Capillarity in Open Top Rough SU8 Micro Channels

6.1 Introduction

Liquid and its interaction with solid surfaces are very important in the scientific subjects of biology, chemistry and physics and the applied and technological subjects of materials science and engineering. To control that interaction, surface chemistry can be used to alter the molecularly determined hydrophobic/hydrophilic properties of the surface (Vogler, 2001). Whilst surface chemistry can cause a droplet of liquid to spread into a film on a particular smooth and flat solid surface, there are many liquids for which a droplet will only partially spread on the same surface. However, if the solid surface is rough or topographically structured on a suitably small length scale the extra surface area can amplify the spreading tendency of a liquid so that it is drawn completely into a film rather than remaining as a partially wetting droplet (McHale, 2004; Aqil, 2006). This type of induced wetting is also known as *hemi-wicking* (Shirtcliffe, 2005).

The flow of liquids can be controlled using differently structured micro-channels using lithographic techniques. If a plane open top micro-channel is brought into contact with a fluid, and the contact angle between the surface and the fluid, θ_e, is less than 90°, the fluid will move into the channel and the rise height depends upon the density and surface tension of fluid, (already discussed in section 2.1). This is the well-known process of capillary filling. These experiments and the detailed analysis of the corresponding results are presented in chapter 4. However, if there are obstacles to the flow, such as micron-scale ridges or posts on the surface, the advancing front can pin for contact angles greater than a certain threshold value ($\theta_{tr} < 90°$), thus halting the filling. It is also possible that far from acting as obstacles, if the additional surface area is wetting/hydrophilic, the effect can be to reduce the threshold value of the contact angle. Moreover, the rate of rise of liquid within a capillary tube, which is usually described by the Lucas-Washburn law (de Gennes, Brochard-Wyart, & Quéré, 2004; Gast., 1997; Dreyer, 2008), can also be expected to be modified (Quéré, 2003; Quéré., 2008).

In this chapter, for the experiments with rough channels, the same video microscopic system is used as that for SU8 plane open top micro channels and glass tubes (Section 3.6) to study the effect of the feature height and alignment of faces of features on faceting shapes of droplets and films. Rough microfluidic channels are

created and capillary penetration and fluid flow is studied. Investigations on the flow behaviour of PDMS oils of various viscosities is carried out using open top SU8 micro channels 400 and 600(±5) μm wide and 300 to 350(±20) μm deep held vertically. The data from a series of experiments is analysed comparing the results to the visco-gravitational capillary model. The deviation of the fitted capillary term 'b' from its predicted value is measured and it is found to be greater in the channels having greater roughness factor values.

6.2 Capillary Rise in Rough Micro Channels

Recalling equation (2.5) which gives the general expression for capillary action,

$$\frac{1}{2}\frac{d}{dt}\left(\frac{dx}{dt}^2\right) = b - gx - ax\left(\frac{dx}{dt}\right) \tag{2.5}$$

here x is the position of liquid meniscus at any time t and a and b are the viscous and capillary terms respectively. In the open top micro channels, the viscous term is given by eq. (2.25),

$$a = \frac{3\eta}{\rho h^2 \zeta_o(\varepsilon)} \tag{2.25}$$

If the channel has smooth walls and bottom surface, then $b = b_s$ and is given by eq. (2.35),

$$b_S = \gamma_{LV}\left[-1 + \cos\theta_e(1 + 2\varepsilon)\right]/\rho h \tag{2.35}$$

In the case of open top rectangular micro channel with smooth bottom surface and two side walls with the same roughness i.e. $r_L = r_R = r$. The contact angle with smooth bottom surface is θ_e, and that with the left and right hand side to the channel is the same Wenzel's angle θ_W (assuming that we have a Wenzel state), then the values of the capillary term b is given by eq. (2.36),

$$b = \frac{\gamma_{LV}}{\rho h}\left[-1 + \cos\theta_e + 2\varepsilon\cos\theta_W\right] \tag{2.36}$$

116

where Wenzel's angle is related to Young's angle as $\cos \theta_W = r \cos \theta_e$, using this value in the above eq. (2.36) and writing it as b_r,

$$b_r = \frac{\gamma_{LV}}{\rho h}\left[-1 + \cos \theta_e (1 + 2r\varepsilon)\right] \tag{6.1}$$

It is clear from the above expression that for wetting liquids, presence of roughness on the wall surface causes the decrease in the value of contact angle, which gives the larger value of b, i.e. $b_r \rangle b_s$. Using the expression $x_e = \dfrac{b}{g}$, the above equation becomes,

$$(x_e)_r = \frac{\gamma_{LV}}{\rho g h}\left[-1 + \cos \theta_e (1 + 2r\varepsilon)\right] \tag{6.2}$$

Therefore, enhanced capillary force is exerted on rising liquid due to which the value of equilibrium height x_e increases linearly with r in rough channels. It is to be noted that the viscous term 'a' is independent of wall roughness.

In order to test the effect of roughness on the capillary flow, SU8 open top rectangular micro channels were fabricated with various roughness factors in the form of triangular steps on channel walls. In the next section, physical parameters are discussed for the experimental setup used.

6.3 Roughness Feature Details:

In order to investigate the effect of roughness on the imbibition in rectangular open top micro channels, rough features were introduced on the side walls of the channels in the form of triangular steps. These steps were identical in shape and in every step the base length was kept constant as shown in Fig. 6.1. The roughness factor is calculated using the formula already discussed in section 3.2.2;
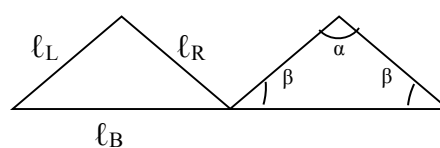
$$r = (\ell_L + \ell_R) / \ell_B$$

$$= 2\ell / \ell_B \qquad\qquad (\text{as } \ell_L = \ell_R = \ell)$$

Fig. 6.1 *Steps of one of the two walls of the sample channel*

The samples used in the experiments were fabricated from mask 4 as discussed in section 3.12 and shown in Fig. 3.12. The base length of each step ℓ_B was set to be 110µm. The length of the two other sides ℓ_L and ℓ_R was taken to be of same value in each step of one channel of a specific roughness factor. The roughness factors of all the channels were set to be 1, 1.2, 1.4, 1.6 and 3.

A plane walled or smooth channel has a roughness factor of 1. For the channels to have roughness factor of 1.2, ℓ was calculated as;

$$r = 2\ell / \ell_B$$
$$1.2 = 2\ell / 110\mu m$$
$$\ell = 66\mu m$$

Similarly for roughness factors 1.4, 1.6 and 3, ℓ is calculated to be 77, 88 and 165µm respectively. β is the angle that the sides ℓ_L and ℓ_R made with base of the triangle. The vertex angle of the triangular step α depends upon the length ℓ. Fig. 6.2 shows the view from above of an open channel with roughness factor of 1.2 and width 600µm.
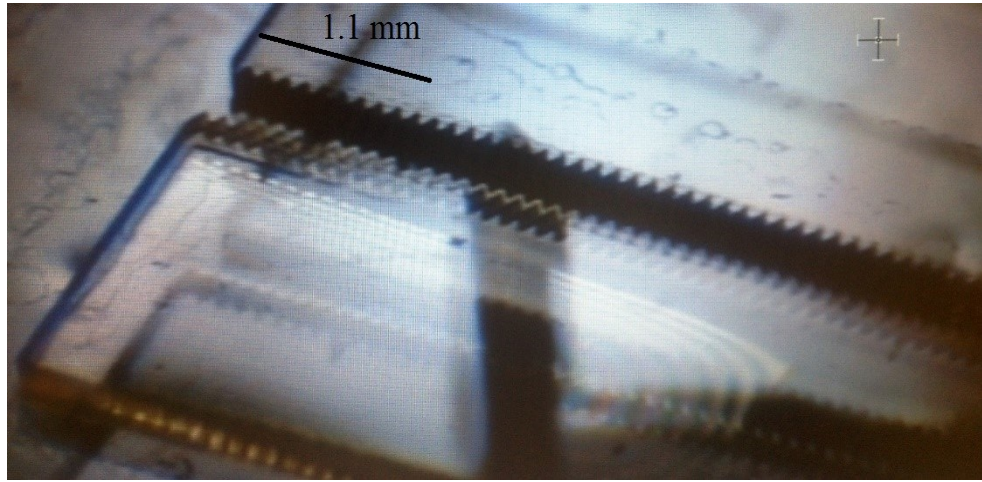
Fig. 6.2   *View from above of an open top rectangular SU8 micro channel with roughness factor of 1.2*

The other samples used were fabricated by using mask 6 (Section 2.3.5) having roughness factor of 1, 1.5, 2 and 2.5 and widths 400 and 600µm and for these roughness factors, the length ℓ is calculated to be 82.5, 110 and 137.5µm respectively. The base length ℓ_B is kept the same as in previous mask i.e. 110µm.

Channel Dimensions and Roughness Features:

Physical dimensions of SU8 open top channels were prepared with roughness features on their side walls in the form of symmetric and periodic triangular steps as shown in Fig. 3.8. The following Table 6.1 shows the channel dimensions and the liquids used.

| Channel Width	400 (±5)µm and 600(±5)µm
Channel Height	300(±15)µm and 350(±15)µm
Liquid	PDMS of viscosity 19.2, 48 and 96 mPas
Roughness factors	1.0, 1.2, 1.4, 1.5, 1.6, 2.0, 2.5, 3.0

Table 6.1 *Table of physical parameters used to investigate capillarity in rough micro channels*

6.4   Experimental Setup

The experimental setup was similar to that used for glass tubes and plane channels shown already in Fig. 3.18 in section 3.6, i.e. samples were held vertical and the liquid reservoir was raised up until liquid surface just came into contact with the lower edges of the channels.

6.5   Results and Discussions

The liquids used to investigate capillary rise in vertically held SU8 open top parallel rough micro channels was PDMS oils of three different viscosity values i.e. 19.2, 48 and 96 mPas. PDMS oil has very low contact angle with SU8 which approaches 0º.

6.5.1   Roughness Effect on Capillary Rise using PDMS Oil

Experiments were performed with 600µm wide and 300µm deep parallel rough micro channels having roughness factor of 1.0, 1.2, 1.4, 1.6 and 3.0. One of the samples used is shown in Fig. 6.3 where roughness factors are 3.0, 1.6, 1.4, 1.2 and 1.0 from left to right. PDMS oil of viscosity 96 mPa.s was used the rising liquid. As $\theta_e = 0º$ for PDMS oils, $b_r \propto r$.
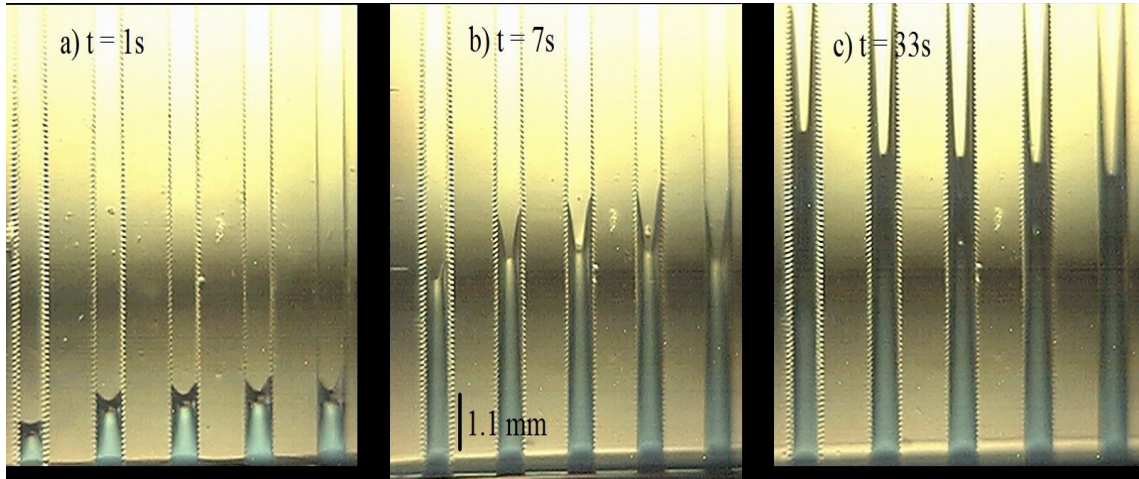
Fig. 6.3   *Different stages of flow of PDMS oil 96 mPas in 600μm wide and 300 μm deep open channels with gradually increasing roughness factor (r=3.0, 1.6, 1.4, 1.2 and 1.0 from left to right)*
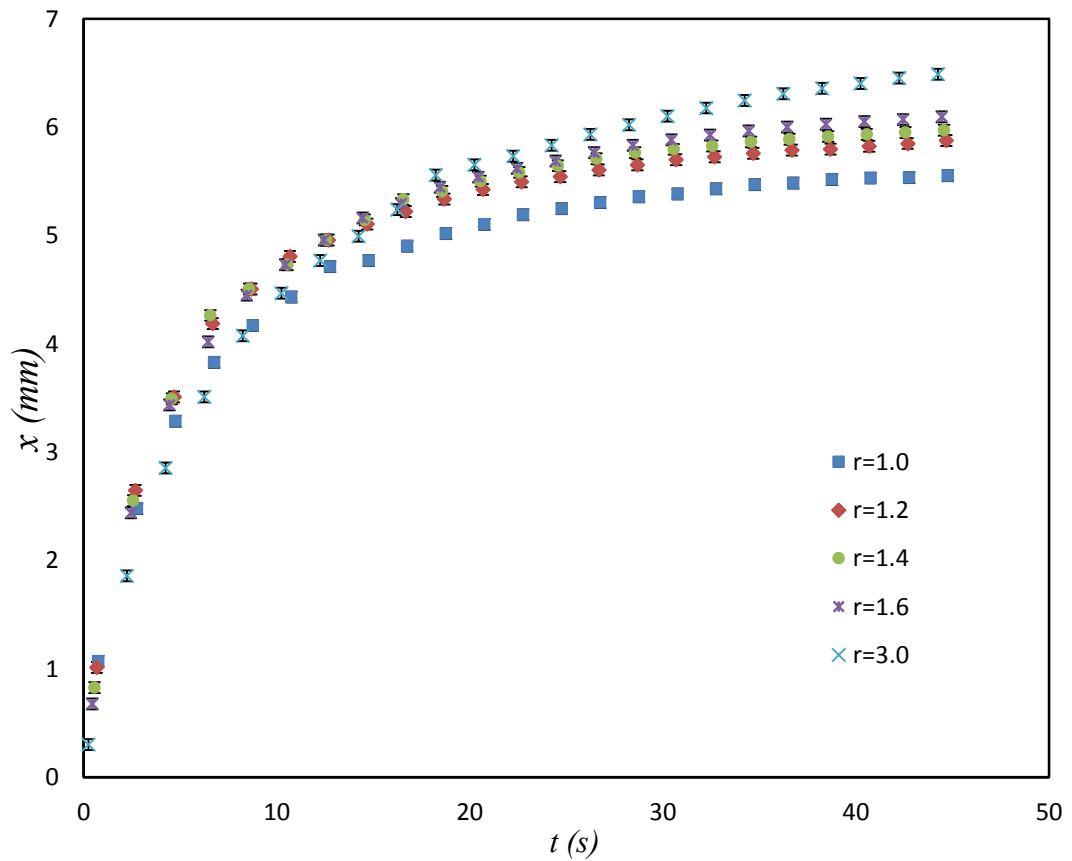
Fig. 6.4   *Effect of roughness on capillary rise of 96 mPas PDMS in 600μm wide and 300μm deep rough channels with roughness factors 1.0, 1.2, 1.4, 1.6 and 3.0*

Fig. 6.4 shows the position of advancing meniscus with time in five parallel channels with gradually increasing roughness factors from 1.0 to 3.0. It can be clearly seen that final height is increased in the channels with increasing roughness thus supporting the argument of an increased capillary force due to increased b with roughness, although not as much as predicted by eq. 6.2. The final heights shown in Fig. 6.4 do not represent equilibrium height. After measuring final height, a snapshot of the capillary flow after every 5 minutes was taken until it gave a constant final height value, which was taken as equilibrium height. The comparison of expected (according to eq. 6.2) and observed equilibrium heights of 96 mPas PDMS oil in 600μm wide and 300μm deep micro channels with roughness factors from 1.0 to 3.0 is shown in Fig. 6.5.
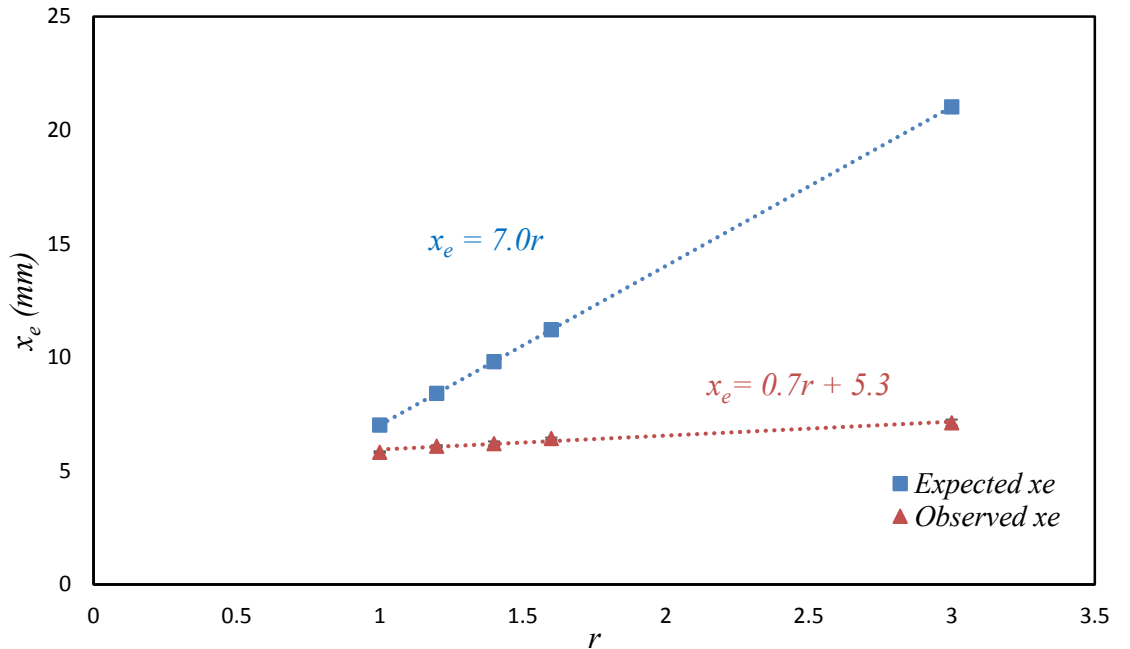
Fig. 6.5   *Comparison of expected and observed equilibrium height of 96 mPas PDMS oil in 600μm wide and 300μm deep micro channels with roughness factors from 1 to 3.*

The sample channels for these experiments were fabricated by using mask 4. The variation in equilibrium height x_e for a particular value of roughness factor r shown by error bars is attributed to the variation in depth and width of sample channels from sample to sample which is unavoidable during fabrication process. It is clear from Fig. 6.5 that there is an increase in equilibrium height with increasing roughness of the

channels which is far less than expected equilibrium height. For 96 mPas PDMS to rise in the particular dimensions of the open top SU8 channels, the expected height should be almost 7 times the roughness factor of the channels, but the rate of rise of the observed equilibrium height was found to be only $1/10^{th}$ of its roughness factor with the intercept of 5.3 instead of zero, as shown by Fig. 6.5.

One of the possible reasons of the reduced equilibrium height compared to its predicted value may be the existence of these liquid fingers that advance along the roughness features and start to become larger in size at the later stage of flow. The liquid fingers were found to be thicker and smaller in size in the channels with the greater roughness. The reason for their smaller size maybe the larger surface area that liquid had to rise in channels with greater roughness. The other possible reason may be the limitation of the theoretical model used to analyse the data.

6.5.2   Visco-gravitational Fitting of PDMS Data:

The data for meniscus position with time, from the experiments discussed in section 6.5.1 was fitted using visco-gravitational approximation. The analysis for liquid fingers was not performed as these fingers advance far along the channel walls beyond the field of view of the microscopic setup which did not give enough points to cover the complete finger dynamics. The experimental data of the smooth channel with roughness factor of 1.2 and its fit is shown in Fig. 6.6.

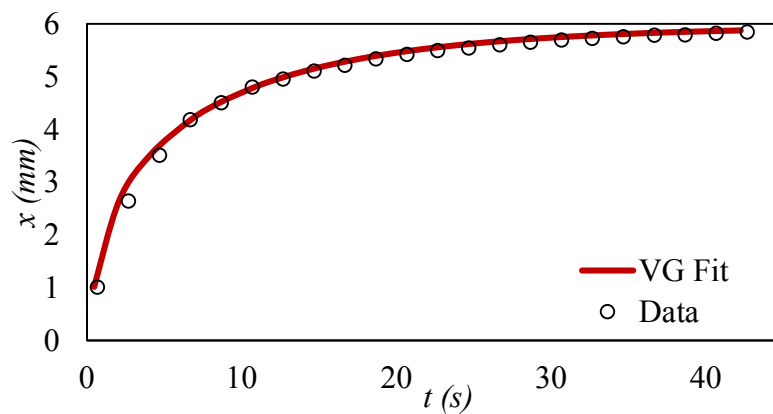**Fig. 6.6**   *Visco-gravitational fit (solid line) to the experimental data (solid symbols) when 96 mPas PDMS rises in 600μm wide and 300μm deep channel. Roughness factor of the channel was 1.2 and contact angle was taken to be 0º.*

The value of viscous co-efficient 'a' came out to be more than twice the predicted 'a' while the fitted value of the capillary term 'b' was found to be 0.72 times its theoretical value.

Similarly channels with roughness factor of 1.4, 1.6 and 3.0 were also analysed using visco-gravitational approximation. The results along with standard error are summarized in Table. 6.2 which gives the average deviation of the three repeat experiments in the values of viscous co-efficient 'a' and the capillary term 'b' with gradually increasing roughness factors in the 600μm wide and 300μm deep channels.

Roughness Factor	a (s^{-1})			b (m/s)^2		
r	Predicted	Fitted	Fit/Predicted	Predicted	Fitted	Fit/Predicted
1	7917.68	23710 (±350)	3.00	0.07	0.0560 (±0.001)	0.82
1.2	7917.68	21410 (±510)	2.70	0.08	0.0590 (±0.001)	0.72
1.4	7917.68	22340 (±28)	2.82	0.10	0.0600 (±0.001)	0.63
1.6	7917.68	22000 (±2200)	2.79	0.11	0.0610 (±0.001)	0.56
3	7917.68	313420 (±130)	3.96	0.21	0.0680 (±0.001)	0.33

Table 6.2 *Variation in the values of viscous co-efficient 'a' and capillary term 'b' in 600μm wide and 300μm deep channels with gradually increasing roughness factor 'r'.*

The mean value of the ratio of fitted 'a' to the corresponding value of predicted 'a' is found to be 3.05. It is to be noted that the viscous term 'a' is independent of the roughness factor (eq. 2.42) but it does alter the value of the capillary term 'b' according to eq. (6.1). The average deviation in the fitted values of viscous term 'a' was found to be (±2.83%). It is most likely due to the channel thickness being a bit variable from sample to sample which is unavoidable during the fabrication process.

The greater values of fitted 'a' compared to their corresponding predicted value show that the actual rise of liquid is slower than the rate predicted by theory. One of the possible reasons of variation in the value of fitted 'a' maybe the effect of dynamic contact angle that liquid interface makes with the capillary walls as soon as it comes

into contact with the capillary. The other reason may be the increased frictional dissipation of the rising liquid (Hamdaoui et al., 2002).

Fig. 6.7(a) shows the comparison of the predicted and fitted values of the capillary term *b* increasing with roughness for the 600μm wide and 300μm deep open top parallel micro channels when PDMS of viscosity 96 mPas rises in them. Roughness factors of these channels were 1.0, 1.2, 1.4, 1.6 and 3.0. Fig. 6.7(b) is the closer look at the fitted values only.

(a)

(b)
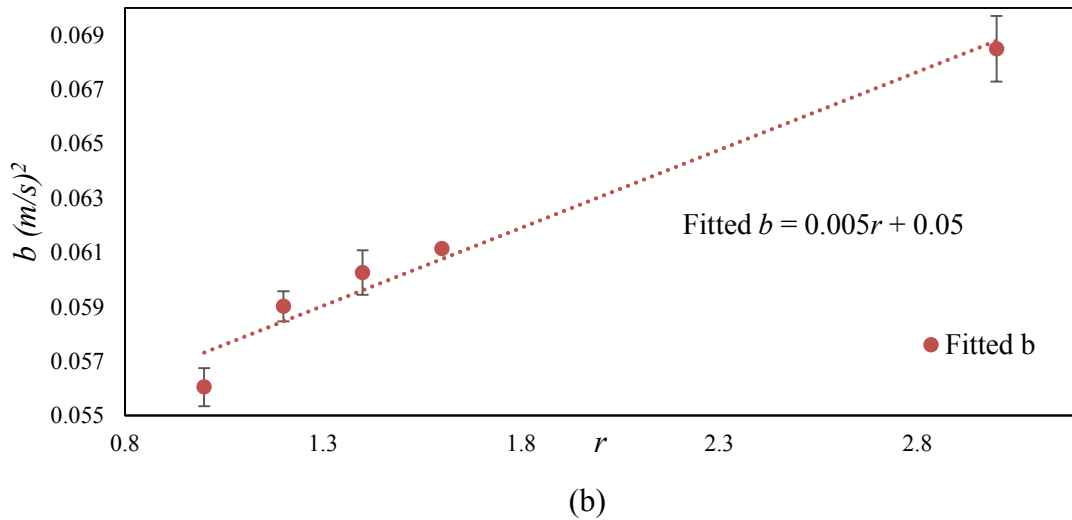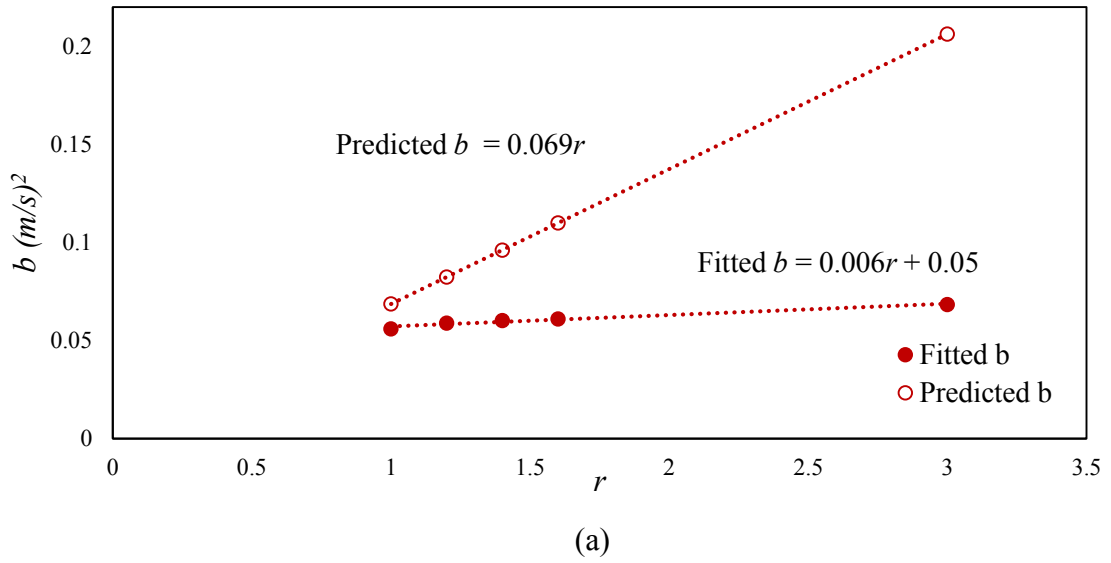
Fig. 6.7   (a) *Variation in the values of the capillary term 'b' in 600μm wide and 300μm deep channels with gradually increasing roughness factor 'r' when 96 mPas PDMS oil was used as rising liquid. (b) a closer look at fitted values.*

This graph in Fig. 6.7 indicates that the fitted value of the capillary term '*b*' increases with roughness but not as much as predicted by considering Wenzel angle. The measured equilibrium height values are found to be far less than the theoretical value in rough channels with larger roughness factor. Again this reduction in equilibrium height is due to the value of fitted '*b*' that came out to be almost 90% less than expected as roughness factor becomes greater. One of the possible reasons of this deviation of the value of fitted '*b*' from the predicted '*b*' may be the presence of liquid fingers which advance ahead of main meniscus along the roughness features of the channels as shown in Table 6.1, the stick-slip behaviour of liquid fingers (will be discussed later in section 6.7), or the limitation of the theory.

Another aspect of the results given in Fig. 6.7 is shown in Fig. 6.8 which gives the comparison between the ratio of fitted '*b*' when the walls are rough to the fitted 'b' when the walls of the channel are smooth for different values of roughness factors in the 600μm wide and 300μm deep open top SU8 channels. This indicates that the fitted value of b_r increases with r but not as fast as expected according to the eq. (6.1). Fig. 6.9 gives a closer look at the fitted values only.
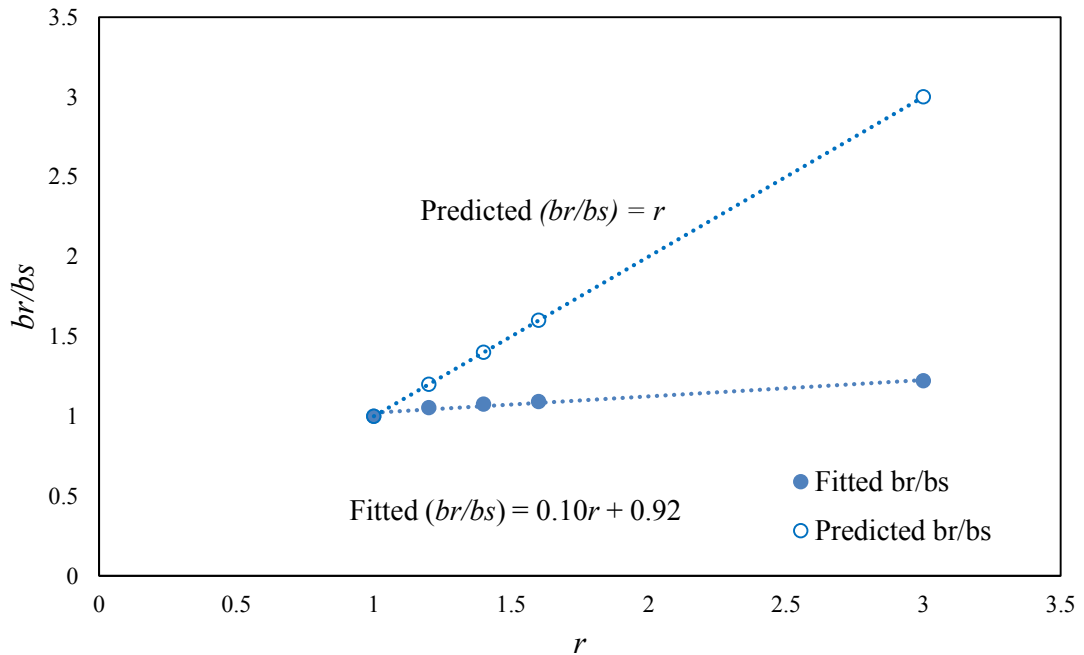
Fig. 6.8   *Comparison between the ratios of fitted and predicted values of b when the walls are rough to when these are smooth in 600μm wide and 300μm deep channels with gradually increasing roughness factor 'r'*

Fitted $(br/bs) = 0.10r + 0.92$
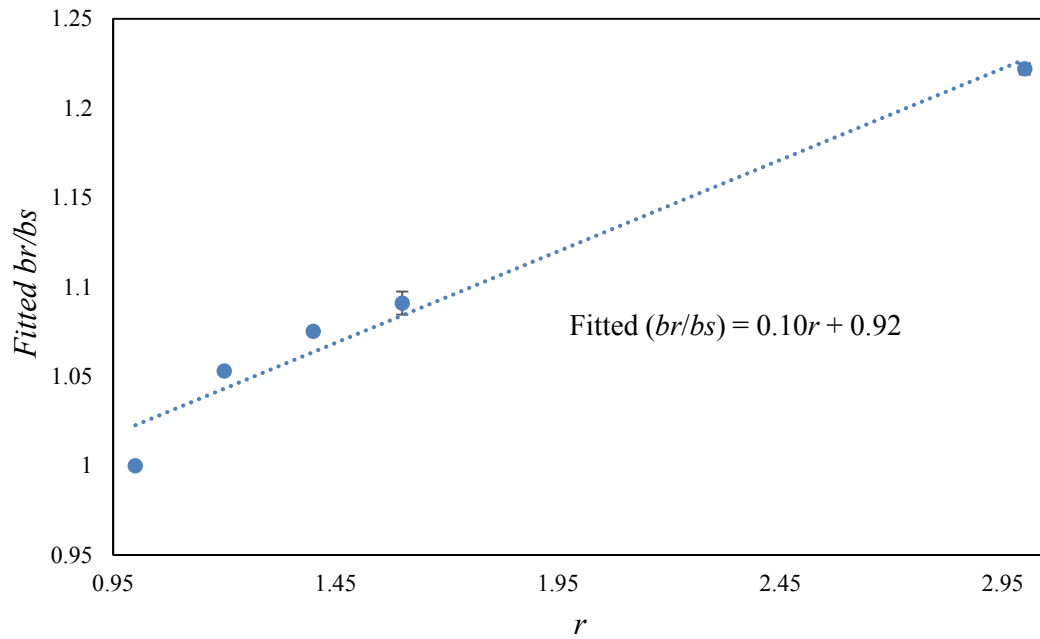
Fig. 6.9   *A closer look at ratio of fitted values of b when the walls are rough to when these are smooth in 600µm wide and 300µm deep channels with gradually increasing roughness factor 'r'.*

6.5.3   Effect of Liquid Viscosity on Capillary Rise in Rough Channels

This set of experiments was performed with 600µm wide and 350µm deep channels with three different viscosities of PDMS oil. The roughness factors of these channels were taken to be 1.0, 1.5, 2.0 and 2.5. The comparison of flow behaviour in the channels with different roughness factors is given in the Fig. 6.10 when rising liquid was PDMS 19.2 mPas.
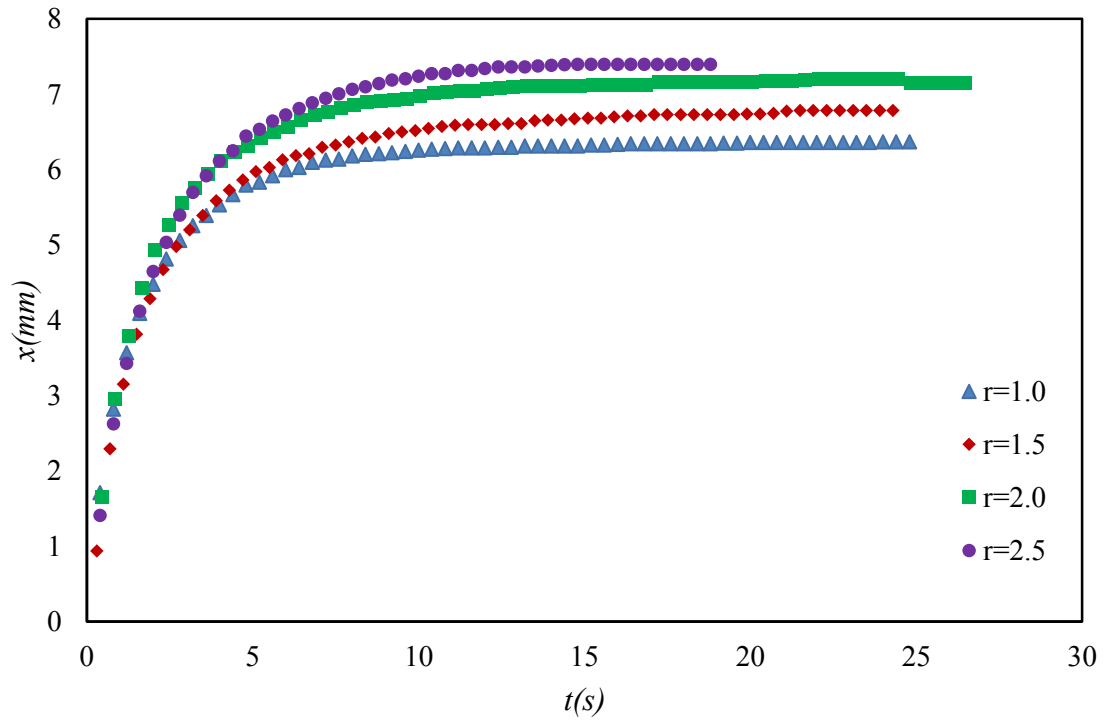
Fig. 6.10   *PDMS 19.2 mPa.s in 600μm wide and 350μm deep channels with roughness factors of 1.0, 1.5, 2.0 and 2.5*

It can be noted from Fig. 6.10 that with increasing roughness, rise height of PDMS in micro channels also increases. The results from experiments performed with other viscosities were also compared with visco-gravitational solution and deviation of viscous co-efficient '*a*' and the capillary term '*b*' was measured in each case. The visco-gravitational fits for the data from the channels with *r* = 1.5 when rising PDMS viscosities were taken to be 19.2, 48 and 96 mPas are shown in Fig. 6.11.
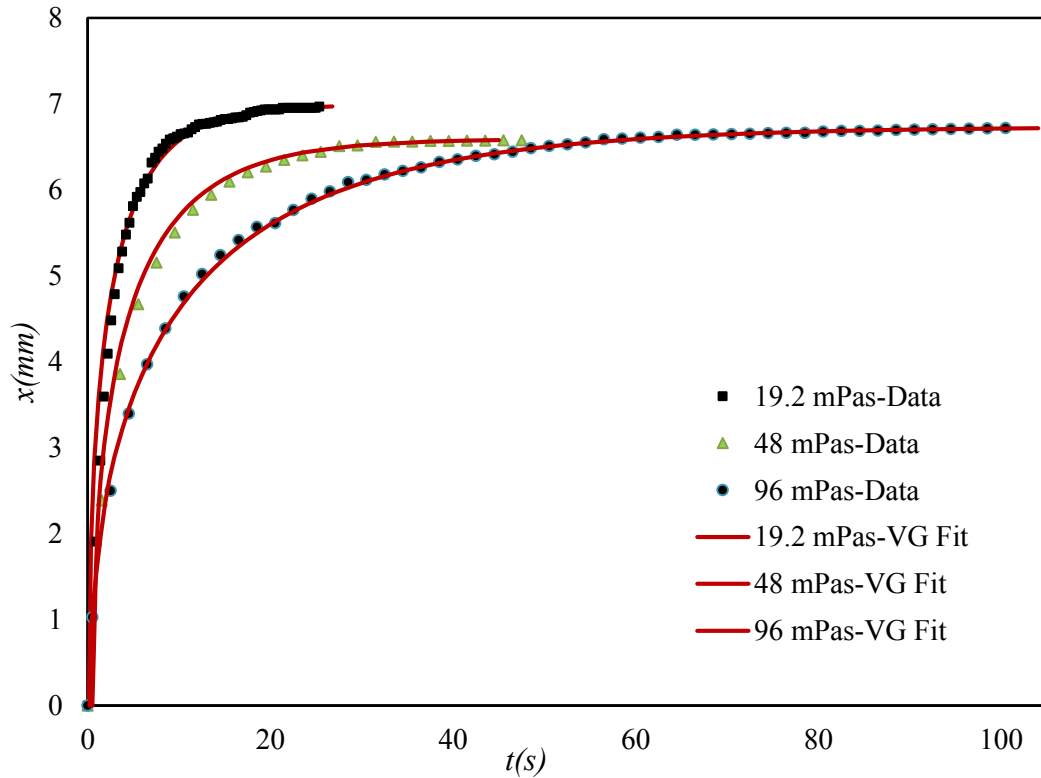
Fig. 6.11 *PDMS 19.2, 48 and 96 mPa.s in 600µm wide and 350µm deep channels with roughness factor of 1.5. Solid symbols represent data points and Solid line gives visco-gravitational fit*

For the experiment performed with PDMS viscosity 19.2 mPas, the viscous co-efficient '*a*' was found to be 4.23 times larger than the theoretical '*a*', whereas in the case of 48 mPas and 96 m Pas, this value was measured to be 3.04 and 4.54 times its theoretical value.

The capillary term '*b*' was measured to be 0.66 times the theoretical '*b*' in case when 19.2 mPas PDMS oil was the rising liquid. For 48 mPas and 96 mPas in the identical channels, the fitted value of '*b*' was found to be 0.64 and 0.66 times the theoretical value of '*b*'.

It is to be noted that the value of '*a*' should be independent of roughness factor but it does depend on viscosity of liquid used and for 19.2, 48 and 96 mPas PDMS, its predicted values are 1374.96, 3437.41 and 7444.69 (s^{-1}) given by eq. (2.44). Table 6.3 lists the ratio of fitted to the predicted values of the viscous term '*a*' for all the roughness factors when 19.2, 48 and 96 mPas PDMS rises in 600 µm wide and

350(±20) μm deep channels. The ratio of fitted '*a*' to predicted '*a*' for *r* = 1.0 increases with channel dimensions from a value of 3 for 300(±20)μm deep (Table 6.2) to a value of 4.00 for 350(±20)μm deep channel (Table 6.3), consistent with the results of chapter 4 (already discussed in section 4.3.4, Fig. 4.12 and 4.13). It is to be noted that the lower value of the ratio of the fitted to the predicted '*a*' for *r* = 2.0 and 2.5 in case of 96 mPas PDMS is because of variation in the depth (280±15μm) of the samples during their fabrication as these two different depths for channels with roughness factors 2.0 and 2.5 were fabricated on the same substrate and the samples were prepared at the same time.

Roughness Factor	*Fitted a/ Predicted a*		
r	For 19mPas	For 48mPas	For 96mPas
1.0	4.00 (±0.28)	4.02 (±0.56)	3.8 (±0.27)
1.5	4.23 (±0.30)	3.04(±0.43)	4.2 (±0.29)
2.0	3.73 (±0.26)	3.77 (±0.53)	2.5 (±0.18)
2.5	3.84 (±0.27)	3.82 (±0.53)	2.5 (±0.17)

Table 6.3   *Variation of the viscous term 'a' in 600 μm wide and 350(±20)μm deep channels when PDMS oil of three different viscosities were used as rising liquids.*

According to eq. (6.1), the value of the capillary term is independent of viscosity of the liquid used but increases by increasing the roughness. The values obtained for '*b*' from visco-gravitational fits in Table 6.4 are supporting this argument, although these values are not as much increasing with roughness as expected from a Wenzel consideration. Table 6.4 lists the mean values of predicted and fitted '*b*' with roughness obtained from three repeat experiments with 600μm wide and 350(±20)μm deep channels when PDMS oil of three different viscosities were used as rising liquids. The value of '*b*' is found to be independent of liquid viscosity as expected.

Roughness Factor	b(m/s)²			
r	Predicted	For 19 mPas (±0.001)	For 48 mPas (±0.001)	For 96 mPas (±0.001)
1.0	0.069	0.063	0.062	0.061
1.5	0.103	0.068	0.067	0.066
2.0	0.138	0.071	0.072	0.072
2.5	0.172	0.075	0.076	0.076

Table 6.4 *The values of the capillary term 'b' in 600(±5)μm wide and 350(±20)μm deep channels when PDMS oil of three different viscosities were used as rising liquids.*

These results are shown graphically for the variation of the fitted and predicted values of the capillary term '*b*' with roughness in Fig. 6.12.
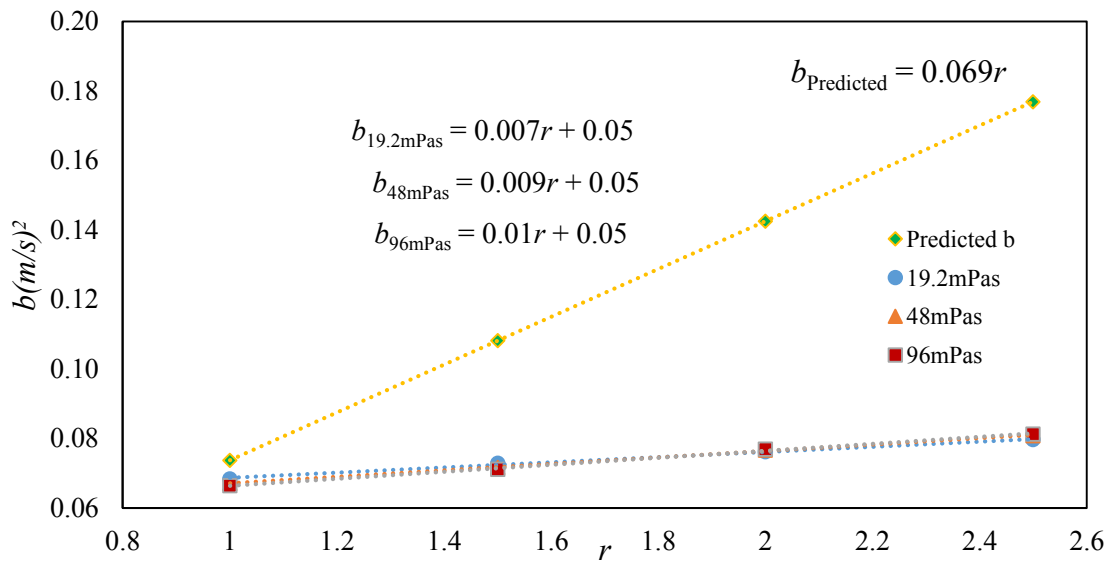
Fig. 6.12 *Comparison between the fitted and predicted values of b in 600 μm wide and 350(±20)μm deep rough channels with gradually increasing roughness factor 'r' from 1.0 to 3.0 when 19.2, 48 and 96 mPas PDMS was used as rising liquid.*

The following Fig. 6.13 gives the graphical representation of only fitted values given in Table in 6.4.
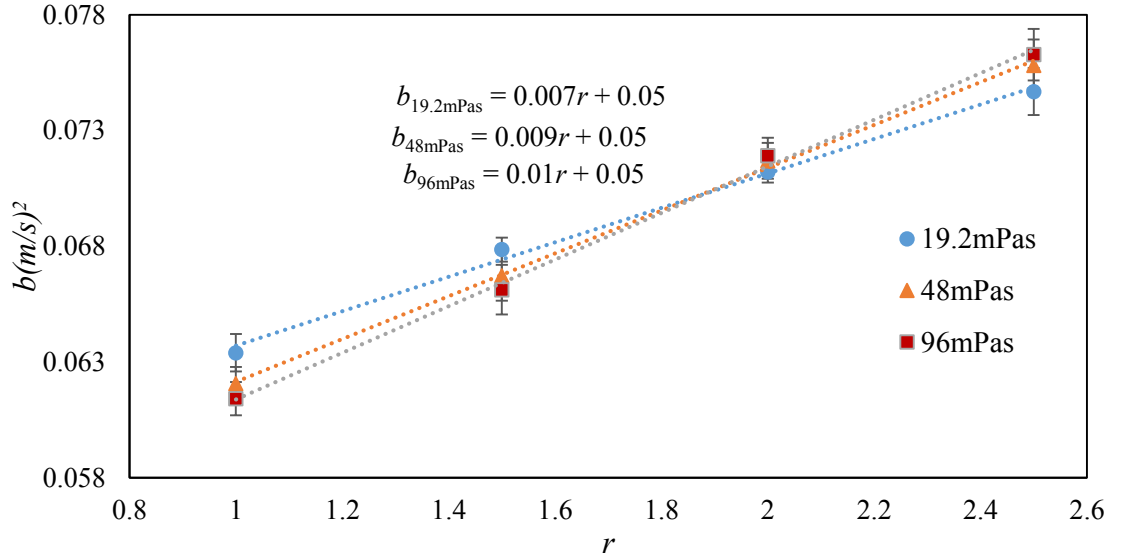
Fig. 6.13 *A closer look at the fitted values of b in 600(±5) μm wide and 350(±20)μm deep rough channels with gradually increasing roughness factor 'r' from 1 to 3 when 19.2, 48 and 96 mPas PDMS was used as rising liquid.*

It is to be noted from fig. 6.14 that the slope of the fitted values of b is found to be about $1/10^{th}$ of its predicted value according to the Wenzel consideration for all viscosities of PDMS oil with a small increase in its value with greater liquid viscosity i.e. for 19.2, 48 and 96 mPas, it is measured to be 0.007, 0.009 and 0.010 times the value of roughness factor of the open top micro channels. The intercept in all cases instead of having zero value, is found to be 0.05 similar to the results presented in section 6.5.2. The above Fig. 6.14 clearly shows that the equilibrium height was not found to be as greater as predicted by the Wenzel case, but almost only one tenth of its value.

The following Fig. 6.14 shows the ratio of fitted b to predicted b for the same value of roughness factor when three liquid viscosities of PDMS oil are used. It should be a horizontal straight line in case of getting same values of fitted and predicted b but it can be seen that this ratio starts decreasing as the roughness of channels becomes greater. It means that deviation of the fitted b from its predicted value becomes greater when larger roughness is introduced in the micro channels. The curve was found to be a

131

better fit than a straight line in this case. It is also observed that this deviation is greater when smaller liquid viscosity rises in the channels.
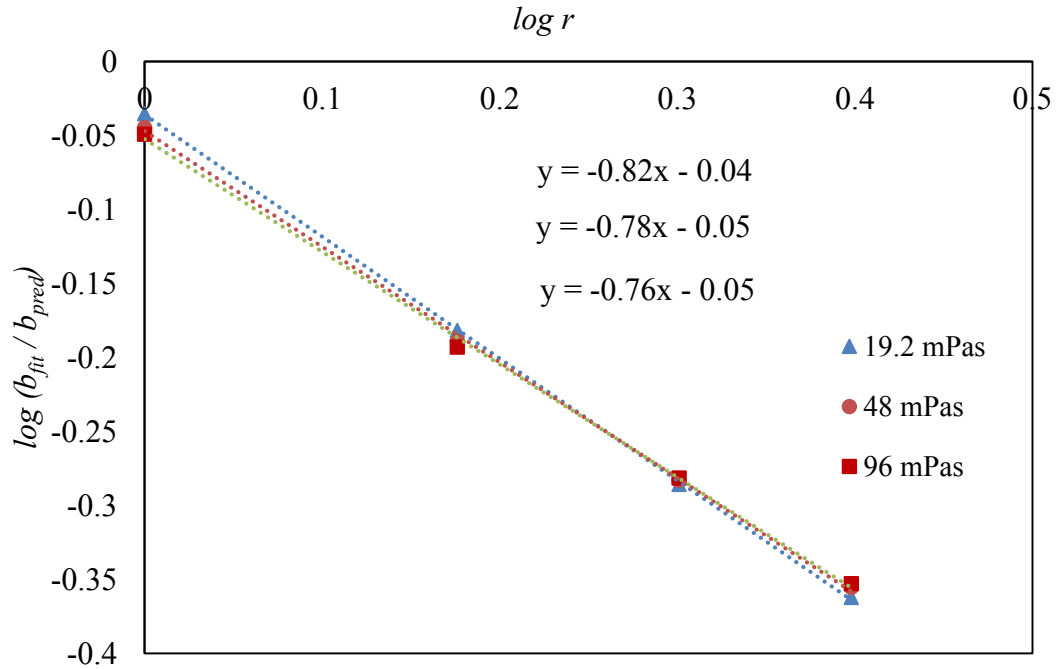
Fig. 6.14   *Graphical representation of reduction of 'b' compared to its predicted value in 600(±5)µm wide and 350(±20)µm deep rough channels when three different viscosities of PDMS were used as rising liquids.*

6.5.4   Effect of Channel Width on Capillary Rise in Rough Channels

This investigation involves the effect of two different widths of 350µm deep SU8 open top micro channels with PDMS oil of viscosity 19.2 mPas. The roughness factors of these channels were taken to be 1.0, 1.5, 2.0 and 2.5. The comparison of flow behaviour of PDMS 19.2 mPas in 400 and 600µm wide channels with different roughness factors is given in Fig. 6.15.
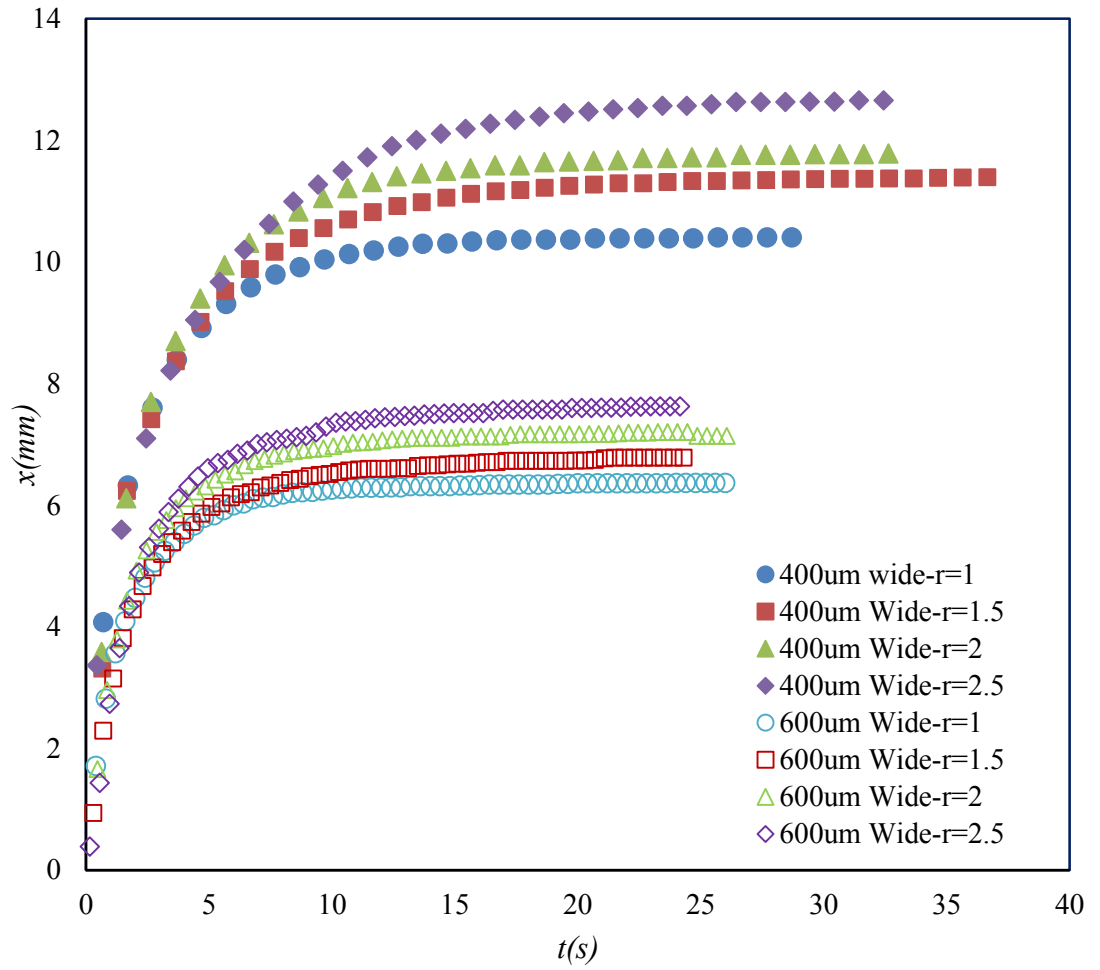
Fig. 6.15 *PDMS 19.2 mPa.s in 400 and 600μm wide and 350μm deep channels with various roughness factors.*

Similar fitting of the data using visco-gravitational approximation was performed as discussed in section 6.5.2 and the deviation of fitted parameters from their predicted values were measured. In Fig. 6.16, the visco-gravitational fitting (solid line) of experimental data (solid symbols) is shown for 400 and 600μm wide micro channels respectively with the same roughness factor of 2.5. These channels were 350μm deep and the viscosity of liquid used was 19.2 mPas.
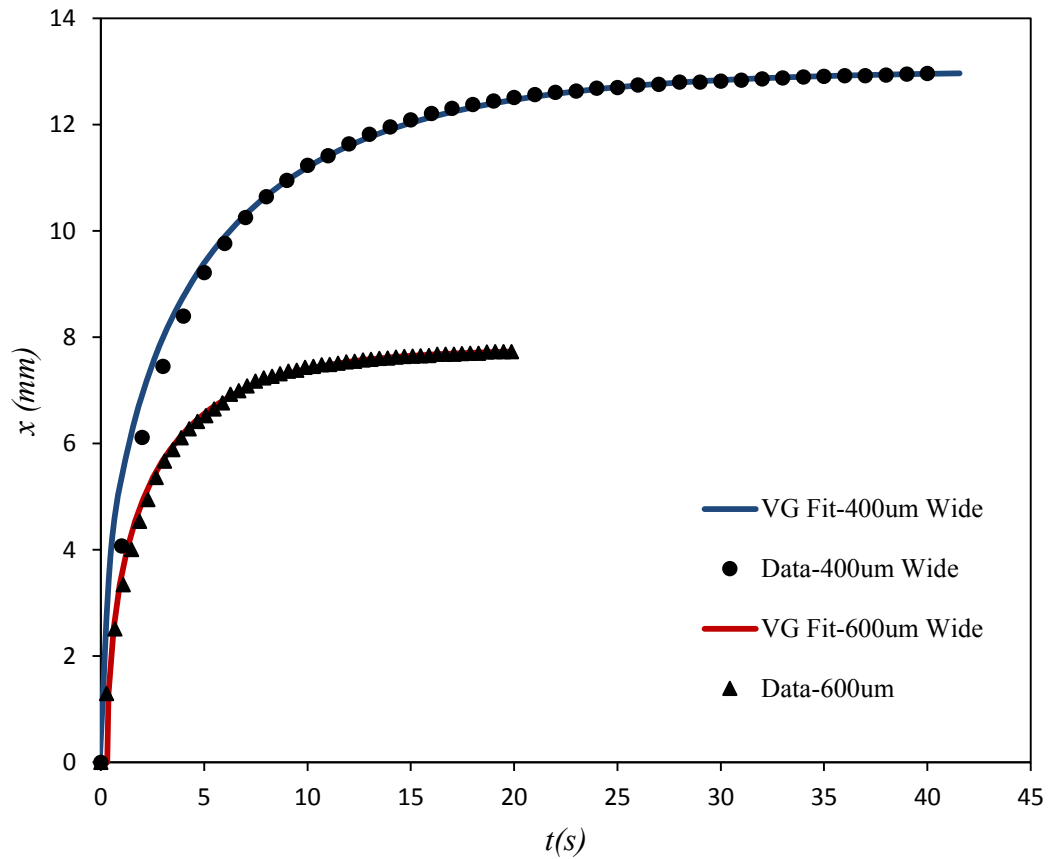
Fig. 6.16 *PDMS 19.2 mPa.s in 400μm and 600μm wide and 350μm deep channels with roughness factor of 2.5. Solid symbols represent data points and Solid line gives visco-gravitational fit*

For 400μm wide open channels, the viscous co-efficient '*a*' was found to be 2.3 times the predicted value of '*a*' while fitted value of capillary term '*b*' was measured to be half of its predicted value in rough channel of roughness factor of 2.5.

In case of 600μm wide channels, roughness factor of 2.5 the viscous co-efficient '*a*' was found to be 3.84 times its predicted value and the capillary term was found to be 56.5% less than the theoretical value of '*b*'.

The deviation of the fitted value of the viscous term '*a*' from its predicted value for all roughness factors for the similar dimensions of the channels was measured and is given in Table 6.5.

Roughness Factor	Fitted *a* / Predicted *a*	
r	For 600μm	For 400μm
1.0	4.00 (±0.28)	1.52 (±0.08)
1.5	4.23 (±0.30)	1.63 (±0.08)
2.0	3.73 (±0.26)	1.87 (±0.09)
2.5	3.84 (±0.27)	2.30 (±0.12)

Table 6.5 *The fitted value of the viscous term 'a' compared to its predicted value when PDMS 19.2 mPas rises in 400μm and 600μm wide and 350μm deep channels with various roughness factors.*

It can be seen that the values of fitted '*a*' becomes in better agreement with their predicted values when smaller widths of the channels i.e. the greater the width of the channels, the slower it rises compared to predicted speed in agreement with the results presented in chapter 4 (section 4.3.4, Fig. 4.12 and Table 6.3).

Similarly, the following Table 6.6 lists the predicted values of the capillary term b for roughness factors from 1 to 2.5 of the open top 300μm deep micro channels with two widths of 400 and 600μm.

Roughness Factor	b (m/s)^2			
r	600μm Wide		400μm Wide	
	Predicted	Fitted	Predicted	Fitted
1	0.07	0.063 (±0.001)	0.10	0.102 (±0.002)
1.5	0.10	0.068 (±0.001)	0.15	0.112 (±0.002)
2	0.14	0.071 (±0.001)	0.21	0.119 (±0.002)
2.5	0.17	0.075 (±0.001)	0.26	0.127 (±0.002)

Table 6.6 *The fitted value of the capillary term 'b' compared to its predicted value when PDMS 19.2 mPas rises in 400μm and 600μm wide and 350μm deep channels with various roughness factors.*

Fig. 6.17 gives graphical representation of the deviation of the capillary term b with increasing roughness in 400 and 600μm wide channels. For 350μm deep with 19.2 mPas PDMS as the rising liquid, the slope of the predicted value of the capillary term b is calculated to be 0.1 and 0.07 times the value of roughness factor in 400 and 600μm wide open top rough micro channels. But it can be seen from the results indicated by Fig. 6.17 that the fitted value of slope is found to be only $1/10^{th}$ of predicted slope value according to the eq. (6.1) with the intercept 0.05 for 600μm wide channels and 0.09 for 400μm wide channels instead of zero value which is consistent with the results discussed in sections 6.5.2 and 6.5.3.
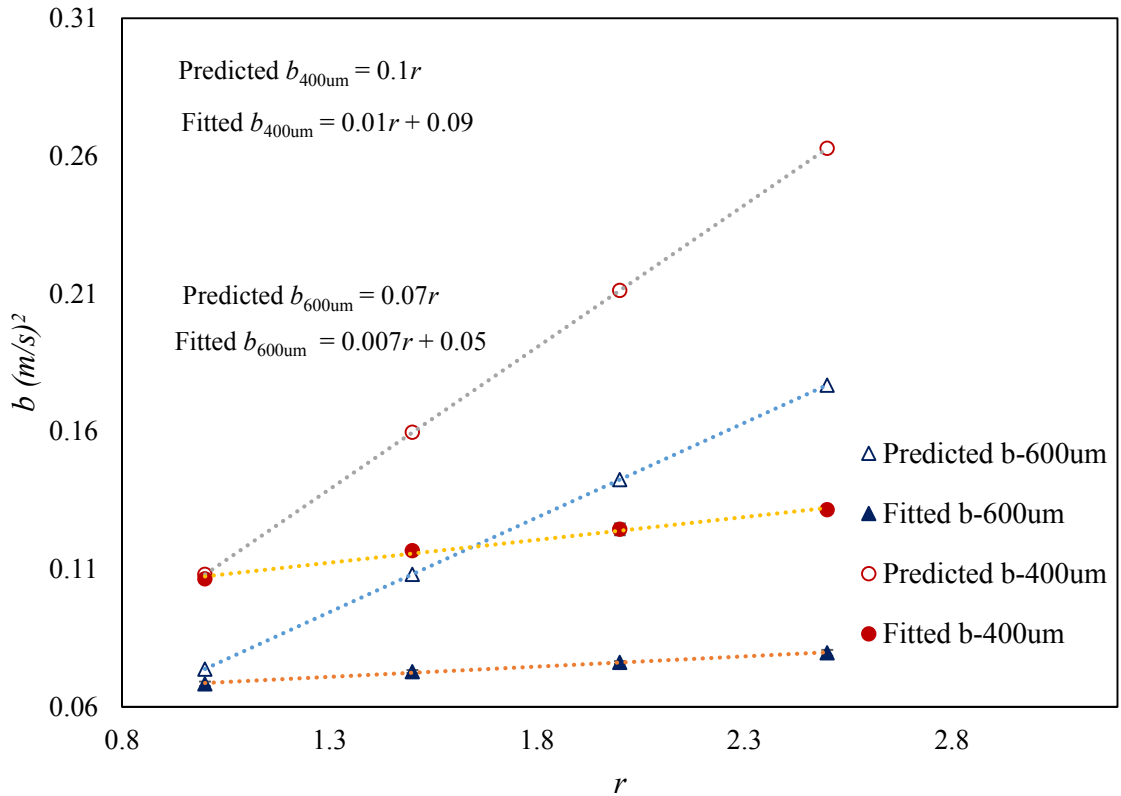
Fig. 6.17   *Graphical representation of variation of 'b' in 400 & 600μm wide and 350μm deep channels when PDMS oil of viscosity 19.2 mPas was used as rising liquid.*

Another aspect of the results from the experiments discussed in this section is shown in Fig. 6.18 below that gives the plot of the log of ratio of fitted b to the predicted b against log of roughness factor r. From the equation of the fitted line, it can

be seen that for 400 and 600μm wide and 350μm deep channels, this ratio is found to be equal to $0.92r^{-0.8}$ and $0.98r^{-0.76}$, where r is the roughness factor of the channel. This ratio is predicted to be proportional to the roughness r according to the Wenzel consideration, and it can be seen that in case of smaller channel dimensions i.e. 400μm width, the fitted ratio is found to be closer to its predicted value.
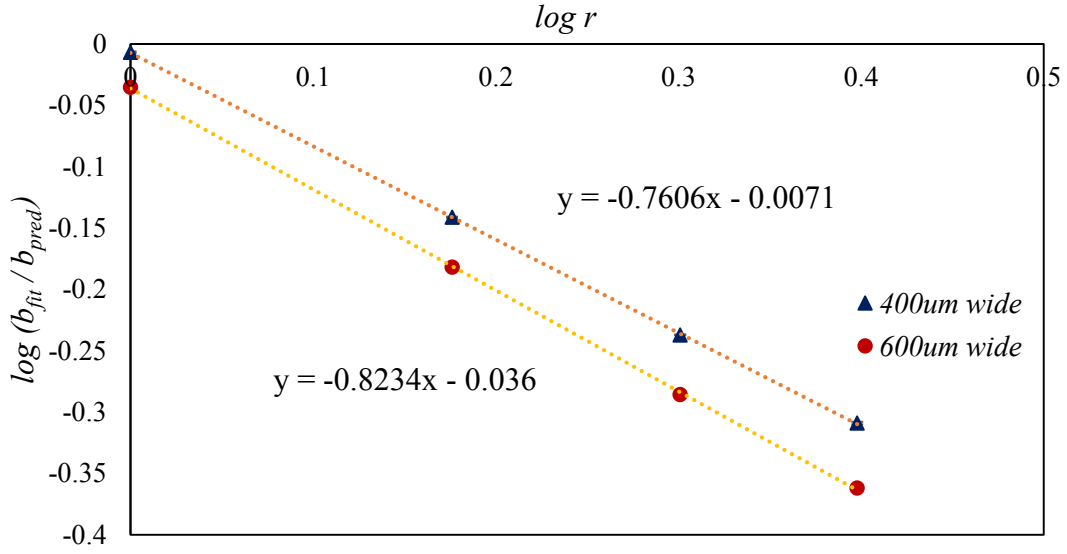
Fig. 6.18   *Graphical representation of deviation of 'b' compared to its predicted value in 400 & 600μm wide and 350μm deep channels when PDMS oil of viscosity 19.2 mPas was used as rising liquid.*

6.6   Effective Roughness

It has been observed (described in Section 6.5.1) that the increase in equilibrium height with increasing roughness is not as much as predicted by eq. 6.2, and as shown by Fig. 6.8 and 6.13 and 6.18, it is found to be linear with roughness as it is predicted by eq. 6.2 but with slope was found to be less than its predicted value by a factor of 10. In this section, the value of effective roughness is calculated, by effective roughness, r_{Eff} we mean that the value of fitted roughness factor for which the predicted equilibrium height becomes equal to the fitted x_e. It means that the ratio (Fitted x_e) / (Predicted x_e) = 1. Recalling eq.6.2 and writing it as "Predicted $(x_e)_r$"

$$\text{Predicted} \quad (x_e)_r = \frac{\gamma_{LV}}{\rho \, g \, h}[-1 + \cos\theta_e(1 + 2r\varepsilon)] \qquad (6.2)$$

137

and,

$$\text{Fitted} \qquad (x_e)_r = \frac{\gamma_{LV}}{\rho\,g\,h}\left[-1 + \cos\,\theta_e\left(1 + 2\,r_{Eff}\,\varepsilon\right)\right] \qquad (6.3)$$

This is shown in Table 6.7 for rough micro channels having roughness factor from 1.0 to 3.0. The experimental data used in this case is the same as represented in section 6.5.2.

Actual r	(b_{fit}/b_{pred}) for Actual r	r_{Eff}	(b_{fit}/b_{pred}) for r_{Eff}
1	0.89	1	0.89
1.5	0.64	1.08	0.89
2	0.52	1.18	0.89
2.5	0.44	1.25	0.89

Table 6.7 *Table showing effective roughness factors for 600µm wide and 350µm deep micro channels with 96 mPas PDMS as rising liquid.*

Fig 6.19 shows the variation in roughness extracted from fitted value of equilibrium height and the actual roughness. The effective roughness factor in the particular case is measured to be 0.17r with intercept 0.83.
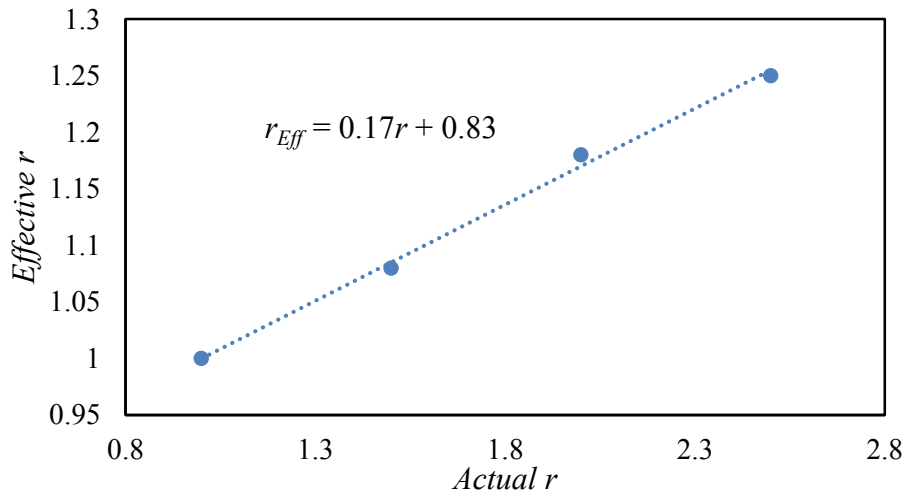
Fig. 6.19 *The graphical representation of the relationship of actual roughness and effective roughness of the channels with roughness from 1 to 2.5 while 96 mPas PDMS was used as rising liquid in 600 µm wide and 300µm deep rough channels.*

One of the possible reasons of the smaller value of effective roughness from the actual roughness may be the attributed to the presence of liquid fingers which advance ahead of main meniscus along the roughness features of the channels as shown in Table 6.1, the stick-slip behaviour of liquid fingers (will be discussed later in section 6.7), or the limitation of the theory.

6.7   Stick-Slip Behaviour and Liquid Fingers

During the rise of PDMS in open top SU8 rough walled micro-channel. it was also observed that liquid fingers do not exist at the early time regime of the flow, but gradually they start to appear as the liquid continues to rise in the channels and at the later time regime until when the liquid is about to attain its equilibrium height, their size becomes greater but their speed decreases gradually similar to the results discussed in chapter 5. Fig. 6.20 shows the propagation of liquid finger along one of the two side walls of the open top rough channel with roughness factor of 3.
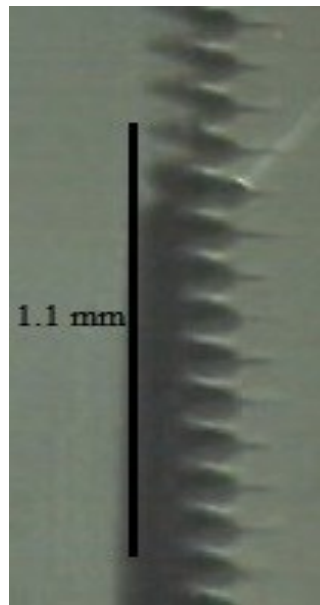
Fig. 6.20   *The liquid finger on one of the two walls of 600 μm wide and 300μm deep rough channel with roughness factors 3 when 48 mPas PDMS is used as rising liquid.*

The pinning of liquid fingers at the sharp edges (pinch) of the triangular roughness steps was observed during its rise in the open top rectangular micro channels at the later time of its flow. It remains pinned at the sharp edges for some time that depends upon viscosity of liquid and channel dimensions, and then slips quickly to the

139

next edge by filling the gap in between the two sharp edges. Fig. 6.21 shows snapshots of the flow of PDMS 48 mPas in 300µm deep and 600µm wide SU8 open top channel held vertically with roughness factor of 3 at three different time intervals (t_o) ms, (t_o+40) ms and (t_o+180) ms, where t_o is any arbitrary time of flow. The graphical representation of stick-slip behaviour is shown by Fig. 6.22 which clearly indicates the pinning and de-pinning of PDMS of viscosity 48 mPas along roughness features at one of the two walls having roughness factor of 3.
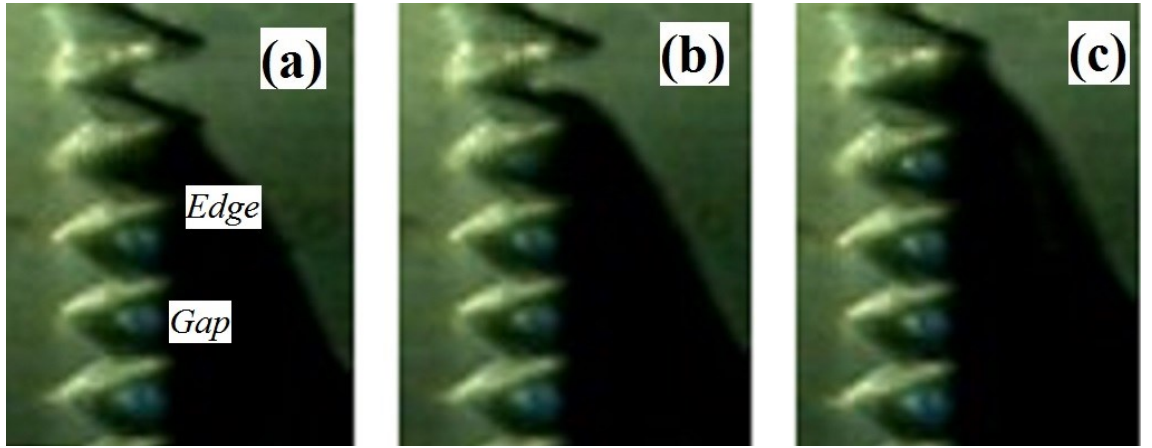
Fig. 6.21   *The snapshots of the 48 mPas PDMS finger rise along one of the two walls of 600 µm wide and 300µm deep rough channel with roughness factor of 3 at **a)** (t_o +0) ms, **b)** (t_o + 40) ms and **c)** (t_o + 180) ms, where t_o is any arbitrary time interval.*
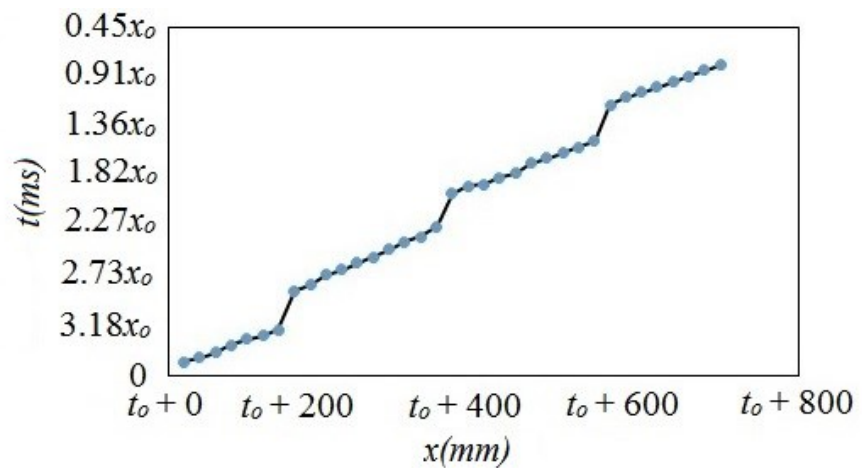
Fig. 6.22   *The pinning and de-pinning of 48 mPas PDMS across one of the two rough walls of 600µm wide SU8 open top micro channel with roughness factor 3.0. Here xo is the gap between the two consecutive edges.*

140

6.8   Summary

Liquid solid interaction can be controlled by altering surface chemistry that can make it more hydrophobic or hydrophilic (Vogler, 2001). If the solid surface is made rough by introducing obstacles to the flow, such as micron-scale ridges or posts on the surface the extra surface area can amplify the spreading tendency of a liquid so that it is drawn completely into a film [McHale, 2004; Shirtcliffe, 2005]. This type of induced wetting is also known as hemi-wicking.

In this chapter, the effect of the roughness on the capillary flow in vertically mounted open top SU8 micro channels is studied. Rough microfluidic channels were created using photolithography with roughness factor ranging from 1 to 3. Investigations on the flow behaviour of PDMS oils of various viscosities is carried out using open top SU8 rough micro channels 400(±5) and 600(±5) microns wide and 300(±20) to 350(±20) microns deep held vertically. It has been found that the equilibrium rise height increases with increase in roughness factor but was found to be far less than the value predicted by the theory considering Wenzel case. It was found that (x_e)fitted $= 0.1(x_e)$predicted with non-zero intercept. The value of the intercept for 400 and 600μm wide open top rough channels is found to be 0.009m and 0.005m respectively. The possible reason of this deviation from the expected value may be the existence of liquid fingers at the later stages of the liquid rise in micro channels that reduce the equilibrium height significantly. It is also possible that stick-slip behaviour of liquid fingers along roughness features may cause it not to attain the expected height according to the Wenzel case, one of the possible reasons may be the limitation of the theory, i.e. it may not be applied to the rough samples used for experimental study. The fitted values of the capillary term '*b*' was observed to be increasing with increasing roughness but it was found to be only 1/10th of the corresponding predicted value given by the eq. (6.1) with non-zero intercept.

The data was also analysed and the result for the fitted values of the viscous co-efficient '*a*' was compared to its predicted value according to visco-gravitational solution. The fitted '*a*' was found to be greater in wider channels which is consistent with the results presented in chapter 4 for plane channels and found to be independent of roughness of the channels which is in agreement with eq. (2.44). The effect of liquid

viscosity, channel depth and channel width on capillary dynamics in rough channels was also observed.

The effective roughness factors for the rough channels were calculated for which *(b_{fit} / b_{pred})* gives the same ratio as in case of smooth channels, i.e. $r = 1$ with the similar dimensions. It has been observed that considering the actual value of roughness factor *r*, r_{Eff} is proportional to 0.17*r*.

7   Conclusion and Future Works

7.1   Conclusion

The experimental work presented in this thesis comprises of three parts, the *first part* involves the testing and validation of the theory for capillary driven imbibition taking into consideration the gravitational effects presented by Ouali et al. (2013) in closed square glass tubes and smooth walled rectangular open top SU8 micro channels. PDMS oil of viscosity from 4.8 to 96 mPas was made to rise in closed square and 135μm deep and 400 and 600μm wide SU8 open top rectangular channels. The experimental work with open top rectangular channels mounted vertically is known to be reported for the first time. The results from these experiments were compared with the visco-gravitational model of capillary rise which is an approximation of the exact differential equation for capillary imbibition presented by Ouali et al. (2013). According to this approximation, the capillary rise can be described above a certain cross-over time by the analytical viscous-gravitational solution, and below this cross-over time, when gravitational effects can be neglected, the analytical Bousanquet model is the better solution. In these experimental conditions, This cross-over time Tc occurs within first 25ms of the rise time when liquid just enters the capillaries, which is during the first time interval to be measured, therefore, visco-gravitational model was found to be the best approximation for the experimental setup presented here. From the fits using visc-gravitational approximation, it has been found that the viscous flow is slower than predicted which is consistent with previously observed data for circular tubes. The viscous coefficient was found to be larger than predicted by theory, but that agreement improves for smaller dimension samples. The reason for this slower flow may be attributed to viscous friction and it may also be due to the possible dynamic contact angle effect during capillary rise or a possible retardation coefficient caused by an increased frictional dissipation of main meniscus. The equilibrium height attained in these capillaries compared to the predicted height was observed to be 5% less in square tubes and 15% less in open channels and the deduction is found to be dependent on sample dimensions. The reason for this reduction is attributed to the presence of propagating liquid fingers ahead of the main meniscus of rising liquid along the edges of the capillaries. It has been shown experimentally that, using one particular liquid viscosity, the data can be scaled for other viscosities in the capillaries having similar physical dimensions. Similarly, scaling method can be applied for fitted value of

viscous term '*a*' and for physical dimensions of capillaries such as height or width of the channels.

Second part is the detailed study of liquid fingers. In non-circular capillaries i.e. square closed glass tubes and rectangular cross-sectional SU8 open top micro channels, the rise of wetting liquid was observed in the form of fingers along all the corners of capillaries where its sides meet at 90° with each other. The shape and size of these liquid fingers depend upon the physical dimensions of the capillaries. It has been observed that these fingers were very prominent and very fast in speed as compared to the main meniscus propagation in SU8 open top micro channels particularly for smaller aspect ratio of the channels. Their size was observed to be increase gradually with time. For the completely wetting liquids ($\theta_e = 0°$), the liquid fingers are thin and form near the corner edges for square tubes with aspect ratio $\varepsilon = 1$, whereas they were found to be prominent for open channels with low values of $\varepsilon = (0.25, 0.225, 0.075)$, in agreement with observations on static fluids. The finger velocity reduced with time which is found to be decayed to $t^{1/2}$ in the long time limit. The capillary dynamics of vertically held open top micro channels in which the liquid fingers were found to be very prominent was analysed using visco-gravitational approximation and it has been found that for capillary rise in channels with very thick and larger liquid fingers, the capillary term '*b*' was reduced significantly. It is assumed that these fingers may attribute to the reduction of the equilibrium rise height. These fingers may have important implications for the design and performance of microfluidic devices based on liquid imbibition of wetting liquids with contact angles $\theta_e \leq 45°$ in rectangular micro channels. It is possible that they might affect the amount and dynamics of liquid flow, cause contamination between the micro-compartments or connect, what would otherwise be, separate area of liquids.

Investigation of capillary rise in rough walled open top SU8 micro channels of rectangular cross-section is the *third part* of the project. Rough microfluidic channels were created using photolithography technique by introducing triangular steps to the side walls of the channel with roughness factor ranging from 1 to 3. Investigations on the flow behaviour of PDMS oil of viscosities 19.2, 48 and 96 mPas has been carried out using vertically mounted open top SU8 rough micro channels 400 and 600(±5) μm wide and 300 to 350(±20) μm deep. It has been found that the equilibrium rise height increases with roughness factor but was found to be less than the value predicted by Wenzel angle consideration. The data from a series of experiments was analysed and

compared to the visco-gravitational capillary model. In rough micro channels, the fitted value of equilibrium height was found to be less than the predicted height, and this deviation was found to increase with increase in roughness factor of the channel. Possible reason for this deviation may be the presence of liquid fingers that advance along the corners of the channels ahead of main meniscus at the later stages of flow or it may also be the indication of the limitation of the Wenzel model. The effective roughness factors were extracted for which the fitted values of the capillary term 'b' from the visco-gravitaional fits was found to be the same as the predicted value. The effective roughness factor is found to increase linearly with the roughness factor r with a slope of 0.17 and an intercept of 0.83

7.2   Suggestions for Further Work

I)   Orientation of Capillaries:

The study of capillary dynamics in plane tubes and open top SU8 micro channels was carried out keeping them vertical i.e. at 90º with horizontal. The visco-gravitational model presents the solution for capillaries at any angle with the vertical. Therefore, it would be possible to validate the model by carrying out experiments with capillaries keeping them at different angles with horizontal other than 90º.

II)   Closed Top Su8 Micro Channels:

Another possibility would be to investigate capillary phenomenon in closed SU8 micro channels by capping the open top samples during their fabrication process of photo lithography. The roughness features may be introduced on the walls of closed channels to investigate their effect on the flow. Due to the presence of the fourth surface, the capillary pull is expected to increase. It would be possible to compare the experimental results with visco-gravitational approximation to check whether this approximation is valid for closed rough channels or gives the similar results as in case of open top SU8 micro channels. In other words, the limitation of Wenzel model can be investigated for closed top rough channels.

III)   Further Investigation on Liquid Fingers:

There is a lot more to be investigated about the dynamics of liquid fingers in non-circular capillaries that may be held at any angle with horizontal. It would also be possible to carry out investigations on liquid fingers in capillaries of non-uniform rectangular cross-sections that may be open top or closed. It may lead to investigation of their speed and their effect on the reduction of the expected rise height in rough as well as smooth walled open or closed top capillaries.

IV)   Stick-Slip Behaviour in Rough Channels:

In rough channel experiments, it has been observed that the equilibrium rise height did not come out to be the same as predicted by the Wenzel theory. It may be assumed that it is due to the pinning effect at the sharper and bigger sized triangular steps fabricated on the channel walls to introduce roughness. In future, in order to reduce the stick-slip behaviour, the size of the steps may be altered to investigate its effect on rise height. In this manner, the liquid flow may be controlled by varying the step size or shape.

V)   Roughness Features:

It may also be suggested to include various other types and shapes of the steps on bottom and side walls as well such as pillars or rectangular ridges on bottom surface, with open or closed top SU8 channels. These ridges may be in different symmetries. This may reduce the stick-slip behaviour and the viscous friction may also be altered due to different shapes and sizes of the obstacles to flow of liquid.

VI)   Non-uniform Cross-section Capillaries:

Another suggestion for future work is to fabricate samples with variable width to make non-uniform cross-section capillaries so that speed of rising liquid can be altered. It may lead to further investigate the effect of variable cross-section on liquid finger speed and its effect on the equilibrium rise height.

References

Ahadian S, Mizuseki H, Kawazoe Y (2009) An efficient tool for modeling and predicting fluid flow in nanochannels. J Chem Phys 131:184506. doi:10.1063/1.3253701

Aqil, S. (2006). Wetting of microstructured surfaces. PhD Thesis. Nottingham Trent University.

Ayyaswamy PS, Catton I, Edwards DK (1974) Capillary flow in triangular grooves. J Appl Mech 41:332–336. doi:10.1115/1.3423288

Baret J-C, Decré MMJ, Herminghaus S, Seemann R (2007) Transport dynamics in open microfluidic grooves. Langmuir 23:5200–5204. doi:10.1021/la063584c

Bertrand E, Blake TD, de Coninck J (2009) Influence of solid-liquid interactions on dynamic wetting: a molecular dynamics study. J Phys: Condens Matter 21:464124. doi:10.1088/0953-8984/21/46/464124

Bico J (2000) Me´canismes d' impre´gnation: surfaces texture´es, Bigouttes, Poreux. PhD thesis, Universite´ de Paris VI

Bico J, C Tordeux, and D Quere. (2001). Rough wetting. Europhysics Letters, 55(2), 214-220.

Bico J, Que´re´ D (2002) Rise of liquids and bubbles in angular capillary tubes. J Colloid Interface Sci 247:162–166. doi: 10.1006/jcis.2001.8106

Bico J, Que´re´ D (2003) Precursors of impregnation. Europhys Lett. 61:348–353. doi:10.1209/epl/i2003-00196-9

Bico J, Thiele U, Que´re´ D (2002) Wetting of textured surfaces. Colloids Surf A 206:41–46. doi:10.1016/S0927-7757(02)00061-4

Blake TD, Coninck J (2004) The influence of pore wettability on the dynamics of imbibition and drainage. Colloids Surf A 250:395–402. doi:10.1016/j.colsurfa.2004.05.024

Blake TD, Haynes JM (1969) Kinetics of liquid/liquid displacement. J Colloid Interface Sci 30:421–423. doi:10.1016/0021-9797(69)90411-1

Bouaidat S, Hansen O, Bruus H et al (2005) Surface-directed capillary system; Theory, experiments and applications. Lab on Chip 5:827–836. doi:10.1039/b502207j

Bousanquet C (1923) On the flow of liquids into capillary tubes. Philos Mag Ser 6(45):525–531. doi:10.1080/14786442308634144

Brody JP, Yager P, Goldstein RE, Austin RH (1996) Biotechnology at low Reynolds numbers. Biophys J 71:3430–3441. doi:10.1016/S0006-3495(96)79538-3

Byon C, Kim SJ (2011) The effect of meniscus on the permeability of micro-post arrays. J Micromech Microeng 21:115011. doi: 10.1088/0960-1317/21/11/115011

Chebbi R (2007) Dynamics of liquid penetration into capillary tubes. J Colloid Interface Sci 315:255–260. doi:10.1016/j.jcis.2007.06.073

Chollet, F. (2013, Feb). SU-8: Thick Photo-Resist for MEMS. Retrieved from memscyclopedia.org: http://memscyclopedia.org/su8.html

Clegg, C. (2008, September). www.ramé-hart.com. Retrieved from http://www.ramehart.com/contactangle.htm

Chen Y, Melvin LS, Rodriguez S et al (2009) Capillary driven flow in micro scale surface structures. Microelectron Eng 86:1317–1320. doi:10.1016/j.mee.2009.02.016

Clime L, Brassard D, Pezacki JP, Veres T (2012) Self-priming of liquids in capillary autonomous microfluidic systems. Microfluid Nanofluid 12:371–382. doi:10.1007/s10404-011-0881-7

Concus P, Finn R (1969) On the behavior of a capillary surface in a wedge. Proc Natl Acad Sci USA 63:292–299. doi:10.1073/pnas.63.2.292

Cox RG (1986) The dynamics of the spreading of liquid on a solid surface. 1. Viscous-flow. J Fluid Mech 168:169–194. doi:10.1017/S0022112086000332

D Bonn, J. E. (2009). Wetting and spreading. Reviews of Modern Physics, 85(2), 739-805.

Darhuber A, Troian S, Reisner W (2001) Dynamics of capillary spreading along hydrophilic microstripes. Phys Rev E 64:1–8. doi:10.1103/PhysRevE.64.031603

de Gennes PG, Brochard-Wyart F., & Que're D. (2004). Capillarity and Wetting Phenomena. Springer.

de Gennes PG (1985) Wetting: statics and dynamics. Rev Mod Phys 57:827–863. doi:10.1103/RevModPhys.57.827

Dong M, Chatzis I (1995) The imbibition and flow of a wetting liquid along the corners of a square capillary tube. J Colloid Interface Sci 172:278–288. doi:10.1006/jcis.1995.1253

F. F. Ouali, G McHale, H Javed, C Trabi, NJ. Shirtcliffe and M. I. Newton (2013) Wetting considerations in capillary rise and imbibition in closed square tubes

and open rectangular cross-section channels, Microfluidics and Nanofluidics, DOI 10.1007/s10404-013-1145-5

Fries N, Dreyer M (2008a) The transition from inertial to viscous flow in capillary rise. J Colloid Interface Sci 327:125–128. doi: 10.1016/j.jcis.2008.08.018

Fries N, Dreyer M (2008b) An analytic solution of capillary rise restrained by gravity. J Colloid Interface Sci 320:259–263. doi: 10.1016/j.jcis.2008.01.009

Fries N, Dreyer M (2009) Dimensionless scaling methods for capillary rise. J Colloid Interface Sci 338:514–518. doi:10.1016/j.jcis.2009.06.036

Gast., A. W. (1997). Physical Chemistry of Surface. Wiley-interscience.

Gentle GT. (2005). Interfacial Science. Oxford press.

Girardo S, Cingolani R, Chibbaro S, Diotallevi F, Succi S, Pisignano D (2009) Corner liquid imbibitions during capillary penetration in lithographically made microchannels. Appl Phys Lett 94: 171901–171903. doi:10.1063/1.3123804

Girardo S, Palpacelli S, De Maio A, Cingolani R, Succi S, Pisignano D (2012) Interplay between shape and roughness in early stage microcapillary imbibition. Langmuir 28:2596–2603. doi:10.1021/la2045724

Hamraoui A, Nylander T (2002) Analytical approach for the Lucas–Washburn equation. J Colloid Interface Sci 250:415–421. doi: 10.1006/jcis.2002.8288

Hamraoui A, Thuresson K, Yaminsky V, Nylander T (2000) Can a dynamic contact angle be understood in terms of a friction coefficient? J Colloid Interface Sci 226:199–204. doi:10.1006/jcis.2000.6830

Han A, Mondin G, Hegelbach NG et al (2006) Filling kinetics of liquids in nanochannels as narrow as 27 nm by capillary force. J Colloid Interface Sci 293:151–157. doi:10.1016/j.jcis.2005.06.037

Hoffman RL (1975) Study of advancing interface. 1. Interface shape in liquid-gas systems. J Colloid Interface Sci 50:228–241. doi: 10.1016/0021-9797(75)90225-8

Ichikawa N, Hosokawa K, Maeda R (2004) Interface motion of capillary-driven flow in rectangular microchannel. J Colloid Interface Sci 280:155–164. doi:10.1016/j.jcis.2004.07.017

Ishino C, Reyssat M, Reyssat E et al (2007) Wicking within forests of micropillars. Europhys Lett. doi:10.1209/0295-5075/79/56005

Jokinen V, Franssila S (2008) Capillarity in microfluidic channels with hydrophilic and hydrophobic walls. Microfluid Nanofluid 5:443–448. doi: 10.1007/s10404-008-0263-y

Jong W, Kuo T, Ho S et al (2007) Flows in rectangular microchannels driven by capillary force and gravity. Int Commun Heat Mass Transfer 34:186–196. doi:10.1016/j.icheatmasstransfer.2006.09.011

Krotov VV, Rusanov AI (1999) Physicochemical hydrodynamics of capillary systems. Imperial College Press, p 222

Kusumaatmaja H, Pooley CM, Girardo S et al (2008) Capillary filling in patterned channels. Phys Rev E 77:3–6. doi:10.1103/PhysRev E.77.067301

Legait B (1983) Laminar flow of two phases through a capillary tube with variable square cross-section. J Colloid Interface Sci 96:28–38. doi:10.1016/0021-9797(83)90005-X

Liou WW, Peng Y, Parker PE (2009) Analytical modeling of capillary flow in tubes of nonuniform cross section. J Colloid Interface Sci 333:389–399. doi:10.1016/j.jcis.2009.01.038

Liu W, Li Y, Cai Y, Sekulic DP (2011) Capillary rise of liquids over a microstructured solid surface. Langmuir 27:14260–14266. doi: 10.1021/la2033884

Lucas R (1918) Ueber das Zeitgesetz des Kapillaren Aufstiegs von Flussigkeiten. Kolloid Z 23:15–22. doi:10.1007/BF01461107

Marmur A. (2003). Wetting of Hydrophobic Rough Surfaces: To be heterogeneous or not to be. Langmuir, 19, 8343–8348.

Marmur A, Cohen RD (1997) Characterization of porous media by the kinetics of liquid penetration: the vertical capillaries model. J Colloid Interface Sci 189:299–304. doi:10.1006/jcis.1997.4816

McHale G, Shirtcliffe NJ, Aqil S et al (2004) Topography driven spreading. Phys Rev Lett 93:1–4. doi:10.1103/PhysRevLett.93.036102

Mehrabian H, Gao P, Feng JJ (2011) Wicking flow through microchannels. Phys Fluids 23:122108. doi:10.1063/1.3671739

Mognetti BM, Yeomans JM (2009) Capillary filling in microchannels patterned by posts. Phys Rev E 80:1–8. doi:10.1103/PhysRevE.80.056309

Mumley TE, Radke C, Williams MC (1986) Kinetics of liquid/liquid capillary rise: I. Experimental observations. J Colloid Interface Sci 109:398–412. doi:10.1016/0021-9797(86)90318-8

N.J. Shirtcliffe, G. M. (2005). Porous materials show superhydrophobic to superhydrophilic switching. Chem. Comm., 25, 3135-3137.

Okumura K. (2008). Wetting transitions on textured hydrophilic surfaces. European Physical Journal, 5 (4), 415-424.

Oh JM, Faez T, Beer S, Mugele F (2009) Capillarity-driven dynamics of water–alcohol mixtures in nanofluidic channels. Microfluid Nanofluid 9:123–129. doi:10.1007/s10404-009-0517-3

Onda, T., Shibuichi, S., Satoh, N. & Tsujii, K. Super water-repellent fractal surfaces. Langmuir 12, 2125–2127 (1996)

Ponomarenko A, Que´re´ D, Clanet C (2011) A universal law for capillary rise in corners. J Fluid Mech 666:146–154. doi: 10.1017/S0022112010005276

Popescu MN, Ralston J, Sedev R (2008) Capillary rise with velocity dependent dynamic contact angle. Langmuir 24:12710–12716. doi:10.1021/la801753t

Que´re´ D (1997) Inertial capillarity. Europhys Lett 39:533–538. doi: 10.1209/epl/i1997-00389-2

Que´re´ D. (2008a). Wetting of Textured Surfaces. Colloids and Surfaces, 206 (1–3), 41-46.

Que´re´ D (2008b) Wetting and roughness. Annu Rev Mater Res 38:71–99. doi:10.1146/annurev.matsci.38.060407.132434

Rame´ E, Weislogel MM (2009) Gravity effects on capillary flows in sharp corners. Phys Fluids 21:042106. doi:10.1063/1.3109685

Ransohoff T, Radke CJ (1988) Laminar flow of a wetting liquid along the corners of a predominantly gas-occupied noncircular pore. J Colloid Interface Sci 121:392–401. doi:10.1016/0021-9797(88)90442-0

Reyssat M, Courbin L, Reyssat E, Stone HA (2008) Imbition in geometries with axial variations. J Fluid Mech 615:335–344. doi: 10.1017/S0022112008003996

Robert N. Wenzel. (1936). Resistance of solid surfaces to wetting by water. Industrial & Engineering Chemistry. doi:10.1021/ie50320a024

Romero LA, Yost FG (2006) Flow in an open channel capillary. J Fluid Mech 322:109–129. doi:10.1017/S0022112096002728

Rosendahl U, Ohlhoff A, Dreyer ME (2004) Choked flows in open capillary channels: theory, experiment and computations. J Fluid Mech 518:187–214. doi:10.1017/S0022112004001041

Schoelkopf J, Gane PAC, Ridgway CJ, Matthews GP (2002) Practical observation of deviation from Lucas–Washburn scaling in porous media. Colloids Surf 206:445–454. doi:10.1016/S0927-7757(02)00066-3

Seemann R, Brinkmann M, Kramer EJ, Lange FF, Lipowsky R (2005) Wetting morphologies at microstructured surfaces. Proc Natl Acad Sci USA 102:1848–1852. doi:10.1073/pnas.0407721102

Shirtcliffe NJ, McHale G, Newton MI et al (2006) Critical conditions for the wetting of soils. Appl Phys Lett 89:094101. doi:10.1063/1.2339072

Shirtcliffe NJ, McHale G, Atherton S, Newton MI (2010) An introduction to superhydrophobicity. Adv Colloid Interface Sci 161:124–138. doi:10.1016/j.cis.2009.11.001

Siebold A, Nardin M, Schultz J et al (2000) Effect of dynamic contact angle on capillary rise phenomena. Colloids Surf A 161:81–87.doi:10.1016/S0927-7757(99)00327-1

Squires T, Quake SR (2005) Microfluidics: fluid physics at the nanoliter scale. Rev Mod Phys 77:977–1026. doi:10.1103/RevModPhys.77.977

Srivastava N, Din C, Judson A et al (2010) A unified scaling model for flow through a lattice of microfabricated posts. Lab Chip 10:1148–1152. doi:10.1039/b919942j

Stange M, Dreyer ME, Rath HJ (2003) Capillary driven flow in circular cylindrical tubes. Phys Fluids 15:2587–2601. doi: 10.1063/1.1596913

Staples TL, Shaffer DG (2002) Wicking flow in irregular capillaries. Colloids Surf A 204:239–250. doi:10.1016/S0927-7757(01)01138-4

Stukan MR, Ligneul P, Crawshaw JP, Boek ES (2010) Spontaneous imbibition in nanopores of different roughness and wettability. Langmuir 26:13342–13352. doi:10.1021/la101995t

T Onda, N Shibuichi, N Satoh, and T Tsuji. (1996). Superwater-repellent fractal surfaces. Langmuir, 2125-2127.

Tartakovsky A, Meakin P (2005) Modeling of surface tension and contact angles with smoothed particle hydrodynamics. Phys Rev E 72:02630. doi:10.1103/PhysRevE.72.026301

Vogler EA. (2001). Chapter 6 'On the origins of water wetting terminology' in 'Water in Biomaterials Surface Science'. (M. Morra, Ed.) New York: John Wiley & Sons.

Washburn EW (1921) *The dynamics of capillary flow*. Phys Rev 17:273–283. doi:10.1103/PhysRev.17.273

Weislogel MM, Baker JA, Jenson RM (2011) *Quasi-steady capillarity-driven flows in slender containers with interior edges*. J Fluid Mech 685:271–305. doi:10.1017/jfm.2011.314

Xiao Y, Yang F, Pitchumani R (2006) *A generalised analysis of capillary flow in channels*. J Colloid Interface Sci 298:880–888. doi:10.1016/j.jcis.2006.01.005

Xue HT, Fang ZN, Yang Y, Huang JP, Zhou LW (2006) *Contact angle determined by spontaneous dynamic capillary*. Chem Phys Lett 432:326–330. doi:10.1016/j.cplett.2006.10.017

Yang D, Krasowska M, Priest C, Popescu MN, Ralston J (2011) *Dynamics of capillary-driven flow in open microchannels*. J Phys Chem C 115:18761–18769. doi:10.1021/jp2065826

Yost F, Holm E (1995) Capillary flow on narrow strips and in V-shaped grooves. Advances in electronic packaging. In: Proceedings of INTERPACK'95 conference, ASME EEP, vol10, pp 1265–1271

Young T. (1805). An Essay on the Cohesion of Fluids. Phil. Trans. R. Soc. Lond, 95, 65-87. doi:10.1098/rstl.1805.0005

Zhu Y, Petkovic-Duran K (2010) Capillary flow in microchannels. Microfluid Nanofluid 8:275–282. doi:10.1007/s10404-009-0516-4